Abstract

This report is a documentation of the project “Plastic Design of Composite Bridges Allowing for Local Buckling” aiming at assessing the feasibility of using plastic design method for continuous steel-concrete composite bridges, in ultimate limit states. The method shall allow for local buckling in the steel girders at internal supports. In order to obtain the moment-rotation relationship for the steel girders at the internal supports, fifteen double-symmetric, welded, I-shaped steel girders were tested. Steel with a nominal yield strength of 700 MPa and 220 MPa was used. The 220 MPa steel was used in the web of two of the tested girders (hybrid girders), while flanges were made of 700 MPa. Flange and web slenderness ratios as well as the length of the girders were varied in the tests. The flange slenderness ratio (flange width over thickness) b_{fl}/t_f varied from 10 to 15, the web slenderness ratio, h_w/t_w from 36 to 110 and the length of the girders from 2.66 to 6.0 m.

The report shows that plastic design of composite bridges, taking into account local buckling in the girders, is feasible. An example using plastic design is outlined in the report. However more work has to be carried out with respect to the moment-rotation relationship and flange induced buckling.

The plastic design method presented in this report saves approximately 10% of material in the steel girders compared to an elastic design.

Preface

This project was carried out in the Department of Civil and Mining Engineering at the University of Technology in Luleå Sweden, during 1993 and 1994. It was conducted with the financial support of SBUF (The Development Fund of the Swedish Construction Industry), through Mr. Helge Nilsson of Skanska Teknik. The author wishes to express his gratitude to the staff of the Department of Civil and Mining Engineering, SSAB Oxelösund and the advisory group of the project consisting of

Mr. Börje Gräfnings,	The Swedish Road Authority
Prof. Torsten Höglund,	Royal Institute of Technology
Prof. Bernt Johansson,	Luleå University of Technology
Mr. Mats Karlsson,	J&W AB
Mr. Sven Krakau,	Skanska Stålteknik AB
Mr. Tore Lundmark,	Scandiaconsult Nord AB
Mr. Helge Nilsson,	Skanska Teknik AB

A special thanks to my professor Bernt Johansson and the research and development engineers Mr. Georg Danielsson and Mr. Lars Åström.

Luleå in April 1995

Frank Axhag

Contents

Notation

A = Area of cross-section
A_f = Area of flange
A_{fc} = Area of flange in compression
A_s = Area of reinforcement bars
A_w = Area of web
C_i = Integration constants, i = 1, 2, 3, ... ,n
C_M = Rotation spring stiffness
E_k,E = Youngs modulus, $2.1 \cdot 10^5$ MPa
E_s = Youngs modulus of the reinforcement bars
G = Shear modulus, $0.81 \cdot 10^5$ MPa
H = Depth of composite bridge cross-section
I = Moment of inertia (an index tells with respect to which axis I should be considered).
K_v = Torsion constant (St. Venant)
K_w = Warping moment of inertia
L = Span length
M = Moment at midspan or moment as a function of a variable, for example M = M(z)
M_e = Effective moment at support
M_{max} = Maximum moment from tests
M_p = Full plastic moment based on f_y from tensile tests (see table 3.6)
M_y = Yield moment based on f_y from tensile tests (see table 3.6)
$M_{y,ef}$ = Effective yield moment with respect to local buckling of cross section according to BSK94 or EC3 with f_y from tensile tests (see table 3.6)
N = Normal force
P = Load at midspan
PNA = Plastic neutral axis
T = Torsion moment
V_{cd} = Shear capacity according to BSK94, column 1 (f_{yw} according to table 3.6 and $f_{yd} = f_{yw}$)
V_{max} = Maximum shear from tests
V_y = Shear force in the direction of y-axis
b_f = Outstand of flange according to BSK94
b_{fl} = Flange width
c = Outstand of flange according to EC3 or concrete cover of reinforcement
d = Depth of web according to EC3 (distance in between weld toes)
f_{cc} = Design compressive strength of concrete
f_{uk} = Ultimate strength
f_{yd} = Design yield strength of flange according to BSK94
f_{yf} = Yield strength of flange
f_y = Yield strength measured from tensile tests
f_{yk} = Characteristic yield strength

f_{yw} = Yield strength of web

h_w = Depth of web

h_{wc} = Depth of part of web in compression from moment, with full plastic cross-section

k = Parameter according to EC3 section 5.7.7
k = 0.3 for flanges in class 1
k = 0.4 for flanges in class 2
k = 0.55 for flanges in class 3 and 4

k_r = Rotation stiffness per unit length and angle for the connection between upper flange and web of girder.

k_θ = Slope of the descending part of moment-rotation curve (see figure 2.1)

s = Distance between center of reinforcement bars

s_{rm} = Mean distance between cracks in concrete

s_1 = Distance from support to the deflection guage at lower flange, closest to support

s_2 = Distance from support to the deflection guage at lower flange, closest to midspan

t_f = Thickness of flange

t_w = Thickness of web

w = Deflection at midspan

Π = Potential (or change in potential)

w_k = Crackwidth in concrete according to BBK94

y = Deflection of girder (in the plane of the web)

α = Coefficient of thermal expansion according to Bro 94 or a help variable in chapter 7.2

β_{fpl} = Slenderness limitation for flanges in class 1 according to BSK94

β_w = Slenderness limitation for webs in class 3 according to BSK94

β_{wel} = Slenderness limitation for webs in class 2 according to BSK94

β_{wpl} = Slenderness limitation for webs in class 1 according to BSK94

ΔT = Temperature difference

ε_{cs} = shrinkage in concrete

ε_f = Strain in flange

ε_s = Strain in reinforcement bars

ε_T = Strain from temperature difference

θ_{fk} = Rotation capacity as defined in figure 2.1

θ_{el} = Elastic rotation at support

θ_p = Plastic (inelastic) rotation at midspan

$\theta_{p,s}$ = Plastic (inelastic) rotation at support

$\theta_{pe,s}$ = Elastic rotation at support when $M = M_p$

θ_{rk} = Required rotation capacity

θ_t = Total (elastic + plastic) rotation at midspan

$\theta_{t,s}$ = Total (elastic + plastic) rotation at support

κ = Curvature of girder

κ_f = Parameter as a function of flange slenderness according to BSK94, table 6:211a, $1.0 \leq \kappa_f \leq 1.5$

κ_1 = Coefficient used when calculating mean distance between cracks (= 0.8 for deformed rebars)

κ_2 = Coefficient used when calculating mean distance between cracks, accounting for the distribution of strain

ν = Either Poisson's ratio (= 0.3) or coefficient in crackwidth calculations expressing the influence of concrete in tension between cracks

ρ_r = Coefficient expressing the ratio of reinforcement to concrete

σ_s = Stress in reinforcement bars

ϕ = Diameter of reinforcement bars

φ = Elastic rotation

$\psi\gamma$ = Loadcoefficient according to Bro 94

Index

DS = Differential settlement

R = Denotes capacity of cross-section

S = Shear centre

T = Linearly varying temperature or tangent modulus (E or G)

d = When applied to notation for loads, it refers to the design load i.e. including load factors.

c = Concrete

comp = Composite section

cr = Critical value with respect to instability

cs = Shrinkage

el = Elastic value

k = Characteristic value

ΔT = Different temperature in concrete slab and girders

0 = Indicates that the indexed value is a constant, for example M_0 = constant

Abbreviations

BBK94 : Bestämmelser för betongkonstruktioner, (Swedish handbook for Concrete constructions, formerly code)

BSK94 : Bestämmelser för Stålkonstruktioner, (Swedish handbook for Steel constructions, formerly code)

EC3 : Eurocode 3, steel structures. Harmonized european code.

K18 : Handboken Bygg chapter 18. Swedish handbook, covering plated structures.

Bro 94 : The swedish bridge code

BS5400 : The british bridge code

Miscellaneous

Moment diagrams are drawn on the side of the construction in which tensile stresses occur from bending moment.

1 Introduction

According to the Swedish bridge code (Bro 94) it is not allowed to use plastic global analysis in ultimate limit states for continuous steel-concrete composite bridges. The plastic strength of a cross-section may only be used if the cross-section is in class 1 according to BSK94. The reason for this is that the rotation capacity of the slender steel girders at internal supports are considered to be insufficient. Also the influence in the fatigue limit state and serviceability state is not known according to the Swedish Road Authority.

By utilizing the descending part of the moment rotation curve, it should be possible to derive a plastic design method, allowing for local buckling, which incorporates the redistribution of moments and possibly cancelling the influences of temperature and shrinkage of the concrete. The advantages of a plastic design would be a simpler design in ultimate limit states and also produce a more cost effective structure.

This procedure requires that the moment-rotation relation can be predicted as a function of the geometry of the composite cross-section and the material properties. To investigate the influence of the length of the girders together with flange and web slenderness, on the moment-rotation relation, fifteen double symmetric, I-shaped steel girders were tested. These tests are part of a project which objective is to derive a plastic design method in ultimate limit states for continuous composite bridges, allowing for local buckling.

Plastic design is usually refered to methods which take advantage of that plastic hinges can develop in stocky members in which the plastic moment is maintained under a considerable plastic rotation. When plastic design is refered to in this report, it is refered to a plastic design method in which account is made for local buckling of the slender cross-section.

The scope of this report is to assess the feasibility of applying a plastic design method for composite bridges. The report is divided into ten chapter and a brief description of the contents in each chapter is given in the following.

Chapter 2 presents a literature study containing compiled references where moment-rotation tests on girders have been performed.

Chapter 3 presents the laboratory tests on the fifteen girders tested.

Chapter 4 evaluates the results derived in chapter 3 and presents formulae of the moment rotation relationships.

Chapter 5 comprises of FEM analyses with the aim to find a model which could simulate the tests performed in the laboratory. This model could then be used for parameter studies of the influence of different parameters on the moment-rotation relationship. However more work needs to be performed to improve the model prior to a FEM parameter study.

Chapter 6 presents a method for predicting the required rotation at an interior support at which a plastic hinge will develop in the sagging moment region.

Chapter 7 deals with problems related to a plastic design method. These are:

- Flange induced buckling (i e a failure mode in which the compressed flange buckles into the web).

- The required distance between lateral bracings in the region ner the internal support where a part of the compressed flange has yielded.

- Requirements in the serviceability state with respect to crackwidths in the concrete slab.

- Effects of imposed deformations from temperature, shrinkage of concrete and settlements of supports.

Chapter 8 points out the advantage of using a plastic design method compared to an elastic method in terms of material savings.

Chapter 9 gives the principles for the procedure when using a plastic design method.

Chapter 10 sums up the findings and the conclusions of this report.

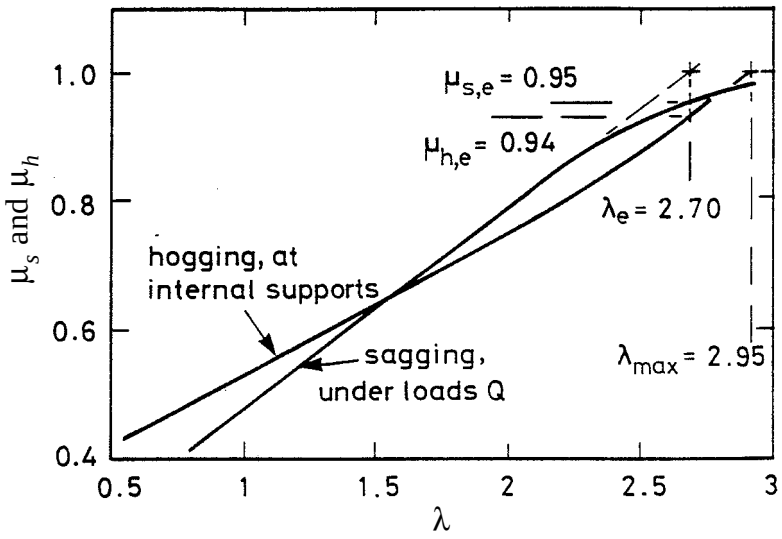

Figure 2.6.2 Redistribution of moments for loadcase (2)

The conclusions from this report is that it is safe to combine elastic global analysis with resistances of sections in sagging bending that are determined by plastic theory, using loads specified in Eurocode 1, Part 3 and in BS5400.

2.6 “Composite Bridge Beams with Mixed-Class Cross-Sections” R.P. Johnson, Dongjie Huang

Johnson and Dongjie Huang have in their report [22] assessed the normal design approach of continuous composite bridges according to BS5400. It consists of using linear-elastic global analysis together with utilizing the plastic resistance in midspan region. In midspan regions the composite section is usually in Class 1 or 2 according to EC3 i.e a compact section. At internal supports the section is often in Class 3 or 4 i.e. slender. The object of the research report was to show whether this approach is safe or not.

The plastic resistance for the section in midspan can exceed the resistance at first yield by 25% or more. The inelastic curvature that develops from using the plastic resistance in midspan is neglected. Hence the hogging moment at the internal support is underestimated.

However since envelopes of the bending moment is used hogging moments are well below their design values under loading that causes maximum sagging moment and vice versa.

The analyses were based on four bridges and it was found that all types of potentially adverse situations could be modelled using only two types of beams, namely two spans with no symmetry and three spans with both load and beam symmetric about the midspan of the centre span. The non-linear analyses were performed using a computer program in which the the loads were applied successively until the bridge failed either by the moment at the internal support reaching the elastic resistance or the sagging moment reaching the plastic resistance. Loading were according to BS5400 and also according to Eurocode 1, Part 3.

An example of one of the analyses performed is loading according to (2) in figure 2.6.1. In Figure 2.21 the result from this loading is presented. Elastic global analysis predicts failure in sagging bending at $\lambda = 2,70$. λ is the value by which the characteristic values of the loads have been multiplied to give failure.The non-linear analysis gives failure in hogging bending at $\lambda = 2,95$. μ_h and μ_s in figure 2.6.2 expresses the ratio of moment to the moment resistance for hogging and sagging moment.

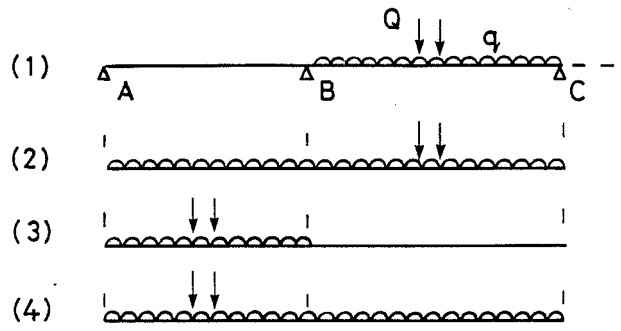

Figure 2.6.1 Loadings analysed in [22].

metrical cross-sections and the third was double-symmetrical.

From the test results, Schilling derived a lower bound relationship for the plastic rotation capacity at various moment levels.

$$\frac{M_e}{M_y} = 2300\theta_p{}^2 - 240\theta_p + 1$$

$$\theta_p \leq 0,04$$

The author proposes two ways of applying this relationship in autostress design for girders that are proportioned at the AASHTO limiting flange and web slenderness ratios, for laterally braced members.

The first concept is to determine the required plastic rotation capacity and corresponding effective plastic moment for a specific girder under consideration.

The second concept is to specify a value of the required plastic rotation capacity, sufficient for all bridges and an effective plastic moment determined from this value.

Schilling states that further study is required before the lower bound relationship can be incorporated into specifications.

2.5 “Plastic Rotation Capacity in Welded Girders” A. Wargsjö

Wargsjö [12] (in Swedish) has assessed the plastic rotation capacity of welded plate girders. Wargsjö tested ten double symmetric plate girders in three point bending tests, with web slenderness varying from $h_w/t_w = 80 - 120$. The flange slenderness was kept constant $b_f/t_f \approx 6,4$. With $f_{yf} = 370\ MPa$ this corresponds to cross section class 1 according to EC3. The length of the girders was also varied. For more detailed information, see table 2.1 and 2.2.

Wargsjö presents a proposal how to predict the moment-rotation relationship as a function of varying web slenderness. Wargsjö proposes following expressions for θ_{fk}:

$$\theta_{fk} = 15 + 60\left(3,2 - \frac{h_w}{t_w}\sqrt{\frac{f_y}{E}}\right) \qquad \text{if} \qquad 2,4 \leq \frac{h_w}{t_w}\sqrt{\frac{f_y}{E}} \leq 3,2$$

$$\theta_{fk} = 15 \qquad \text{if} \qquad 3,2 < \frac{h_w}{t_w}\sqrt{\frac{f_y}{E}} < 4,8$$

The value of the descending slope k_θ of the moment-rotation relationship is set to 7 kNm/mrad, constant for all girders according to Wargsjö.

For the determination of the parameter K_2 an insufficient number of test data with the falling branch of the M - θ_t curve were available so K_2 had to be determined by an trial-and-error method as compared with the results. K_2 was taken as 3.1 K_1 that is $K_2 = 415 - 22,5\lambda_c$.

A parametric study was then performed on a continuous two span beam of uniform section and uniformly distributed loading. The M - θ_t curves derived were then used in the study. The interesting conclusions from the study can be summed up accordingly:

- Increasing the span ratio from 1.0 to 1.25 reduces the design ultimate load. If the span ratio is higher than approximately 1.6, the ultimate design load will be less than that according to Eurocode 4.

- A rigid-plastic global analysis performed on a class 2 section will give an overestimation of the resistance. This confirms the restrictions in Eurocode 4 that a rigid-plastic analysis is not allowed for class 2 sections.

  However design based on rigid-plastic global analysis makes use of the full bending resistance of both hogging and sagging regions of span, which will require some plastic deformation capacity. It should also be emphasised that this study performed by Johnson and Chen only considers uniformly distributed loading which is not the type of loading a bridge is subjected to.

2.4"Moment-Rotation Tests of Steel Bridge Girders." C.G. Schilling

Schilling [9] has tested three laterally braced girders to obtain moment-rotation curves for use in autostress design of continuous-span, non-compact bridge girders. The autostress method is a procedure that extends the limit state criteria as stated in the American bridge code [20]. The improved limit state criteria permit inelastic load redistribution in continuous beam bridges under heavy loads. The autostress method is incorporated in the AASHTO “Guide Specification for Alternate Load-Factor Design Procedures for Steel Beam Bridges Using Braced Compact Sections”.

The flange and web slenderness ratios were close to the limiting AASHTO values for laterally braced, non-compact girders. For a steel with 50 ksi (345 MPa) and double symmetric cross-section, the AASHTO limitations are:

$h_w / t_w = 86$

$b_f / t_f \approx 9,2$

Therefore the girders should be able to reach the yield moment. Each specimen was tested as a simply supported beam with a single load at midspan. Two of the specimens had single-sym-

$$R = \frac{\theta_{p,s}}{\theta_{pe,s}}$$

The maximum elastic curvature $\Phi_{pe,s}$ is related to $\theta_{pe,s}$ by:

$$\Phi_{pe,s} = 2\,(\theta_{pe}/L_c)$$

where

L_C = Length of cantilever.

If the inelastic rotation $\theta_{p,s}$ is assumed to result from an inelastic curvature $\Phi_{p,s}$, constant over a length of h/2 adjacent to a support, K_1 can be expressed as:

$$K_1 = \frac{L_c}{h}R$$

The authors claimed that since the test data were too few to enable an expression for K_1 as a function of both the compression flange and the web, they instead used a combined slenderness λ_c based on the definitions for slenderness in Eurocodes 3 and 4.

$$\lambda_c = \sqrt{\frac{\alpha d 3 A_w}{t_w \varepsilon A} \cdot \frac{c 3 A_f}{t_f \varepsilon A}}$$

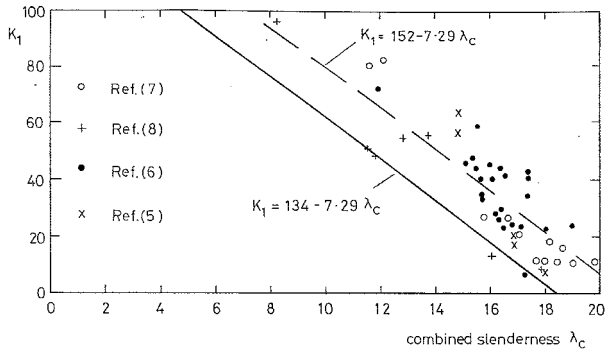

Fig. 2.3.3 K_1 as a function of λ_c.

where

$\varepsilon = \sqrt{235/f_y}$

λ_c express the geometric mean of the slenderness of the web (left part of expression) and flange (right part). From the tests, K_1 was estimated to $K_1 = 134 - 7,29\lambda_c$.

2.3 "Local Buckling and Moment Redistribution in Class 2 Composite Beams." R.P. Johnson, S. Chen

Johnson and Chen [6] has derived moment-curvature curves based on experimental results. These curves have then been used in a parametric study of failure loads for two span beams with distributed loading. The cross sections were of class 2 according to EC4 and for the structural steel a trilinear stress-strain curve was used.

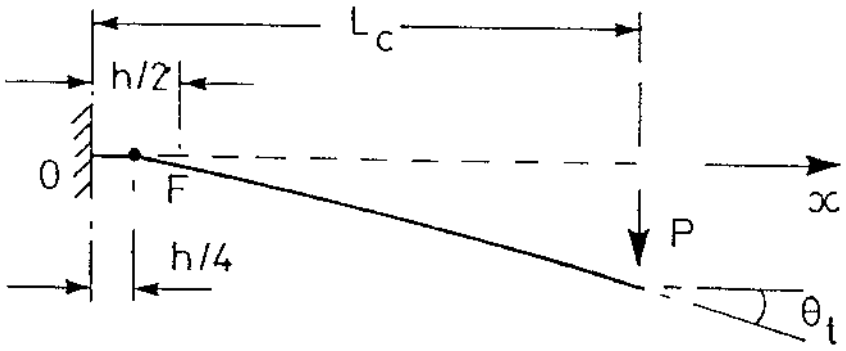

Fig. 2.3.1 Composite cantilever with local buckling at x=h/4.

The effect of local buckling was modelled by replacing the portion AB by ACD defined by the parameters K_1 and K_2.

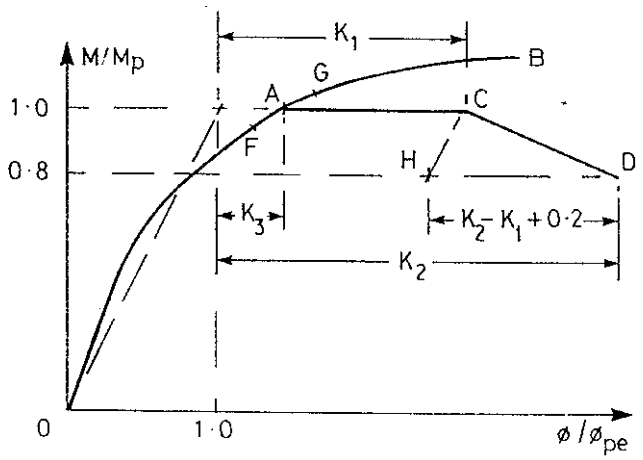

Fig. 2.3.2 Moment-curvature curve in hogging bending.

with rotation capacity R defined by:

It should be noted that Spangemacher used true $\sigma - \varepsilon$ diagram as input to the FEM-analyses, see appendix D, figure D5. By FEM parameter studies, Spangemacher presents the influence of:

- Variation in span length, appendix D, figure D6

- Flange thickness and flange width, appendix D, figure D8

- b_{fl}/t_f ratio, appendix D, figure D10

- Stiffness of the web, appendix D, figure D12

- Steel quality, appendix D, figure D14

From the tests and FEM-analyses, Spangemacher presents a formula for the rotation capacities, according to figure 2.2.3, where K_ϑ is a parameter that expresses the influence of the web as a torsion spring according to Lay.

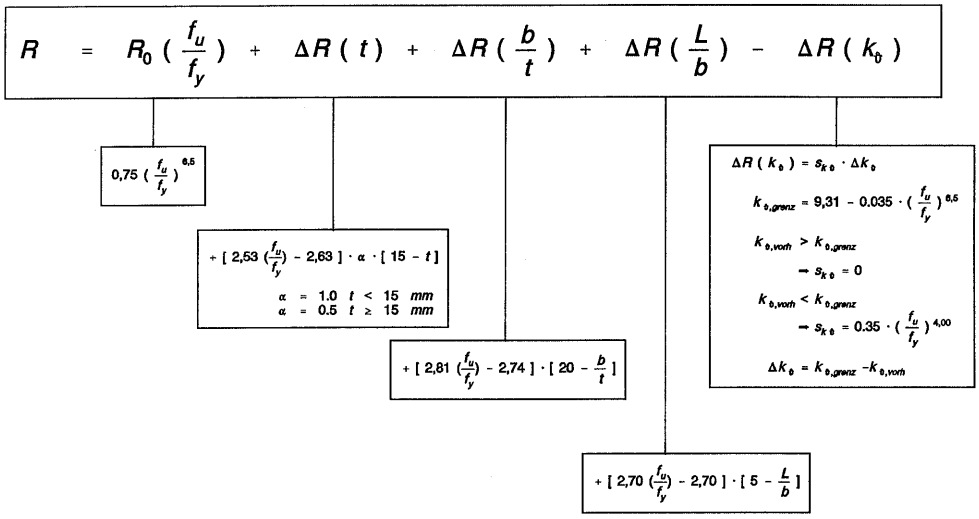

Figure 2.2.3 Rotation capacity according to Spangemacher.

Spangemacher also gives examples of structures that are not suitable for plastic hinge theory. Classical examples are systems that from geometry and loading require a high rotation capacity. These are:

- Continuous beams with extreme difference in span lengths, cross-section properties and loading conditions.

- Frames with extreme ratios of the lengths of vertical and horizontal members.

- Systems with concentrated load near supports.

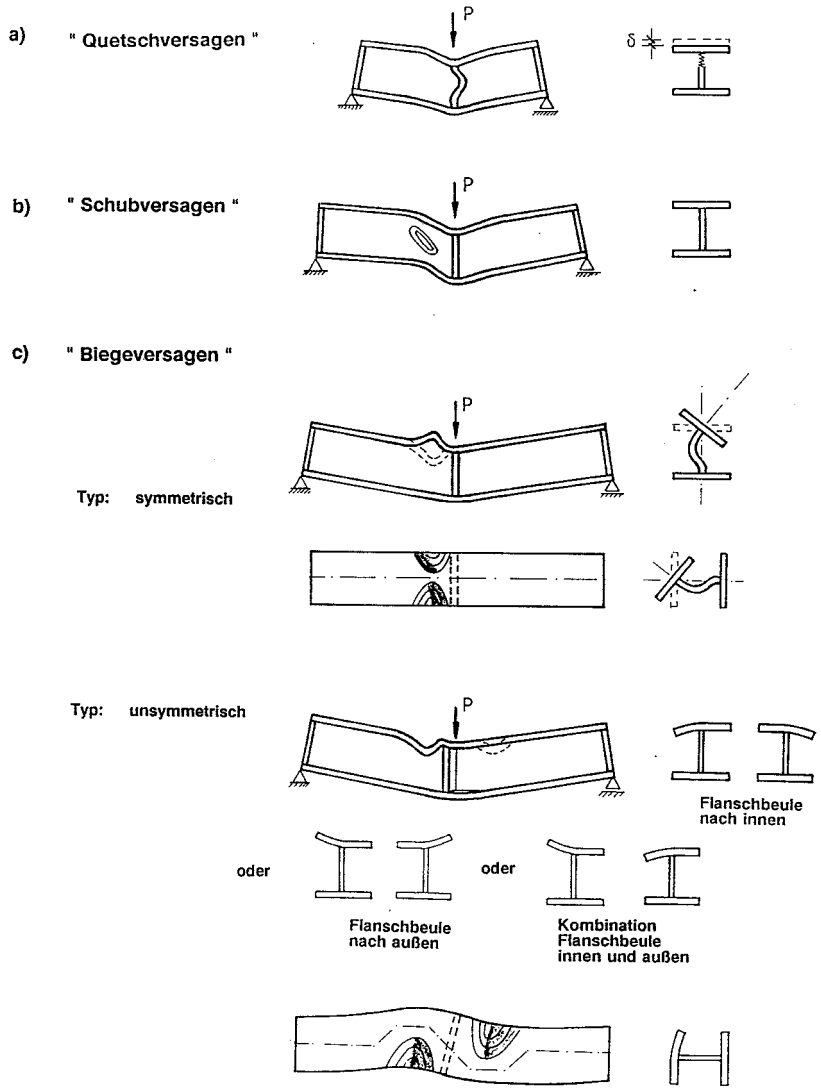

Figure 2.2.2 Different types of failure modes according to Spangemacher.

Spangemacher used the results from the tests to calibrate FEM-analyses and then used a model of reference beams from which he varied the following parameters:

- Length of half span 0.5 - 2.5 m

- Thickness of flange 7.5 - 20 mm

- Thickness of web 5 - 12.5 mm

- b_{fl}/t_f ratio of flange 12.5 - 25.0

- h/w ratio 25.0 - 100.0

- Steel quality St37 - StE690

to Spangemacher that while R is constant for the span over depth ratio, different steel qualities and the position of a concentrated load, ϑ is linear varying. This is presented in diagrams in appendix D, figures D1, D2 and D3. ϑ_{erf} can be determined by use of the principle of virtual work together with methods to locate the last plastic hinge to form.

Spangemacher has compiled some previous tests on beams with respect to rotation capacity and plotted them in a diagram as a function of $b/t \cdot \sqrt{f_y/235}$, according to appendix D, figure D4. The diagram shows clearly that the rotation capacity does not depend on the $b/t \cdot \sqrt{f_y/235}$ parameter only.

To determine the rotation capacity R_{vorh} both laboratory tests on beams and FEM-analyses were performed. A total of 30 beams were tested of which 26 were rolled profiles and four plate girders. The flange slenderness b_{fl}/t_f varied from 13.4 to 22.3 and h_w/t_w from 18.8 to35.0. For all beams the yield strength of the steel varied from 275 to 540 MPa except for the plate girders where a maximum yield strength of 990 MPa was reported.

The tested beams were simply supported with a concentrated load at midspan. Spangemacher reports three types of failure modes that can be expected, assuming the beam is laterally braced. These failure modes are presented in figure 2.2.2 and are:

- Web crippling (flange induced buckling)

- Shear failure

- Bending failure

2.2 “Zum Rotationsnachweis von Stahlkonstruktionen, die nach dem Traglastverfahren berechnet werden.” R. Spangemacher

Spangemacher [11] has in his research work assessed the rotation capacity of plastic hinges for I-shaped beams. The scope of this work consisted of:

- The influence of b_f/t_f ratios on the rotation capacity.

- The rotation requirements in typical steel structures.

- Tests on steel beams and numerical analyses.

- Numerical analyses of the rotation capacitites in order to discover limitations in the plastic hinge theory.

Spangemachers aim was to include class 2 members (EC3) into plastic hinge theory. The required rotation is defined through a parameter R_{erf}.

$$R_{erf} = \frac{\varphi_{erf} - \varphi_{pl}}{\varphi_{pl}}$$

and the rotation capacity of the structure as R_{vorh}.

$$R_{vorh} = \frac{\varphi_{rot} - \varphi_{pl}}{\varphi_{pl}}$$

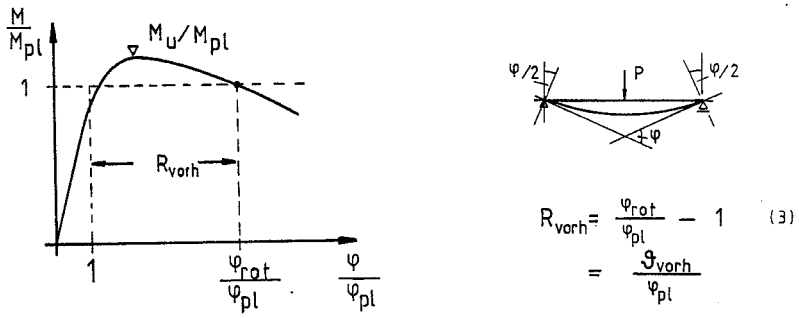

Figure 2.2.1 Explanations of φ_{rot} , φ_{pl} and R_{vorh}

The requirement is then

$$R_{erf} \leq \frac{R_{vorh}}{\gamma_m}$$

The advantage of using the parameter R_{erf} instead of the angle $\vartheta_{erf} = \varphi_{erf} - \varphi_{pl}$ is according

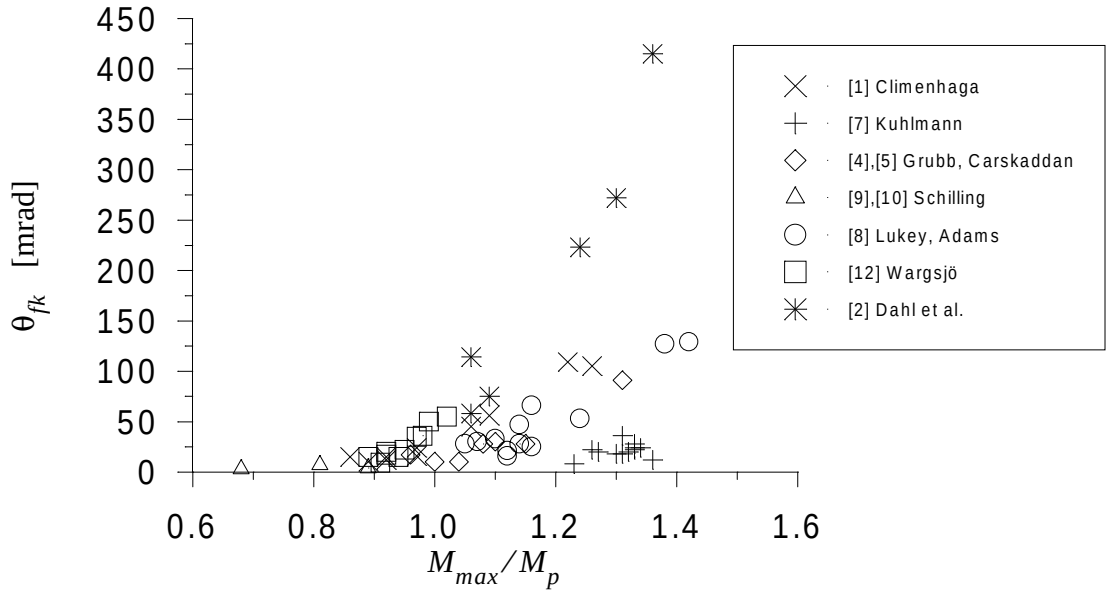

Figure 2.1.14 $\theta_{fk} - M_{max}/M_p$ *diagram*

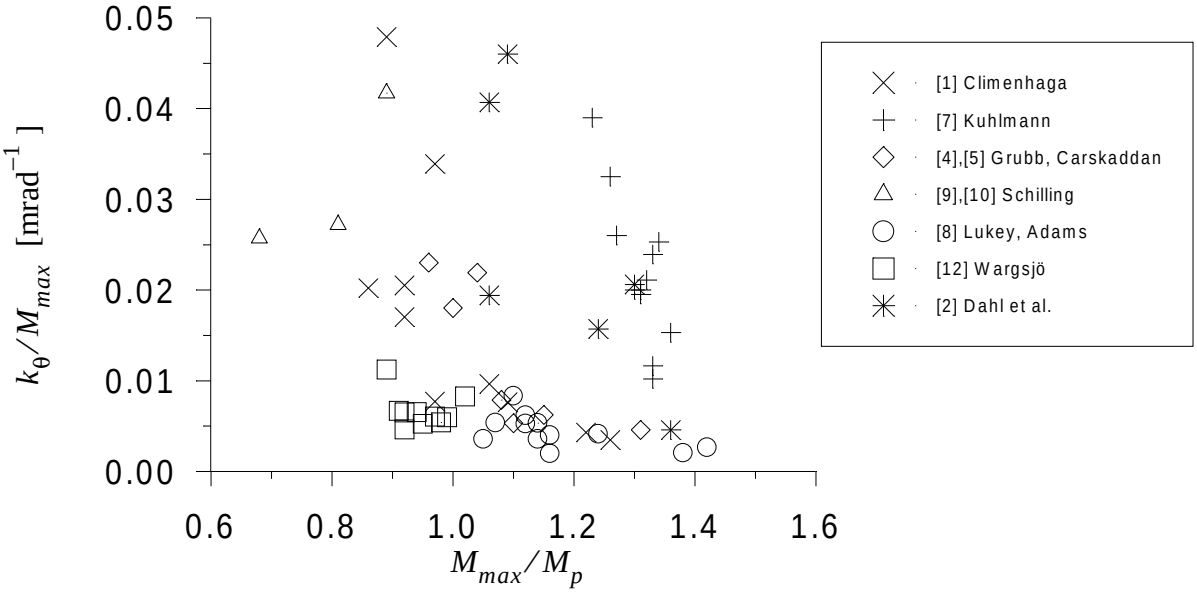

Figure 2.1.15 $k_\theta/M_{max} - M_{max}/M_p$ *diagram*

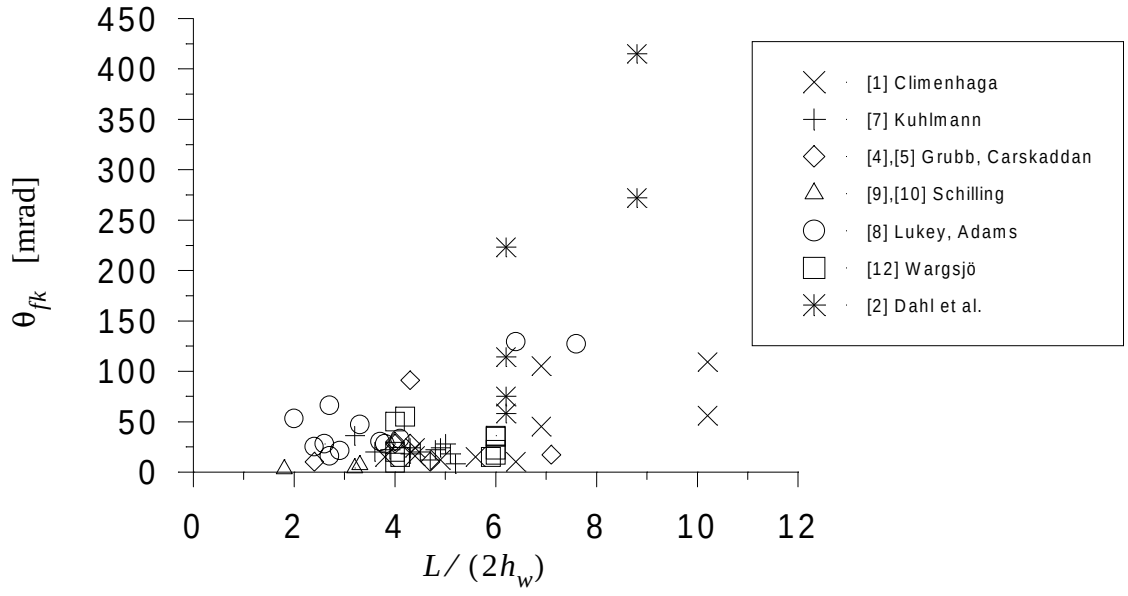

Figure 2.1.12 $\theta_{fk} - L/(2h_w)$ *diagram*

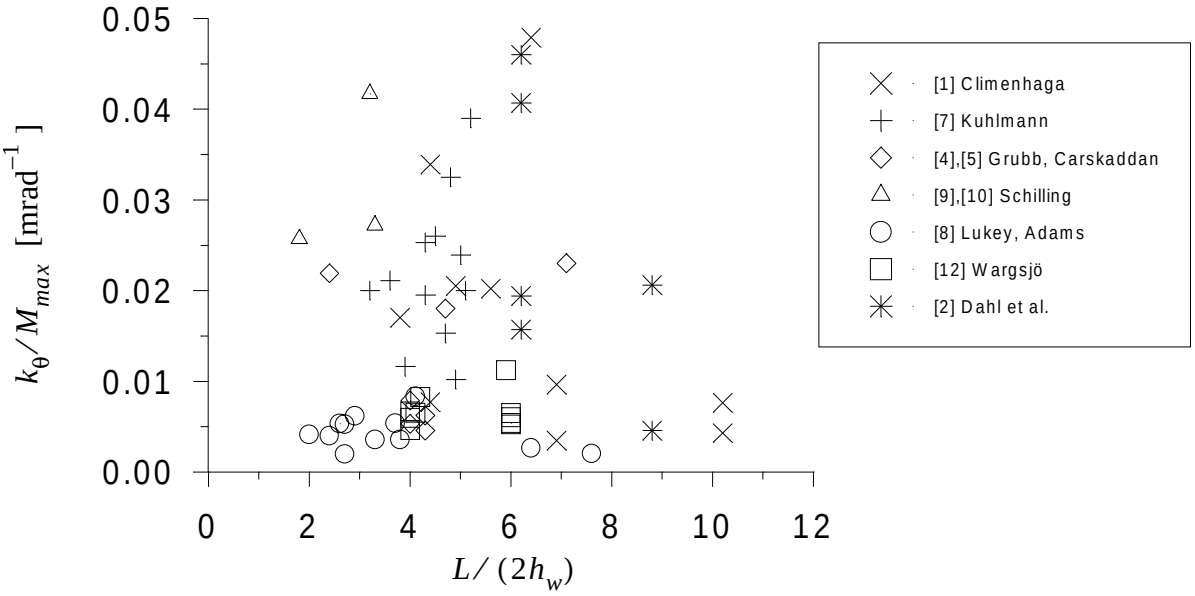

Figure 2.1.13 $k_\theta / M_{max} - L/(2h_w)$ *diagram*

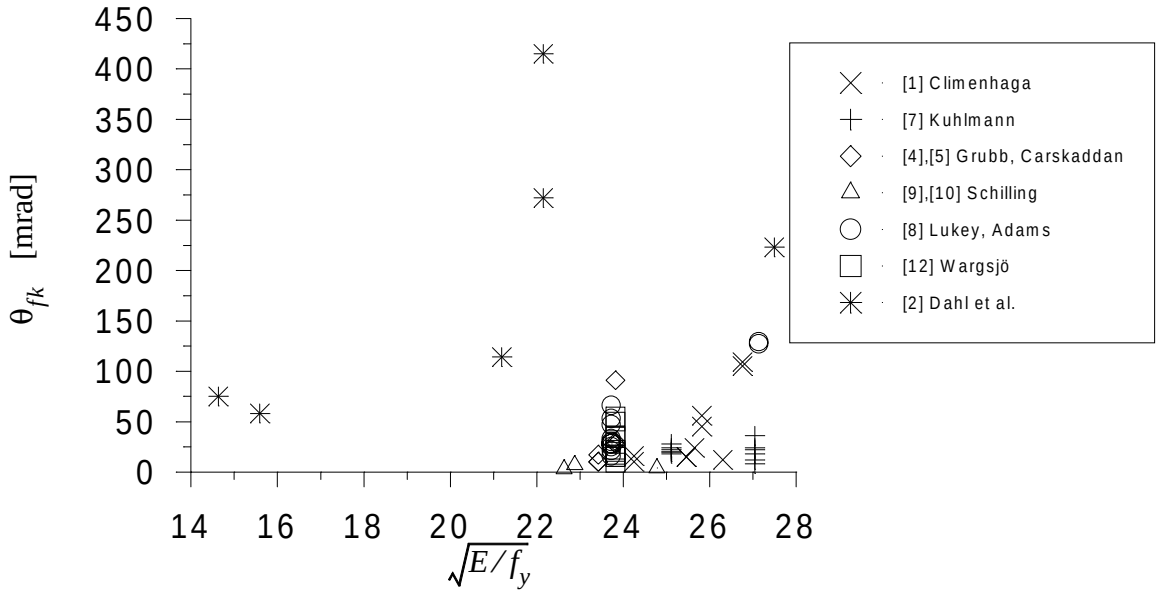

Figure 2.1.10 $\theta_{fk} - \sqrt{E/f_y}$ *diagram*

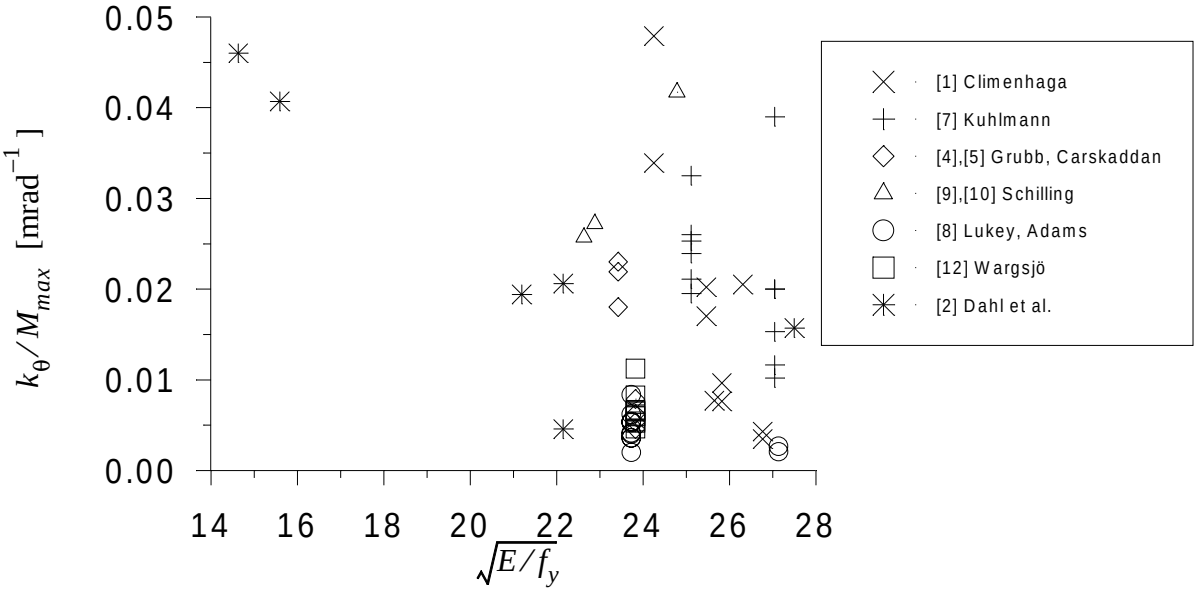

Figure 2.1.11 $k_\theta / M_{max} - \sqrt{E/f_y}$ *diagram*

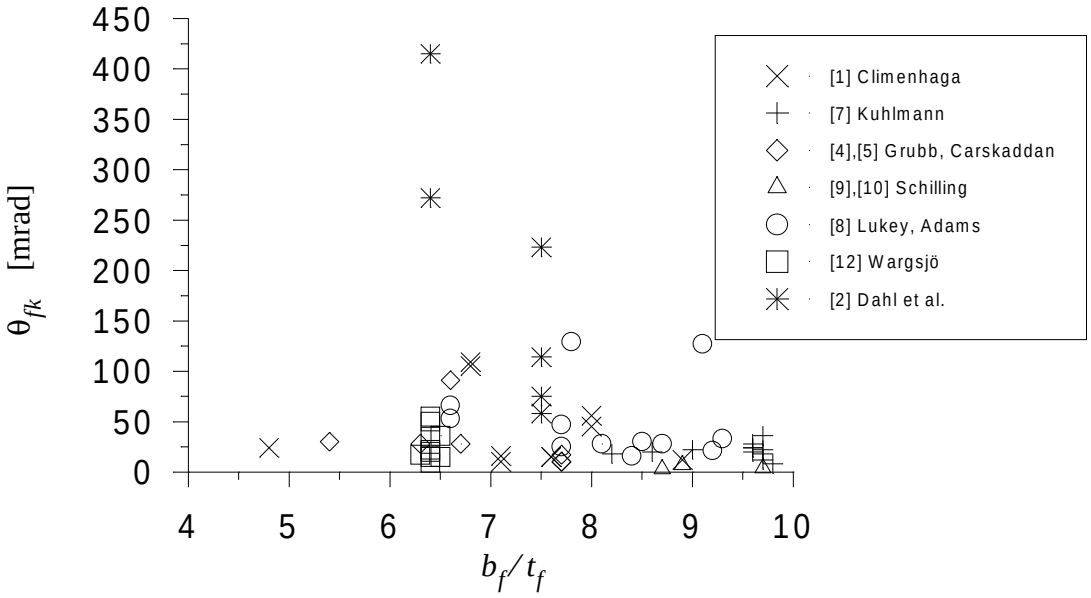

Figure 2.1.8 $\theta_{fk} - b_f/t_f$ *diagram*

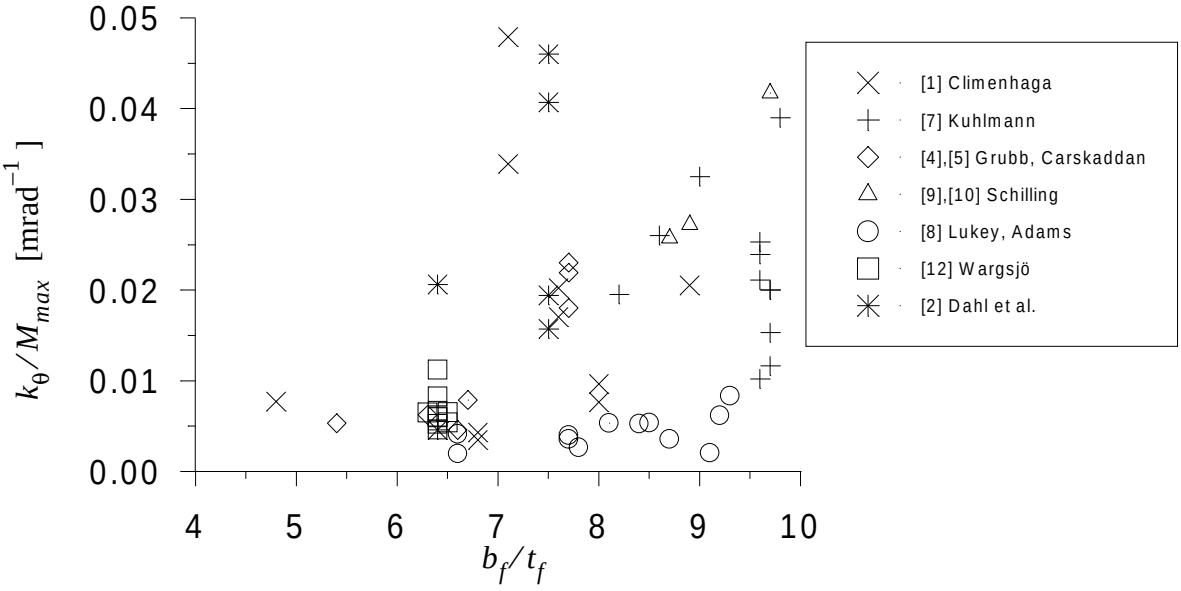

Figure 2.1.9 $k_\theta/M_{max} - b_f/t_f$ *diagram*

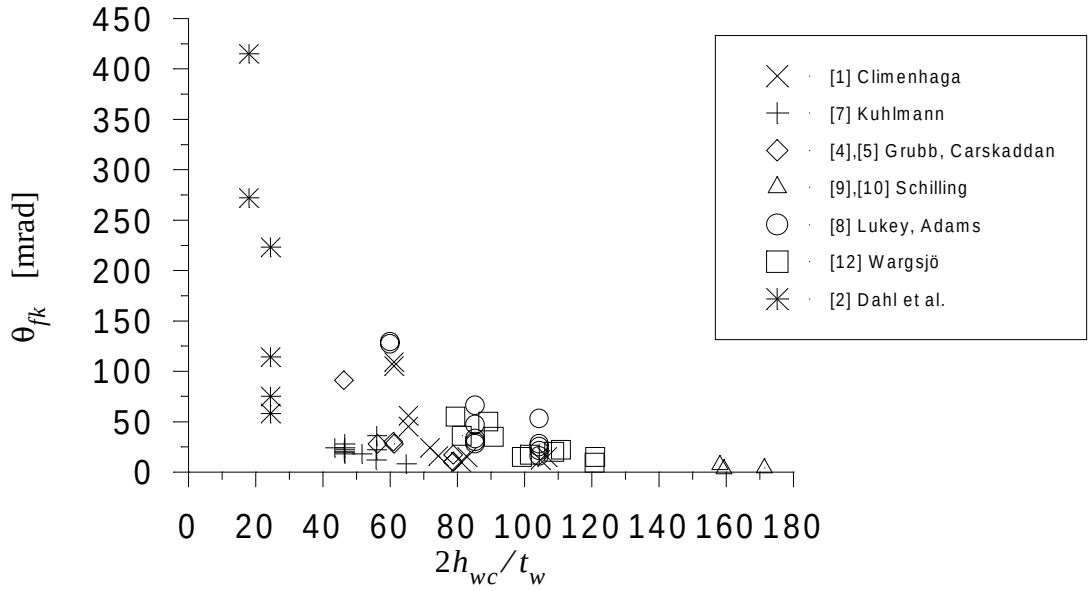

Figure 2.1.6 $\theta_{fk} - 2h_{wc}/t_w$ *diagram*

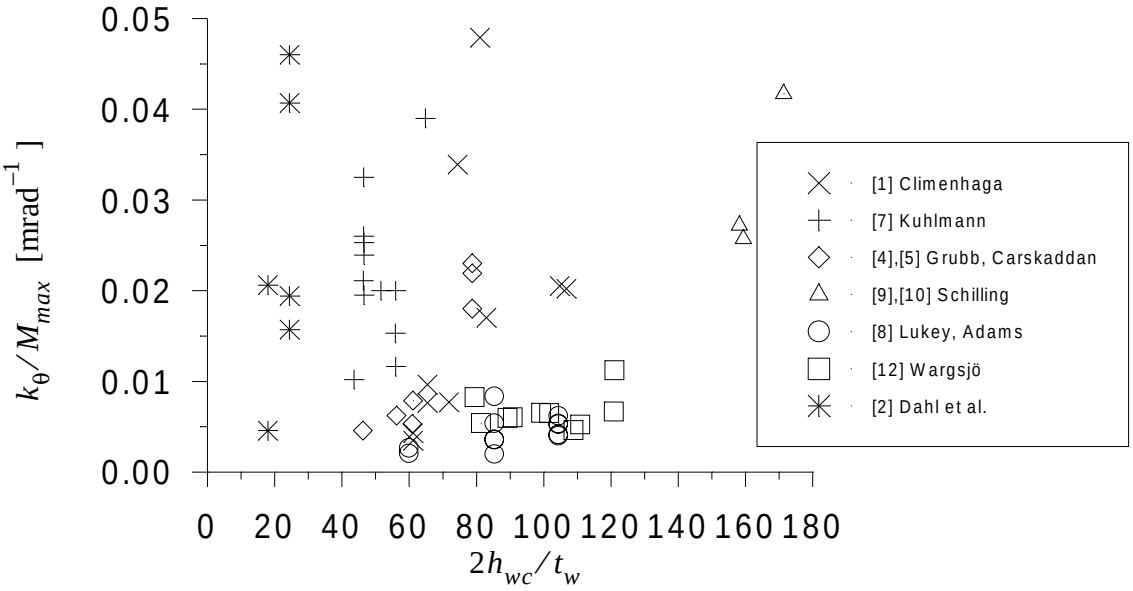

Figure 2.1.7 $k_\theta/M_{max} - 2h_{wc}/t_w$ *diagram*

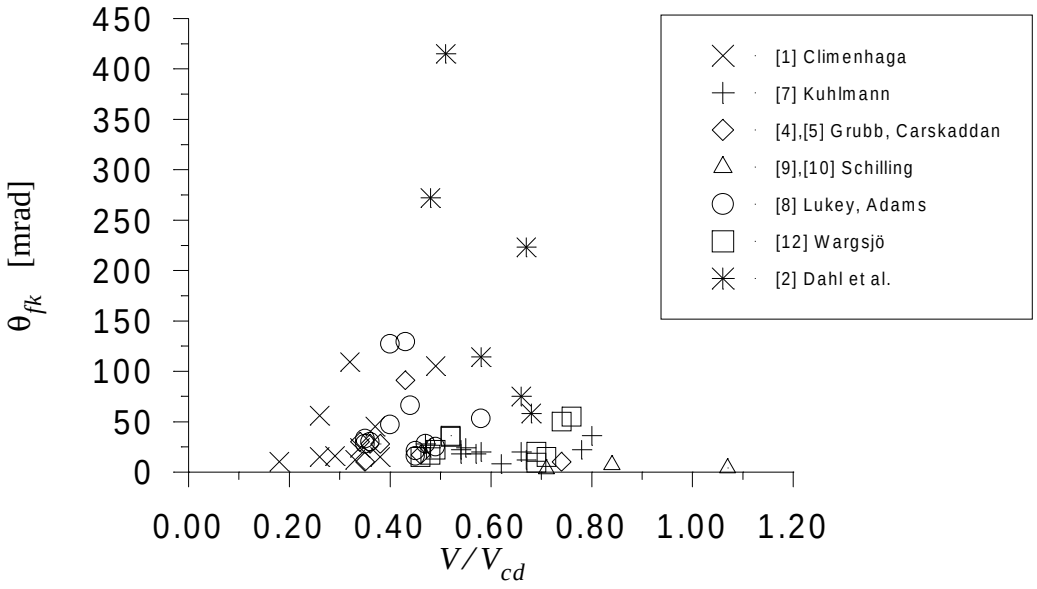

Figure 2.1.4 $\theta_{fk} - V/V_{cd}$ *diagram*

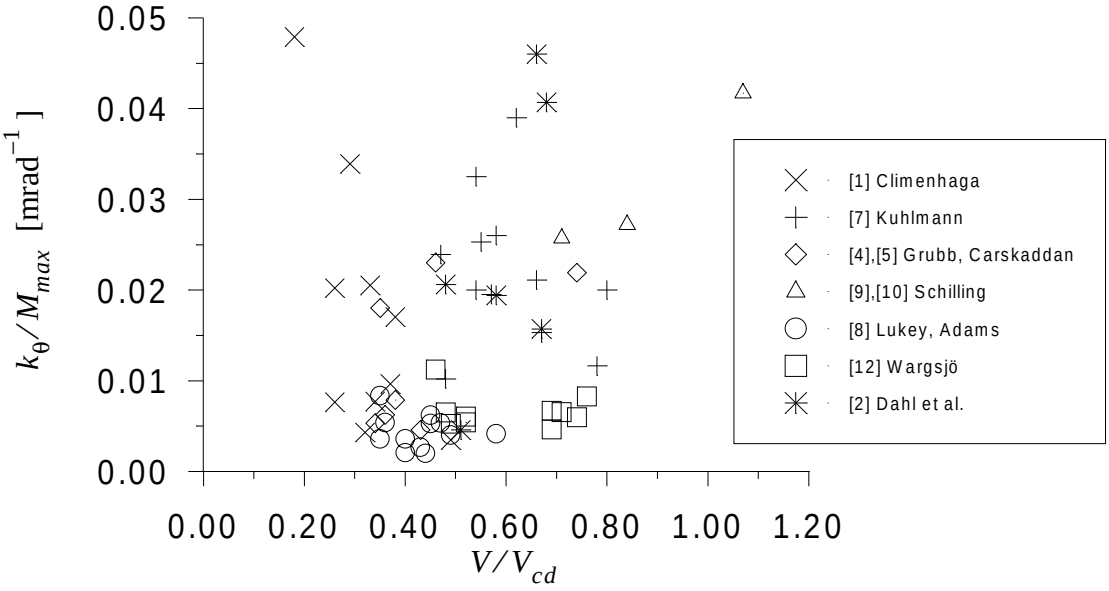

Figure 2.1.5 $k_\theta / M_{max} - V/V_{cd}$ *diagram*

Table 2.1.2 Test results from literature survey

Ref.	Test	$\frac{2h_{wc}}{t_w}$	$\frac{b_f}{t_f}$	$\sqrt{\frac{E}{f_y}}$	$\frac{L}{2h_w}$	$\frac{V_{max}}{V_{cd}}$	$\frac{M_{max}}{M_p}$	θ_{fk} $[mrad]$	k_θ / M_{max} $[mrad^{-1}]$
	B-3	85.3	7.7	23.7	3.31	0.40	1.14	47	$3,57 \cdot 10^{-3}$
	B-4	85.3	8.5	23.7	3.68	0.36	1.07	30	$5,36 \cdot 10^{-3}$
	B-5	85.3	8.7	23.7	3.82	0.35	1.05	28	$3,57 \cdot 10^{-3}$
	C-1	104.4	9.2	23.7	2.86	0.45	1.12	21	$6,17 \cdot 10^{-3}$
	C-2	104.4	6.6	23.7	2.00	0.58	1.24	53	$4,11 \cdot 10^{-3}$
	C-3	104.4	7.7	23.7	2.43	0.49	1.16	25	$4,00 \cdot 10^{-3}$
	C-4	104.4	8.4	23.7	2.70	0.45	1.12	16	$5,26 \cdot 10^{-3}$
	C-5	104.4	8.1	23.7	2.58	0.47	1.14	28	$5,33 \cdot 10^{-3}$
[12]	1A	120.8	6.4	23.8	3.97	0.69	0.91	9	$6,67 \cdot 10^{-3}$
	1B	121.0	6.4	23.8	5.94	0.46	0.89	15	$11,2 \cdot 10^{-3}$
	2A	108.8	6.4	23.8	4.03	0.69	0.92	20	$4,63 \cdot 10^{-3}$
	2B	110.8	6.4	23.8	6.02	0.49	0.95	22	$5,24 \cdot 10^{-3}$
	3A	99.2	6.5	23.8	4.08	0.71	0.94	15	$6,52 \cdot 10^{-3}$
	3B	101.6	6.3	23.8	5.97	0.48	0.92	17	$6,49 \cdot 10^{-3}$
	4A	89.2	6.4	23.8	4.05	0.74	0.99	50	$5,96 \cdot 10^{-3}$
	4B	90.8	6.4	23.8	6.00	0.52	0.97	35	$6,05 \cdot 10^{-3}$
	5A	79.4	6.4	23.8	4.15	0.76	1.02	55	$8,25 \cdot 10^{-3}$
	5B	81.3	6.5	23.8	6.01	0.52	0.98	36	$5,38 \cdot 10^{-3}$
[2]	EB20D33	17.9	6.4	22.2	8.82	0.51	1.36	415	$4,57 \cdot 10^{-3}$
	D3-CRM	17.9	6.4	22.2	8.82	0.48	1.30	272	$20,6 \cdot 10^{-3}$
	ETB2883	24.4	7.5	14.6	6.15	0.66	1.09	75	$46,0 \cdot 10^{-3}$
	ETB2863	24.4	7.5	15.6	6.15	0.68	1.06	58	$40,7 \cdot 10^{-3}$
	ETB2843	24.4	7.5	21.2	6.15	0.58	1.06	114	$19,4 \cdot 10^{-3}$
	ETB2833	24.4	7.5	27.5	6.15	0.67	1.24	223	$15,7 \cdot 10^{-3}$

It should be noted that the values of θ_{fk} and k_θ are based on measurements in diagrams and that their definition is a bit subjective.

Table 2.1.2 Test results from literature survey

Ref.	Test	$\frac{2h_{wc}}{t_w}$	$\frac{b_f}{t_f}$	$\sqrt{\frac{E}{f_y}}$	$\frac{L}{2h_w}$	$\frac{V_{max}}{V_{cd}}$	$\frac{M_{max}}{M_p}$	θ_{fk} $[mrad]$	k_θ / M_{max} $[mrad^{-1}]$
	SB9	61.1	6.8	26.8	6.9	0.49	1.26	105	$3,47 \cdot 10^{-3}$
	SB10	74.3	7.1	24.2	4.4	0.29	0.97	16	$33,9 \cdot 10^{-3}$
	SB11	82.9	7.6	25.5	3.8	0.38	0.92	15	$17,0 \cdot 10^{-3}$
	SB14	71.8	4.8	25.6	4.4	0.34	0.97	24	$7,69 \cdot 10^{-3}$
[7]	4	43.5	9.6	27.0	4.9	0.48	1.33	24	$10,2 \cdot 10^{-3}$
	5	51.6	9.7	27.0	5.1	0.54	1.30	18	$20,0 \cdot 10^{-3}$
	6	64.8	9.8	27.0	5.2	0.62	1.23	8	$39,0 \cdot 10^{-3}$
	7	56.0	9.7	27.0	3.2	0.80	1.31	36	$20,0 \cdot 10^{-3}$
	8	56.0	9.7	27.0	3.9	0.78	1.33	22	$11,6 \cdot 10^{-3}$
	9	55.8	9.7	27.0	4.7	0.67	1.36	12	$15,3 \cdot 10^{-3}$
	19	46.3	9.6	25.1	3.6	0.66	1.32	20	$21,1 \cdot 10^{-3}$
	20	46.5	9.6	25.1	4.3	0.55	1.34	24	$25,3 \cdot 10^{-3}$
	21	46.5	9.6	25.1	5.0	0.47	1.33	28	$23,9 \cdot 10^{-3}$
	22	46.5	8.2	25.1	4.3	0.57	1.31	18	$19,5 \cdot 10^{-3}$
	23	46.4	8.6	25.1	4.5	0.58	1.27	20	$26,0 \cdot 10^{-3}$
	24	46.4	9.0	25.1	4.8	0.54	1.26	22	$32,5 \cdot 10^{-3}$
[4],[5]	188-3-1	78.7	7.7	23.4	2.36	0.74	1.04	10	$21,9 \cdot 10^{-3}$
	188-3-2	78.7	7.7	23.4	4.72	0.35	1.00	10	$18,0 \cdot 10^{-3}$
	188-3-3	78.7	7.7	23.4	7.08	0.46	0.96	17	$23,0 \cdot 10^{-3}$
	188-3-5	46.2	6.6	23.8	4.25	0.43	1.31	91	$4,57 \cdot 10^{-3}$
	188-3-6	56.2	6.3	23.8	4.33	0.36	1.15	28	$6,22 \cdot 10^{-3}$
	188-3-7	60.9	5.4	23.8	3.99	0.34	1.10	30	$5,31 \cdot 10^{-3}$
	188-3-8	61.1	6.7	23.8	3.96	0.38	1.08	28	$7,86 \cdot 10^{-3}$
[9],[10]	US	159.4	8.6	22.6	1.79	0.71	0.68	3	$25,7 \cdot 10^{-3}$
	UL	158.2	8.9	22.9	3.32	0.84	0.81	7	$27,2 \cdot 10^{-3}$
	SL	171.4	9.7	24.8	3.17	1.07	0.89	4	$41,7 \cdot 10^{-3}$
[8]	A-1	59.9	9.1	27.1	7.60	0.40	1.38	127	$2,02 \cdot 10^{-3}$
	A-2	59.9	7.8	27.1	6.44	0.43	1.42	129	$2,64 \cdot 10^{-3}$
	B-1	85.3	9.3	23.7	4.10	0.35	1.10	33	$8,33 \cdot 10^{-3}$
	B-2	85.3	6.6	23.7	2.73	0.44	1.16	66	$1,96 \cdot 10^{-3}$

Table 2.1.1 Test results from literature survey

Ref.	Test	h_w [mm]	t_w [mm]	b_{fl} [mm]	t_f [mm]	f_{yf}/f_{yw} [MPa]	L [mm]	V_{max} [kN]	M_{max} [kNm]
	C-5	240	4.6	90	5.3	373/352	1240	121	75
[12]	1A	481	4.0	131	9.9	370/335	3820	149	285
	1B	482	4.0	130	9.9	370/335	5720	97	276
	2A	437	4.0	131	10.0	370/335	3520	147	259
	2B	439	4.0	131	9.9	370/335	5280	101	267
	3A	395	4.0	132	9.8	370/335	3220	143	230
	3B	402	4.0	130	10.0	370/335	4800	96	231
	4A	360	4.0	131	9.9	370/335	2920	149	218
	4B	360	4.0	131	9.9	370/335	4320	100	215
	5A	316	4.0	131	10.0	370/335	2620	148	194
	5B	320	3.9	131	9.8	370/335	3840	97	186
[2]	EB20D33	170	9.5	202	15	428/456	3000	233	350
	D3-CRM	170	9.5	202	15	428/456	3000	252	378
	ETB2883	244	10	280	18	982/984	3000	1053	1579
	ETB2863	244	10	280	18	864/813	3000	899	1348
	ETB2843	244	10	280	18	468/536	3000	509	764
	ETB2833	244	10	280	18	278/323	3000	353	530

Table 2.1.2 Test results from literature survey

Ref.	Test	$\frac{2h_{wc}}{t_w}$	$\frac{b_f}{t_f}$	$\sqrt{\frac{E}{f_y}}$	$\frac{L}{2h_w}$	$\frac{V_{max}}{V_{cd}}$	$\frac{M_{max}}{M_p}$	θ_{fk} $[mrad]$	k_θ/M_{max} $[mrad^{-1}]$
[1]	SB2	65.4	8.0	25.8	10.2	0.26	1.09	56	$7,63 \cdot 10^{-3}$
	SB3	61.1	6.8	26.8	10.2	0.32	1.22	109	$4,29 \cdot 10^{-3}$
	SB4	81.0	7.1	24.2	6.4	0.18	0.89	10	$47,9 \cdot 10^{-3}$
	SB5	106.7	7.6	25.5	5.6	0.26	0.86	15	$20,2 \cdot 10^{-3}$
	SB6	104.7	8.9	26.3	4.9	0.33	0.92	12	$20,5 \cdot 10^{-3}$
	SB8	65.4	8.0	25.8	6.9	0.37	1.06	45	$9,65 \cdot 10^{-3}$

Table 2.1.1 Test results from literature survey

Ref.	Test	h_w [mm]	t_w [mm]	b_{fl} [mm]	t_f [mm]	f_{yf}/f_{yw} [MPa]	L [mm]	V_{max} [kN]	M_{max} [kNm]
	6	259	4	160	8	287/259	2716	104	141
	7	280	5	160	8	287/252	1796	189	170
	8	280	5	160	8	287/252	2196	158	173
	9	279	5	160	8	287/252	2598	136	177
	19	278	6	160	10	333/349	2000	256	256
	20	279	6	160	10	333/349	2402	217	261
	21	279	6	160	10	333/349	2804	185	259
	22	279	6	170	10	333/349	2406	222	267
	23	278	6	183	10.3	333/349	2500	225	281
	24	279	6	190	10.2	333/349	2700	212	286
[4],[5]	188-3-1	387	6.7	156	9.7	383/345	1828	429	392
	188-3-2	387	6.7	156	9.7	383/345	3658	200	366
	188-3-3	387	6.7	156	9.7	383/345	5486	265	726
	188-3-5	286	8.3	157	11.2	370/337	2438	305	372
	188-3-6	352	8.4	150	11.2	370/337	3048	274	418
	188-3-7	382	8.4	130	11.2	370/337	3048	272	414
	188-3-8	385	8.4	158	11.2	370/337	3048	301	458
[9],[10]	US	597	5.3	127	7.0	410/450	2134	353	377
	UL	597	5.3	229	12.5	401/450	3962	422	836
	SL	914	5.3	311	15.7	342/450	5791	596	1726
[8]	A-1	229	7.6	203	10.8	285/309	3480	143	248
	A-2	229	7.6	176	10.8	285/309	2946	154	227
	B-1	190	4.4	103	5.3	373/396	1554	77	60
	B-2	190	4.4	74	5.3	373/396	1036	98	51
	B-3	190	4.4	86	5.3	373/396	1254	89	56
	B-4	190	4.4	94	5.3	373/396	1396	80	56
	B-5	190	4.4	97	5.3	373/396	1448	77	56
	C-1	240	4.6	102	5.3	373/352	1372	118	81
	C-2	240	4.6	74	5.3	373/352	960	152	73
	C-3	240	4.6	86	5.3	373/352	1168	128	75
	C-4	240	4.6	93	5.3	373/352	1296	117	76

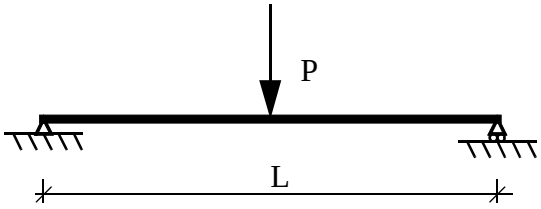

Figure 2.1.2 Test setup of tested beams in literature survey

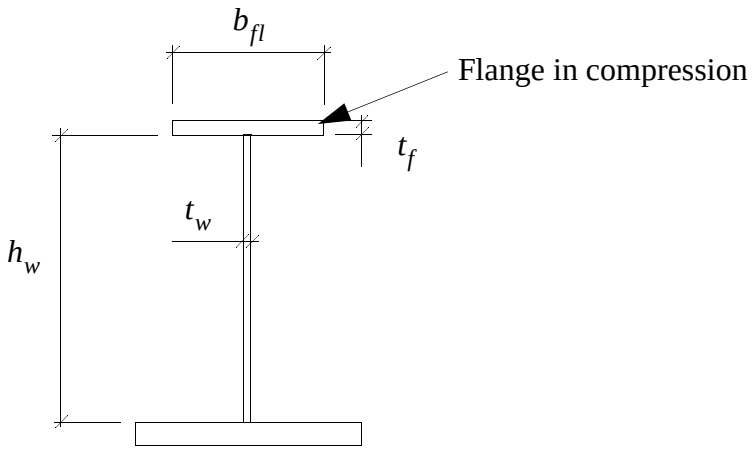

Figure 2.1.3 Notation used in table 2.1.1

Table 2.1.1 Test results from literature survey

Ref.	Test	h_w [mm]	t_w [mm]	b_{fl} [mm]	t_f [mm]	f_{yf}/f_{yw} [MPa]	L [mm]	V_{max} [kN]	M_{max} [kNm]
[1]	SB2	185	5.7	135	8.0	315/344	3912	62	118
	SB3	185	6.0	134	9.5	293/310	3912	74	140
	SB4	292	6.0	104	6.9	357/412	3912	88	167
	SB5	336	6.0	128	8.0	324/363	3912	117	218
	SB6	383	6.2	141	7.6	303/379	3912	162	292
	SB8	185	5.7	135	8.0	315/344	2692	89	114
	SB9	185	6.0	134	9.5	293/310	2692	114	144
	SB10	292	6.0	104	6.9	357/412	2692	139	174
	SB11	336	6.0	128	8.0	324/363	2692	167	212
	SB14	288	6.2	105	10.3	319/384	2692	155	195
[7]	4	261	6	160	8	287/260	2540	131	166
	5	258	5	160	8	287/252	2636	118	155

2 Literature survey

2.1 Test results from literature survey

This literature survey consists of compiled references from which the rotation capacity θ_{fk} and the slope of the descending part of the moment-rotation curve k_θ can be calculated. Several more papers were found by the survey but were excluded in this chapter due to the fact that they did not present complete test results.

The rotation capacity is presented in table 2.1.1 below and a definition of the rotation capacity θ_{fk} is given i figure 2.1.1. In addition, five recent papers have been reviewed to give an idea of the state of the art in this field.

Following table 2.1.1 are diagrams in which θ_{fk} and k_θ are plotted against the parameters presented in table 2.1.1.

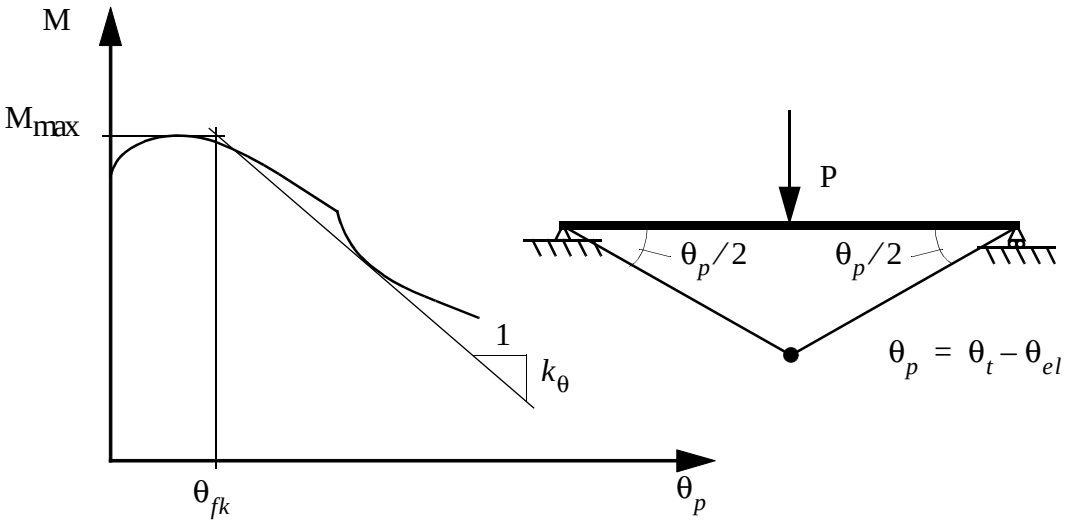

Figure 2.1.1 Definition of rotation capacity θ_{fk}.

Table 2.1.1 and 2.1.2 presents a total of 60 tests of rolled or welded steel beams found from the literature survey. These were both of double and single symmetrical cross-sections. b_f/t_f in table 2.1.2 is the dimensions of the compressed flange for a single symmetrical cross-section. There were also sometimes extra plates welded to one flange, to simulate the influence of a concrete slab. The tests were all performed as three point bending tests i.e. the beams were subjected to a concentrated load at midspan, see figure 2.1.2.

influence on the results. The slope should probably be steeper than the results imply.

Girders A7 and A8 were the most "stocky" girders of all. Girder A7 shows a very large moment-rotation capacity while A8 is surprisingly low taking into account the low h_w/t_w ratio of the web.

Another observation from the moment-rotation curves for varying slenderness of the web is that for increasing slenderness, the descending branch of the curve is not linear but a sudden drop in moment appers as the rotation increases. The boundary between a linear and a non-linear descending branch seems to be at A3 and A4. This phenomenon is due to the fact that the flange buckles down into the web (flange induced buckling) instead of showing an asymmetrical buckled shape of the flange. This behaviour has to be assessed more carefully so that it can be predicted as this has a negative influence of the moment-rotation capacity for the girder.

Another parameter that influences the moment-rotation relationship is the flange slenderness. Girders A3, B3 and B4 have identical geometries except for the flanges. The flange thickness for all girders are 12 mm while the width is 120, 150 and 180 mm respectively. This is equal to a flange slenderness of 10, 12.5 and 15. Comparing the moment-rotation curves for these girders one notices that the descending branch of these tests are parallel but that the curves start dropping earlier for more slender flanges.

The third parameter that has been studied in the laboratory tests are the influence of the length of the girders. Four girders, B5, B2, A3 and B1 had the same geometry except for their lengths, which was 2660, 3500, 5000 and 6000 mm respectively. Comparing the moment-rotation curves for these girders it can be seen that B5, which was the shortest of these girders, shows the least favourable moment-rotation relationship. B5 did however fail in shear. All the other girders tested failed in bending. This implies that shear failure is not a desireable failure.

Comparing B2, A3 and B1 they are fairly similar in appearance until they reach approximately $0.8M_{max}$ on the descending branch. Then suddenly both B1 and B2 lose their moment capacity wery rapidly with increasing rotation. This is due to the fact that the flange buckles down into the web. There is no obvious pattern when comparing B2, A3 and B1 as far as the length is concerned because the length of A3 is between B2’s and B1’s. As mentioned earlier from the influence of the web slenderness, it is important that the phenomenon of the flange buckling into the web is studied in more detail so that such a behaviour can be predicted.

4th stop at P = 570 kN and w = 80 mm. Measurements of web buckling. Duration of stop approximately 10 min.

Girder HB1 (test performed June 20 1994):

Stroke rate: 3 mm/min

At approximately P = 109 kN the measurements at the stiffener towards the cellar was taken away due to the girder moving outside measurement range.

1st stop at P = 360 kN and w = 60 mm. Measurements of web buckling. Duration of stop approximately 10 min.

2nd stop at P = 370 kN and w = 52 mm. No measurements of web buckling because the upper flange was too distorted.

Unloading rate: 30 mm/min

Girder HB2 (test performed June 21 1994):

Stroke rate: 2 mm/min

1st stop at P = 627 kN and w = 50 mm. Measurements of web buckling. Duration of stop approximately 10 min.

2nd stop at P = 635 kN and w = 65 mm. Measurements of web buckling. Duration of stop approximately 10 min. The midspan deflection measurement device was taken away to prevent the device from being squeezed between the girder and the floor.

3rd stop at P = 485 kN and w = 80 mm. No measurements of web buckling. The stroke rate was increased to 3 mm/min.

3.8 Discussion

Some observations from the tests can be stated. Firstly, the large amount of lateral supports required of the flange in compression was a bit discourageing. This demand of lateral bracing is probably connected with the high yield strength of the steel used in the test. Thus a design based on plastic design will require lateral bracings fairly close to internal supports.

Secondly, when assessing the descending slope of the moment-rotation curves the observation is that the slope for girders A1, A2 and A3 are somewhat parallel. Going from girder A3 to A4 it is obvious that the slope increases and thus implying a faster drop in moment-rotation capacity for girder A4. Girder A5 is showing an even more rapidly descending curve.

The results from girder A6 should not be relied on as far as the descending slope is concerned. This was the test where the hydraulic jack accelerated out of control and thus giving a dynamic

3rd stop at P = 580 kN and w = 46 mm. Measurements of web buckling. Duration of stop approximately 10 minutes.

4th stop at P = 574 kN and w = 54 mm. Measurements of web buckling. Duration of stop approximately 10 minutes.

5th stop at P = 490 kN and w = 65 mm. The stroke rate was now increased to 2 mm/ minute.

Girder B3 (test performed March 22 1994):

1st stop at P = 135 kN and w = 18 mm. Measurements of web buckling. Duration of stop approximately 10 minutes.

2nd stop at P = 280 kN and w = 37 mm. Measurements of web buckling. Duration of stop approximately 10 minutes.

3rd stop at P = 430 kN and w = 59 mm. Measurements of web buckling. Duration of stop approximately 10 minutes.

4th stop at P = 459 kN and w = 64 mm. Measurements of web buckling. Duration of stop approximately 10 minutes.

5th stop at P = 479 kN and w = 72 mm. Measurements of web buckling. Duration of stop approximately 10 minutes.

6th stop at P = 480 kN and w = 77 mm. Measurements of web buckling. Duration of stop approximately 10 minutes.

7th stop at P = 360 kN and w = 108 mm. The stroke rate was now increased to 2 mm/ minute.

Girder B4 (test performed March 23 1994):

Stroke rate: 1 mm/min

1st stop at P = 350 kN and w = 39 mm. Measurements of web buckling. Duration of stop approximately 10 min.

2nd stop at P = 460 kN and w = 52 mm. Measurements of web buckling. Duration of stop approximately 10 min.

3rd stop at P = 520 kN and w = 60 mm. Measurements of web buckling. Duration of stop approximately 10 min.

Girder A8 (test performed September 16 1993):

1st stop at P = 600 kN and w = 57 mm. Measurements of web buckling. Duration of stop approximately 10 minutes. P = 592 kN prior to starting the jack .

2nd stop at P = 620 kN and w = 72 mm. Measurements of web buckling. Duration of stop approximately 10 minutes. P = 608 kN prior to starting the jack.

3rd stop at P = 578 kN and w = 88 mm. Measurements of web buckling. Duration of stop approximately 10 minutes. P = 565 kN prior to starting the jack.

4th stop at P = 565 kN. The stroke rate was now increased to 2 mm/minute.

This test had to be terminated earlier than desired due to the fact that the hydraulic jack was inclined during the test. Under the circumstance of very high load this could have permanently damaged the hydraulic jack if the test had continued.

Girder B1 (test performed March 17 1994):

1st stop at P = 50 kN and w = 15 mm. Measurements of web buckling. Duration of stop approximately 10 minutes.

2nd stop at P = 150 kN and w = 43 mm. Measurements of web buckling. Duration of stop approximately 10 minutes.

3rd stop at P = 245 kN and w = 69 mm. Measurements of web buckling. Duration of stop approximately 10 minutes.

4th stop at P = 290 kN and w = 82 mm. Measurements of web buckling. Duration of stop approximately 10 minutes.

5th stop at P = 312 kN and w = 94 mm. Measurements of web buckling. Duration of stop approximately 10 minutes.

6th stop at P = 310 kN and w = 106 mm. Measurements of web buckling. Duration of stop approximately 10 minutes. The stroke rate was now increased to 2 mm/minute.

7th stop at P = 277 kN and w = 129 mm. Measurements of web buckling. Duration of stop approximately 10 minutes.

Girder B2 (test performed April 15 1994):

1st stop at P = 400 kN and w = 26 mm. Measurements of web buckling. Duration of stop approximately 10 minutes.

2nd stop at P = 515 kN and w = 36 mm. Measurements of web buckling. Duration of stop approximately 10 minutes.

stop approximately 10 minutes. P = 462.4 kN prior to starting the jack.

5th stop at P = 440 kN and w = 76 mm. Measurements of web buckling. Duration of stop approximately 10 minutes. P = 427 kN prior to starting the jack. The stroke rate was now increased to 2 mm/minute.

During the test it was noted that one part of the upper flange got stuck to the lateral support closest to the left support. The jack was then halted and the flange came loose and got back into position.

Girder A6 (test performed October 5 1993):

1st stop at P = 275 kN and w = 29 mm. Measurements of web buckling. Duration of stop approximately 10 minutes. P = 274.2 kN prior to starting the jack .

2nd stop at P = 410 kN and w = 40 mm. Measurements of web buckling. Duration of stop approximately 10 minutes. P = 407 kN prior to starting the jack.

At P = 480 kN web buckles could be clearly detected visually. Without any warning, the hydraulic jack suddenly went out of control and in 5 seconds the jack had loaded the girder to failure before anyone could stop the jack.

Later the cause to the fault of the jack was detected. The gauge controlling the stroke of the hydraulic jack had got stuck. As the jack was controlled by stroke, this led to an continuously increasing flow of hydraulic oil into the jack since no stroke was detected by the guage.

Girder A7 (test performed September 20 1993):

1st stop at P = 433 kN and w = 61 mm. Measurements of web buckling. Duration of stop approximately 10 minutes. P = 428.7 kN prior to starting the jack .

2nd stop at P = 470.7 kN and w = 84 mm. Measurements of web buckling. Duration of stop approximately 10 minutes. P = 460.5 kN prior to starting the jack.

3rd stop at P = 473.2 kN and w = 97 mm. This stop was caused by the fact that the hydraulic jack was not in line with the web of the girder. The girder was therefore unloaded, the jack adjusted to the correct position and then continuing the test by loading the girder once again. Stroke rate 1 mm/minute. Duration of stop approximately 2 hours.

4th stop at P = 472.2 kN and w = 109 mm. Measurements of web buckling. Duration of stop approximately 10 minutes. P = 460 kN prior to starting the jack.

Girder A3 (test performed Sept 9 1993):

1st stop at P = 333 kN and w = 56 mm. Measurements of web buckling. Duration of stop approximately 10 minutes.

2nd stop at P = 390 kN and w = 71 mm. Measurements of web buckling. Duration of stop approximately 10 minutes. P = 384 kN prior to starting the jack.

3rd stop at P = 393 kN and w = 85 mm. Measurements of web buckling. Duration of stop approximately 10 minutes. P = 384.5 kN prior to starting the jack.

4th stop at P = 365 kN and w = 103 mm. Measurements of web buckling. Duration of stop approximately 10 minutes. P = 353 kN prior to starting the jack. The stroke rate was now increased to 2 mm/minute.

Girder A4 (test performed September 10 1993):

1st stop at P = 325 kN and w = 44 mm. Measurements of web buckling. Duration of stop approximately 10 minutes. P = 322.1 kN prior to starting the jack .

2nd stop at P = 400 kN and w = 56 mm. Measurements of web buckling. Duration of stop approximately 20 minutes. P = 391 kN prior to starting the jack.

3rd stop at P = 439.6 kN and w = 70 mm. Measurements of web buckling. Duration of stop approximately 10 minutes. P = 430.3 kN prior to starting the jack.

4th stop at P = 418 kN and w = 83 mm. Measurements of web buckling. Duration of stop approximately 10 minutes. P = 404.3 kN prior to starting the jack. The stroke rate was now increased to 2 mm/minute.

Just passing the maximum load it was discovered that two of the lateral supports (connected to the floor) on the right hand side of the girder, had slipped approximately 10 mm and 15 mm respectively. This resulted in tightening the bolts connecting the lateral supports to the floor.

Girder A5 (test performed September 14 1993):

1st stop at P = 275 kN and w = 29 mm. Measurements of web buckling. Duration of stop approximately 10 minutes. P = 274 kN prior to starting the jack .

2nd stop at P = 370 kN and w = 40 mm. Measurements of web buckling. Duration of stop approximately 10 minutes. P = 368.5 kN prior to starting the jack.

3rd stop at P = 430.5 kN and w = 49 mm. Measurements of web buckling. Duration of stop approximately 10 minutes. P = 428 kN prior to starting the jack.

4th stop at P = 470 kN and w = 60 mm. Measurements of web buckling. Duration of

3.7 Notes from test of girders

The hydraulic jack was controlled using a stroke rate of 1mm/minute for all girders except the hybrid girders, during the ascending part of the moment-rotation curve. For some of the girders the stroke rate was increased during the descending part of the curve.

Girder A1 (test performed July 9 1993):

1st stop at P = 200 kN and w = 60 mm. Measurements of web buckling. Duration of stop approximately 10 minutes. P = 198.9 kN prior to starting the jack .

2nd stop at P = 275 kN and w = 88 mm. Measurements of web buckling. Duration of stop approximately 14 minutes. P = 270.8 kN prior to starting the jack.

3rd stop at P = 281.6 kN and w = 99 mm. Measurements of web buckling. Duration of stop approximately 9 minutes. P = 277.1 kN prior to starting the jack. A ticking sound was heard from the girder.

4th stop at P = 264 kN and w = 109 mm. Measurements of web buckling. Duration of stop approximately 15 minutes. P = 252 kN prior to starting the jack.

The test was brought to an end at P = 220 kN and w = 120 mm. It was now discovered that the laterally bracings had not been stiff enough, enabling the upper flange to deflect sideways approximately 30 mm. At which point of the test this sideways deflection started, is not known. Stroke rate of unloading 10 mm/minute.

Girder A2 (test performed August 25 1993):

1st stop at P = 280 kN and w = 61 mm. Measurements of web buckling. Duration of stop approximately 10 minutes. P = 278.6 kN prior to starting the jack . Electrical disturbancies occur when measuring the web buckles which can be seen in the moment-rotation diagram.

2nd stop at P = 318 kN and w = 72 mm. Measurements of web buckling. Duration of stop approximately 10 minutes. P = 315.1 kN prior to starting the jack.

3rd stop at P = 335.5 kN and w = 83 mm. Measurements of web buckling. Duration of stop approximately 10 minutes. P = 329.1 kN prior to starting the jack.

4th stop at P = 326 kN and w = 105 mm. Measurements of web buckling. Duration of stop approximately 10 minutes. P = 320.4 kN prior to starting the jack. Now it is discovered that the lateral supports, which are connected eccentrically to the upper flange, have distorted the flange about an axis paralell to the length of the girder. This is due to the eccentricity of the connection and the force in the lateral supports. The test was terminated at this stage.

Table 3.6.1 Test results versus capacities

Girder	V_{max} [kN]	V_{cd} [kN]	V_{max}/V_{cd}	M_{max} [kNm]	M_p [kNm]	M_{max}/M_p
B2	291	333	0.874	508	494	1.028
B3	241	346	0.697	602	593	1.015
B4	288	332	0.867	719	705	1.020
B5	363	334	1.087	484	485	0.998
HB1	185	230	0.804	325	307	1.059
HB2	318	349	0.911	733	701	1.046

Table 3.6.2 Test results versus capacities

Girder	M_y [kNm]	M_{max}/M_y	$M_{y,ef}$ BSK94 [kNm]	$M_{max}/M_{y,ef}$ BSK94	$M_{y,ef}$ EC3 [kNm]	$M_{max}/M_{y,ef}$ EC3
A1	317	1.117	317	1.117	317	1.117
A2	377	1.119	377	1.119	367	1.150
A3	442	1.120	438	1.130	425	1.165
A4	501	1.100	489	1.127	474	1.162
A5	562	1.048	545	1.081	527	1.118
A6	633	1.063	606	1.111	583	1.154
A7	496	1.206	496	1.206	496	1.206
A8	660	1.180	660	1.180	660	1.180
B1	441	1.079	441	1.079	423	1.125
B2	441	1.152	441	1.152	423	1.201
B3	544	1.107	540	1.115	525	1.147
B4	652	1.103	634	1.134	634	1.134
B5	441	1.098	441	1.098	423	1.144
HB1	292	1.113	a	-	a	-
HB2	684	1.072	a	-	a	-

a. Calculation of effective cross section is not covered in BSK94 and EC3 for hybrid girders.

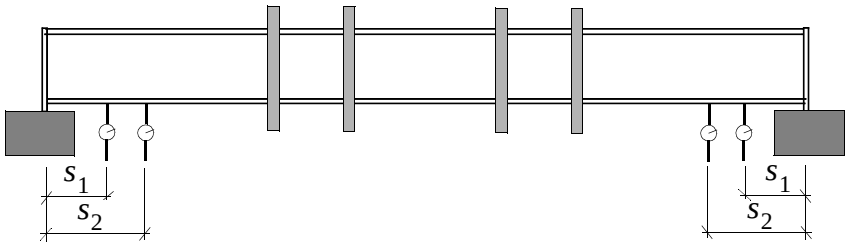

Figure 3.6.1 Distance s_1 and s_2 in equation 3.6.1.

The moment values in the moment-rotation diagrams are given both as their measured values and also in nondimensional form. In the case of the nondimensional diagrams, the moment is related to the full plastic moment M_p, based on the obtained values on f_y in table 3.4.2.
The test results with respect to moment and shear are presented in table 3.6.1 and 3.6.2. V_{cd} is calculated according to K18 using column 1 in table K18:26a and λ_w according to (18:26d), where:

$$V_{cd} = \omega_v \cdot h_w \cdot t_w \cdot f_y$$
$$\omega_v = 0,79 / (\lambda_w + 0,70)$$
$$\lambda_w = 0,35 \cdot h_w / t_w \cdot \sqrt{f_y / E}$$

M_y for hybrid girders HB1 and HB2 is defined at which yielding starts in the extreme fibres of the flanges.

Table 3.6.1 Test results versus capacities

Girder	V_{max} [kN]	V_{cd} [kN]	V_{max}/V_{cd}	M_{max} [kNm]	M_p [kNm]	M_{max}/M_p
A1	141	293	0.481	354	348	1.017
A2	168	307	0.547	422	413	1.022
A3	198	335	0.591	495	486	1.019
A4	220	330	0.667	551	552	0.998
A5	235	338	0.695	589	623	0.945
A6	269	345	0.780	673	702	0.959
A7	239	997	0.240	598	557	1.074
A8	311	1118	0.278	779	747	1.043
B1	190	345	0.551	476	486	0.979

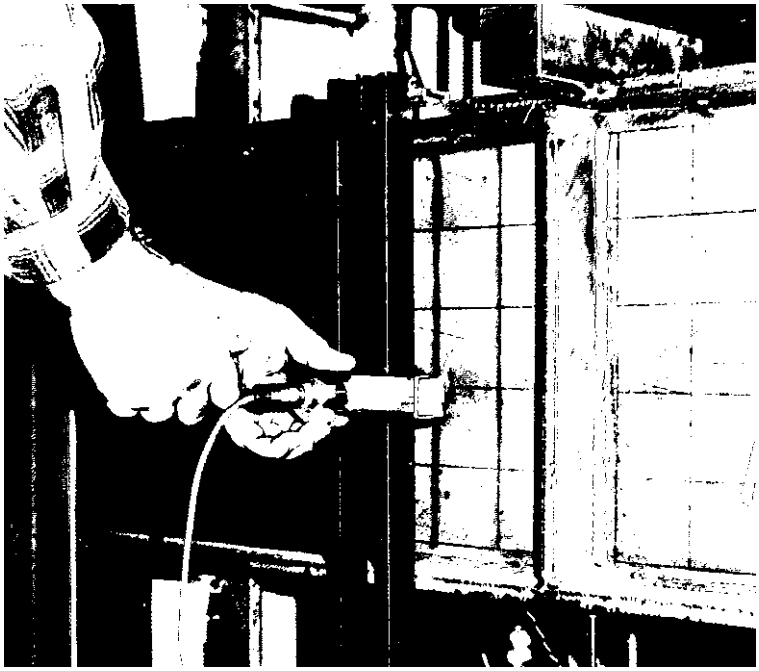

Figure 3.5.8 Measurements of local web buckling

3.6 Presentation of test results

Results in the form of moment-rotation curves and web buckles, from the tests on the fifteen steel girders, are presented in appendix C. The rotation in the diagrams are the sum of the plastic rotation $\theta_{p,s}$ at the left and the right supports . $\theta_{t,s}$ is the total rotation at each support that is measured in the tests. The plastic rotation at one support is obtained by the following expression:

(3.6.1)

$$\theta_{p,s} = \theta_{t,s} - M\left[\frac{2}{GA_w L} + \frac{L}{4EI}\left(1 - \frac{4}{3L^2}\left(s_1^2 + s_1 s_2 + s_2^2\right)\right)\right]$$

where s_1 and s_2 are are distances from support to the deflection guages, see figure 3.6.1.

Rotation was measured at each end of the girders. The rotation was measured by pairwise deflection gauges applied at the lower flange and also at the vertical support stiffener of the girder. Thus the measurement of the rotation at each end was duplicated. The deflection at mid-span was also measured.

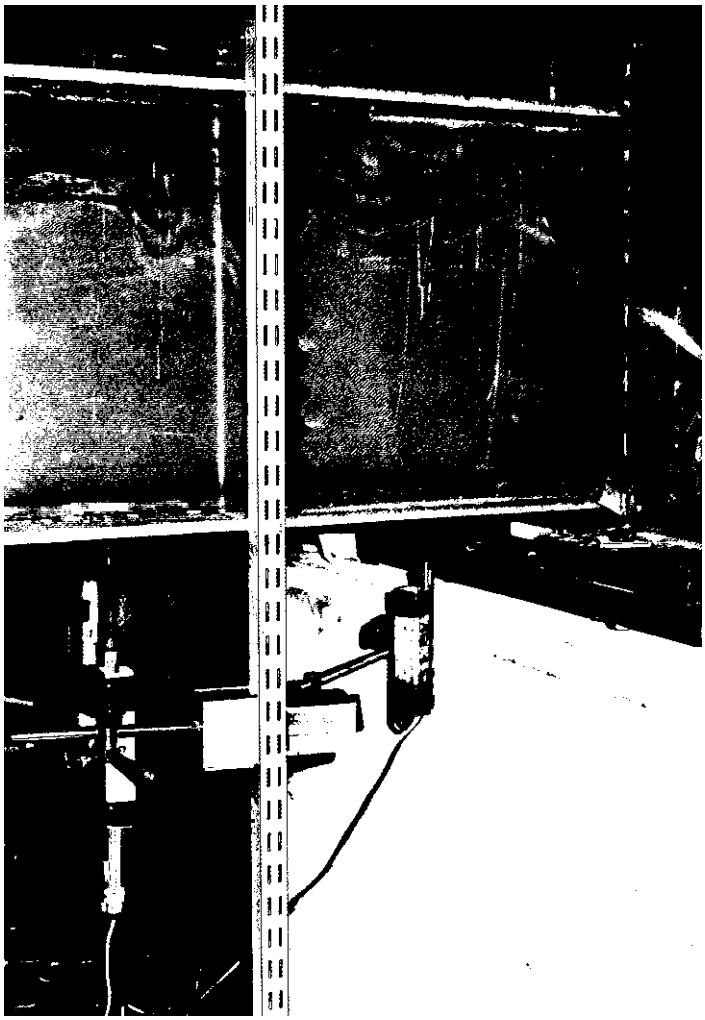

Figure 3.5.7 Measurement of rotation at end of girder

In the vicinity of midspan, eight strain gauges, four on the upper flange and four on the lower flange, was applied in line with the web except for girder B5 in which no gauges were applied. This will make it possible to estimate the curvature of the girders at four sections.

Local buckles in the web at midspan were measured during the tests using a deflection guage except for girder B5. The measurements were performed with the edges of the upper and lower flanges defining a vertical reference plane. From this reference plane the distance to the web was measured in a prescribed mesh. The presented isographs in appendix C represents the increase in distance at specified load levels, from the distance measured prior to loading.

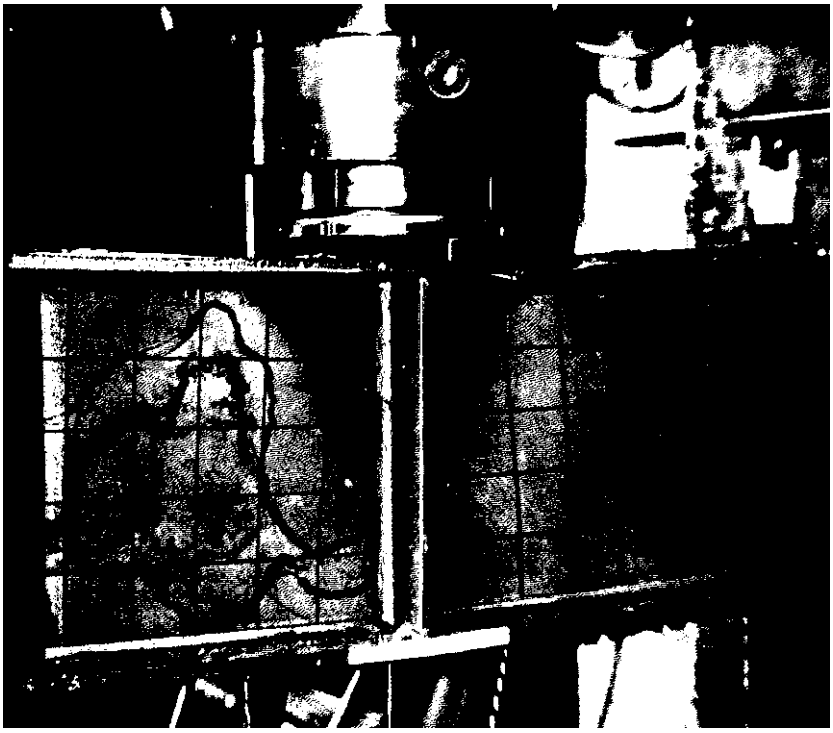

Figure 3.5.5 Bearing between the jack and the crossbar

The ends of the girders were put on steel plates with low-friction material in between to avoid normal forces in the girder.

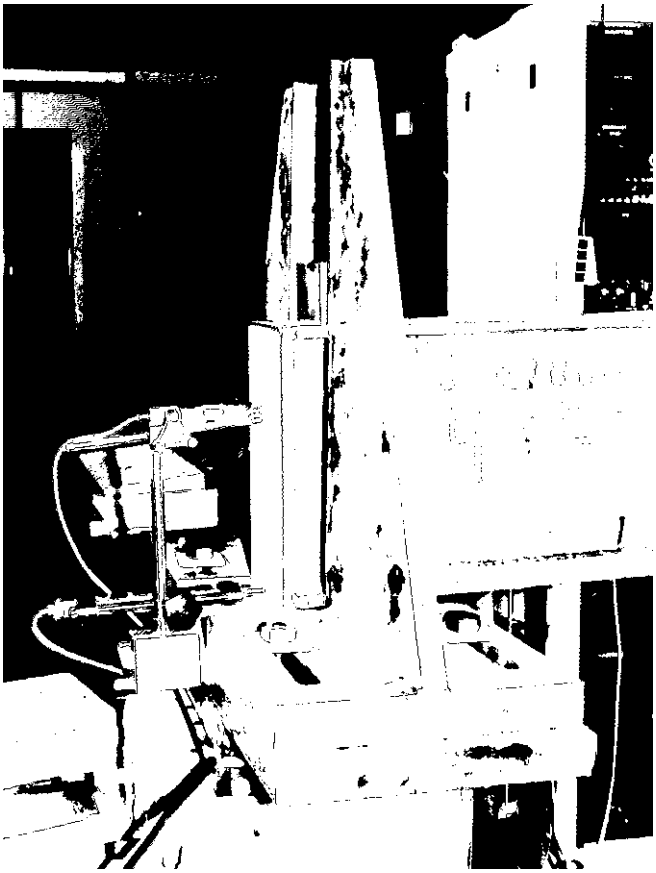

Figure 3.5.6 Photo of girder support

Table 3.5.1 Locations of lateral supports along the girders measured from midspan

Girder	Distance lateral support 1 and 2 from midspan [mm]	Distance lateral support 3 and 4 from midspan [mm]
A1	900	-
A2	400	900
A3	500	1000
A4	500	1000
A5	500	1000
A6	500	1000
A7	500	1000
A8	500	1000
B1	500	1000
B2	500	1000
B3	500	1000
B4	500	1000
B5	500	-
HB1	500	1000
HB2	500	1000

The midspan load was applied using one 1000 kN-capacity hydraulic jack. The load was applied through a crossbar (50x50 mm^2 cross section) resting on the upper flange. For all girders except girder A1 there was also a bearing between the jack and the crossbar, allowing the girder to rotate about a vertical axis relative to the jack.

Lateral supports were placed at the ends of the girders and in four additional points, symmetric with respect to midspan except for girder A1 and B5 which was only supported in two additional points. The location of the lateral supports in figure 3.5.4 was determined from BSK94 but also where attachment to the floor was possible in the laboratory hall. Both the upper and lower flanges were laterally supported except for girders A1 and A2 where only the upper (in compression) flange were attached through pins.The lateral supports for A1 and A2 were found too weak so the lateral supports were redesigned according to figure 3.5.3. The distances of the lateral supports from midspan are presented in table 3.5.1.

Figure 3.5.3 Lateral bracings in test setup

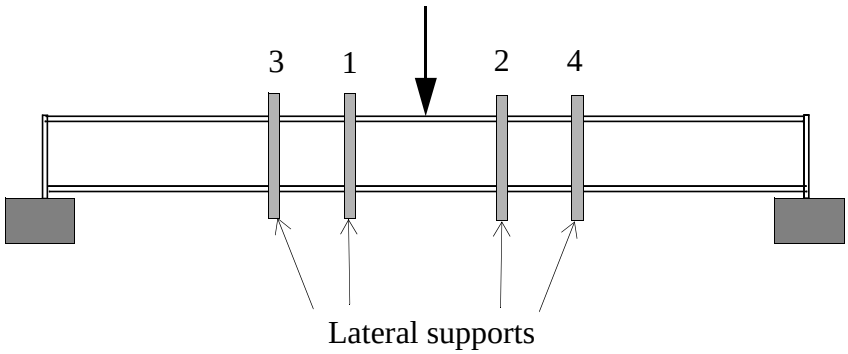

Figure 3.5.4 Numbering of lateral supports in table 3.8.

3.5 Test Setup and Procedures

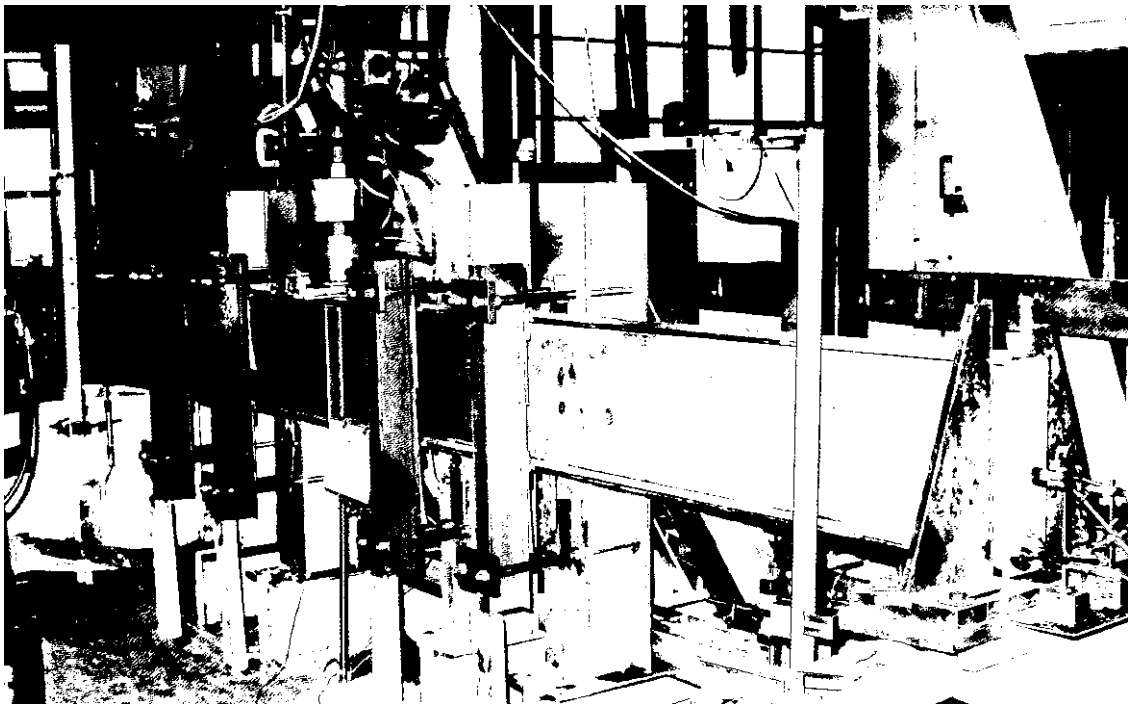

Figure 3.5.1 Photo of test setup

Each test was performed as a simply supported girder with a single load at midspan. This loading arrangement simulates an interior support of a continuous span bridge. The center load in the test simulated the reaction at the interior support in the bridge and the simple supports in the test simulated the nearest points of contraflexure in the bridge, see figure 3.5.2.

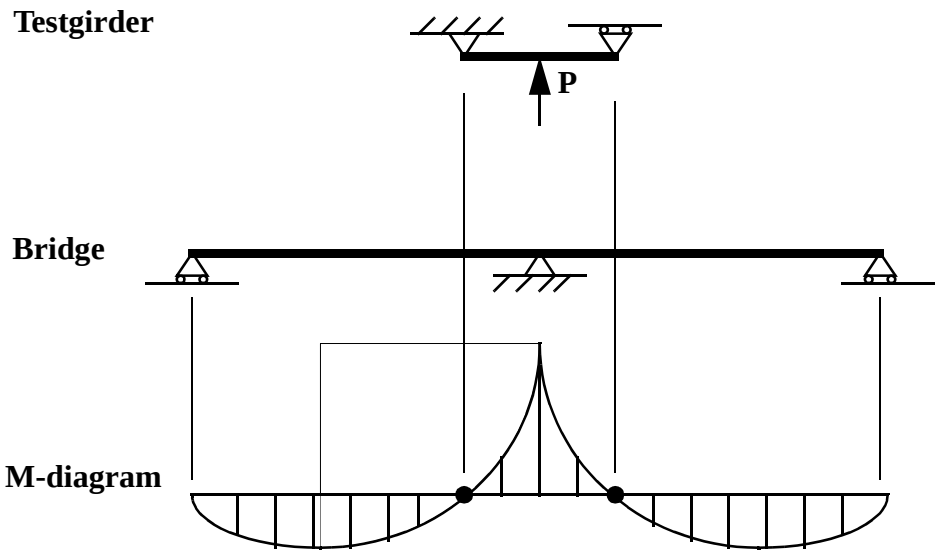

Figure 3.5.2 Testgirders simulating girder of a bridge at interior support

Table 3.4.2 Tensile specimen reference to girders

Girder	Part	Specimen	Mean yield [MPa]	Mean ult. strength [MPa]
A5, A6	web	A1PL1, A2PL1	830	860
A3, A4	flange	AC1, AC2	844	882
	web	A1PL2, A2PL2	832	871
A7, A8	flange	AC1, AC2	844	882
	web	AB1, AB2	762	802
B1, B2, B5	flange	E1, E2	846	883
	web	D1PL1, D2PL1, D3PL1	819	855
B3, B4	flange	E1, E2	846	883
	web	D1PL2, D2PL2, D3PL2	820	857
HB1, HB2	flange	E1, E2	846	883
	web	HB2, HB3	242	362

The width, thickness and area are mean values. The stroke is the speed of the grips of the Dartec machine and the strainrate is the increase in strain per second for the material within the measure length of the extensometer in the elastic region of the material.

Specimen AC1 developed the failure zone outside the guage length of the MTS extensometer which means that the reported strain after yielding is not comparable with the other specimen tests. Also, for specimen D2PL1 and E2 the failure zone developed near one end of the extensometer.

For specimen A1PL1 the strainrate was by mistake set too high. This has the effect that the reported stress will be somewhat higher than if the same specimen had been tested with a strainrate comparable with the other specimen tests. The results from the tensile tests are presented in appendix B. Note that the $\sigma - \varepsilon$ relation in the diagrams is only registered within the MTS extensometers measure range. Thus the “end” of the $\sigma - \varepsilon$ diagram might not be the strain at which the specimens fail but the end of the measure range of the MTS extensometer.

In table 3.4.1 below are the data of the tensile specimens presented.

Table 3.4.1 Tensile test specimens

Speci-men	Width [mm]	Thick-ness [mm]	Area [mm^2]	Max. load [kN]	Ser-ies	f_y [MPa]	f_u [MPa]	Stroke [mm/s]	Strainrate [s^{-1}]
AC1	30.09	12.01	361.38	318.9	A	842	882	0.037	$7,5 \cdot 10^{-5}$
AC2	30.13	12.02	362.16	319.9	A	846	883	0.037	$7,3 \cdot 10^{-5}$
AB1	20.06	7.66	153.66	123.1	A	763	801	0.025	$8,4 \cdot 10^{-5}$
AB2	20.05	7.65	153.38	123.2	A	761	803	0.025	$8,2 \cdot 10^{-5}$
A1PL1	15.03	3.88	58.32	50.00	A	835	857	0.020	$4,2 \cdot 10^{-4}$
A2PL1	15.04	3.86	58.05	50.13	A	825	864	0.020	$9,5 \cdot 10^{-5}$
A1PL2	15.03	3.91	58.77	51.34	A	835	874	0.020	$9,6 \cdot 10^{-5}$
A2PL2	15.02	3.91	58.73	51.00	A	828	868	0.020	$9,7 \cdot 10^{-5}$
D1PL1	15.03	3.86	58.02	49.80	B	823	859	0.020	$9,7 \cdot 10^{-5}$
D2PL1	15.07	3.92	59.07	50.11	B	817	848	0.020	$9,3 \cdot 10^{-5}$
D3PL1	15.05	3.92	59.00	50.69	B	818	859	0.020	$8,8 \cdot 10^{-5}$
D1PL2	14.99	3.92	58.76	50.10	B	817	852	0.020	$9,6 \cdot 10^{-5}$
D2PL2	14.99	3.91	58.61	50.39	B	820	860	0.020	$9,5 \cdot 10^{-5}$
D3PL2	15.00	3.91	58.65	50.39	B	824	859	0.020	$8,9 \cdot 10^{-5}$
E1	30.04	11.95	358.98	317.58	B	848	885	0.020	$7,5 \cdot 10^{-5}$
E2	30.07	11.95	359.34	316.7	B	843	881	0.020	$7,5 \cdot 10^{-5}$
HB2	19.96	6.08	121.36	44.11	HB web	240	363	0.020	$4,6 \cdot 10^{-5}$
HB3	20.02	6.07	121.52	44.02	HB web	245	362	0.050	$12,6 \cdot 10^{-5}$

Table 3.4.2 Tensile specimen reference to girders

Girder	Part	Specimen	Mean yield [MPa]	Mean ult. strength [MPa]
A1, A2,	flange	AC1, AC2	844	882

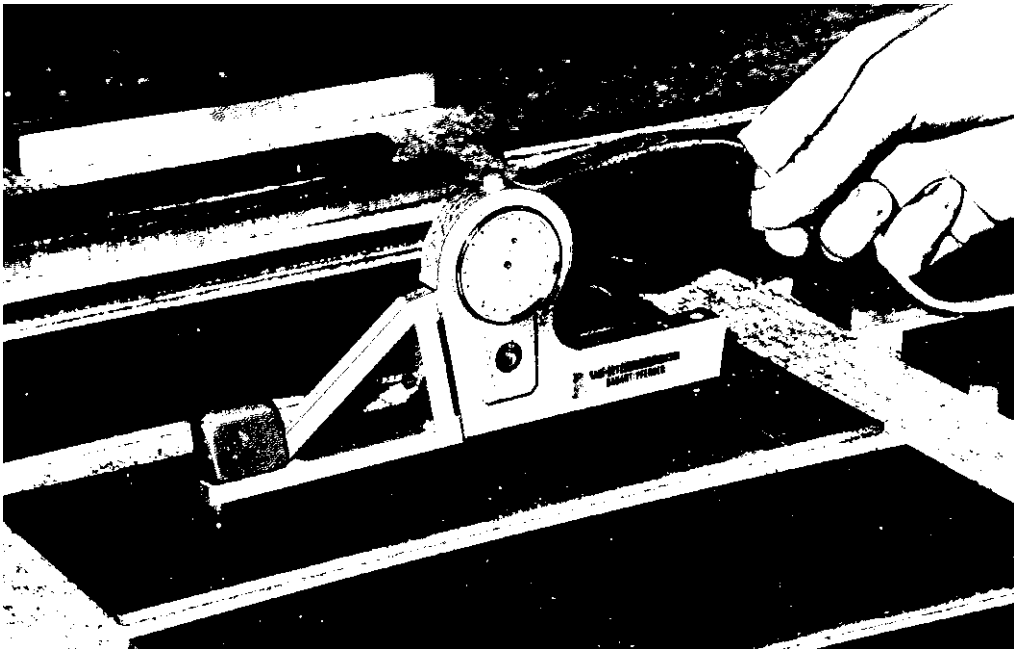

Figure 3.3.1 Measurement device for residual stresses

This procedure enables an estimation of the residual stresses in the girder as they will be relieved when the parts of the girders are cut in strips. The residual stresses are presented in appendix A.

The reason for the differences between A6 and B2 is that first girder A6 was assessed. It was found that the gradient of the residual stresses was high in the flanges, therefore the decision was taken to increase the number of steel balls (measure points) for girder B2. In addition, the residual stresses increase from the ends of the girder until they reach a constant value. To be confident that the measurements is undertaken in the part of the girder where the residual stresses have grown to a constant value, the measurements were performed further away from the end in girder B2. If this latter measure was necessary is somewhat difficult to say as it is a bit hard to compare the stresses in corresponding points of girder A6 and B2, due to the high gradient of the residual stresses.

3.4 Tensile tests on steel used in girders

The steel girders of series A were fabricated from steel plates of 4 mm, 8 mm and 12 mm thickness, series B of 4 mm and 12 mm plates and series HB from 6 mm and 12 mm plates. Material from two steel plates of 4 mm, one of 8 mm and one of 12 mm thickness were used for the fabrication of the girders of series A. Series B was made from material from two plates of 4 mm and one plate of 12 mm. Girder series HB was made from one plate of 6 mm and one plate of 12 mm, which was the same used for series B. Two tensile test specimens were fabricated from each steel plate except for the 4 mm plates of series B where three specimens were fabricated. This means that a total of 18 test specimens were tested.

The specimens were tested in a Dartec machine with a maximum capacity of 600 kN. The elongation was measured by an MTS extensometer with an original length $L_0 = 50$ mm.

difference that assumptions have been included in the latter. The limitation of the classes have not been derived for such high yield strengths as is present in this report.

3.2 Fabrication

The girders were fabricated at Verkstads AB Eric Erlandsson. The girders were made from steel plates, Weldox 700 (f_{yk} = 700 MPa) and (f_{yk} = 220 MPa) courtesy of SSAB, Oxelösund. From these plates the flanges and webs were cut out using flame cutting. The I-shaped girders were welded with hand-held MIG equipment. The fillet welds were of 3 mm size

Girders A4 and A6 were straightened at the fabrication workshop to keep the transverse curvature of the girder within the limits of BSK94. The straightening was only performed on the outer thirds of the girders to keep the midpart unaffected. All girders were kept within the imperfection limits of BSK94 chapter 8:62 with respect to transverse curvature of the girder i.e $e_b \leq 0,0015L$ (see figure 3.2.1), flange imperfection and web imperfection.

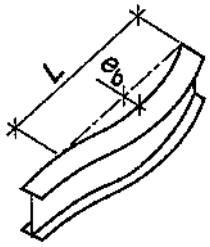

Figure 3.2.1 Transverse curvature

3.3 Residual stresses

Girder A6 was intentionally made 500 mm longer from the fabrication workshop. On these 500 mm, situated at the end of the girder, steel balls of approximately 1 mm in diameter were applied at the mid 200 mm of the 500 mm long part. Similarly, girder B2 was made 1500 mm longer from which a 300 mm part was taken out approximately 1100 mm from the end of the girder.

The balls served as marks for measuring the length between the balls in the direction of the girder. A total of 32 pair of steel balls were applied on girder A6 on each side of both the upper and lower flange and on the web. For girder B2 the amount of steel balls was increased to 68 pairs. The distance within each pair was measured with a Steiger measuring equipment, capable of measuring 1/1000 mm of accuracy. The parts were then cut off from the girders and the distance between the balls was then measured again. Finally the parts were cut in strips (17 strips for A6 and 37 strips for B2) along the length of the girder (using a cold-saw for A6 and a spark cutting machine for B2) and the distance within each pair of balls was measured once again.

Table 3.1.3 Limiting values according to EC3, section 5.7.7 for the girders

Girder	EC3, section 5.7.7
B4	103
B5	69
HB1	71
HB2	105

Table 3.1.4 Classification of cross-sections according to BSK94 and EC3

Girder	$\frac{b_f}{t_f}$ $\frac{c}{t_f}$	$\frac{d}{t_w}$	BSK94 flange	BSK94 web	EC3 flange	EC3 web
A1	4.4	61	Class 1	Class 2	Class 1	> Class 4
A2	4.5	71	Class 1	Class 2	Class 1	> Class 4
A3	4.5	80	Class 1	Class 3	Class 1	> Class 4
A4	4.5	92	Class 1	Class 3	Class 1	> Class 4
A5	4.5	102	Class 1	$\beta_w > 99$	Class 1	> Class 4
A6	4.5	114	Class 1	$\beta_w > 99$	Class 1	> Class 4
A7	4.4	40	Class 1	Class 2	Class 1	Class 2
A8	4.3	49	Class 1	Class 2	Class 1	Class 3
B1	4.5	76	Class 1	Class 3	Class 1	> Class 4
B2	4.4	79	Class 1	Class 3	Class 1	> Class 4
B3	5.6	77	Class 2	Class 3	Class 3	Class 4
B4	6.9	79	Class 2	Class 3	Class 3	Class 4
B5	4.5	79	Class 1	Class 3	Class 1	> Class 4
HB1	4.3	35	Class 1	Class 1[a]	Class 1	Class 1[a]
HB2	4.4	77	Class 1	Class 3[a]	Class 1	Class 4[a]

a. The webs of the hybrid girders have been classed with f_{yk} = 845 MPa.

Girders marked with “>Class 4” for webs according to EC3 have failed the EC3 criterion in section 5.7.7. The limitation of EC3, section 5.7.7, gives a lower value for girders A1 and A2 than the limitation for class 3 due to the fact that f_{yk} (and f_{yf}) equals a high value (845 MPa) and because of the web over flange ratio A_w/A_{fc}. The formula in EC3, section 5.7.7 and the limitation of class 3, for formulae given in table 3.1.2 in BSK94 are basically the same with the

Table 3.1.2 Limiting values for cross-section classes in BSK94 and EC3

Part of Cross-section	BSK 94 class	EC3 class	BSK94	EC3
Web	1	1	$\beta_{wpl} = 2.4\sqrt{\frac{E}{f_{yk}}} = 38$	$\frac{d}{t_w} = 72\sqrt{\frac{E}{f_{yk}}} = 38$
		2		$\frac{d}{t_w} = 83\sqrt{\frac{235}{f_{yk}}} = 44$
	2	3	$\beta_{wel} = 3.2\kappa_f\sqrt{\frac{E}{f_{yk}}} = 76$	$\frac{d}{t_w} = 124\sqrt{\frac{235}{f_{yk}}} = 65$
	3	sec-tion 5.7.7	$\frac{h_w + 2t_f}{t_w} < 0.4\frac{E}{f_{yk}} = 100$	$\frac{d}{t_w} \le k\frac{E}{f_{yf}}\sqrt{\frac{A_w}{A_{fc}}} = 60 - 114$

Since there are three classes in BSK94 and four in EC3, the comparable classes from each code has been put on the same line.

The formula according to EC3, section 5.7.7 is dependent of the geometry of the cross-section. The limiting values of h_w / t_w for the girders according to this formula are according to table 3.1.3.

Table 3.1.3 Limiting values according to EC3, section 5.7.7 for the girders

Girder	EC3, section 5.7.7
A1	60
A2	64
A3	69
A4	73
A5	76
A6	80
A7	99
A8	111
B1	70
B2	69
B3	114

Table 3.1.1 Geometry of tested girders

Girder	h_w [mm]	t_w [mm]	b_{fl} [mm]	t_f [mm]	L [mm]
A3	319.7	3.9	120.1	12.0	5008
A4	359.6	3.8	120.5	11.9	5009
A5	397.7	3.8	120.0	12.0	5006
A6	439.9	3.8	120.0	12.0	5007
A7	320.7	7.9	120.5	11.9	5012
A8	400.5	8.0	120.4	12.0	5013
B1	318.1	4.0	120.2	12.0	5999
B2	319.9	3.9	120.2	12.2	3497
B3	318.7	4.0	149.3	12.2	4999
B4	321.9	3.9	180.4	12.2	4999
B5	318.9	3.9	120.3	12.0	2664
HB1	219.0	6.1	120.0	12.3	3512
HB2	481.0	6.1	121.0	12.2	4606

The values in table 3.1.1 are mean values based on measured dimensions in midspan of girder.

The classification of the cross-sections are presented in table 3.1.2 according to the Swedish Regulations for Steel Structures (BSK94) and Eurocode 3 (EC3). If a mean value of $f_y = 845$ MPa from table 3.6 is used (from flange material), the limiting values according to these regulations are :

Table 3.1.2 Limiting values for cross-section classes in BSK94 and EC3

Part of Cross-section	BSK 94 class	EC3 class	BSK94	EC3
Flange	1	1	$\beta_{fpl} = 0.3\sqrt{\frac{E}{f_{yk}}} = 4.73$	$\frac{c}{t_f} = 9\sqrt{\frac{235}{f_{yk}}} = 4.75$
		2		$\frac{c}{t_f} = 10\sqrt{\frac{235}{f_{yk}}} = 5.27$
	2	3	$\beta_{fel} = 0.44\sqrt{\frac{E}{f_{yk}}} = 6.94$	$\frac{c}{t_f} = 14\sqrt{\frac{235}{f_{yk}}} = 7.38$
	3		$\beta_f < 2\sqrt{\frac{E}{f_{yk}}} = 31.5$	

3 Laboratory Tests

3.1 Geometry of girders

Fifteen welded, I-shaped steel plate girders were fabricated for the test. For simplicity, the steel girders were tested without a composite concrete slab since the objective of the test was to investigate the influence of the geometry of the steel girders. Also, the concrete is cracked over an internal support and assumed not to contribute to the resistance of the composite cross section. It is therefore only the girder and the reinforcement that contributes to the resistance of the cross-section. The neutral axis will be situated close to the midpart of the web. Hence, the tested girders were made double-symmetric. The geometry of the girders in the test are presented in table 3.1.1.

The girder called B5 (formerly called LABBALK) is actually an extra girder that was used in a student laboratory experiment. It is actually a part of girder B1 that was taken out of the girder after it had been tested. B5 differs from the rest of the girders in the respect that no strain guages were applied on the girder and that no web buckles were measured. An curvature measurement device was however applied at the midspan of the girder.

Girders HB1 and HB2 are hybrid girders, i e the web is made of steel with lower yield strength than the flanges. In this case the nominal yield strength of the webs were 220 MPa and for the flanges 700 MPa.

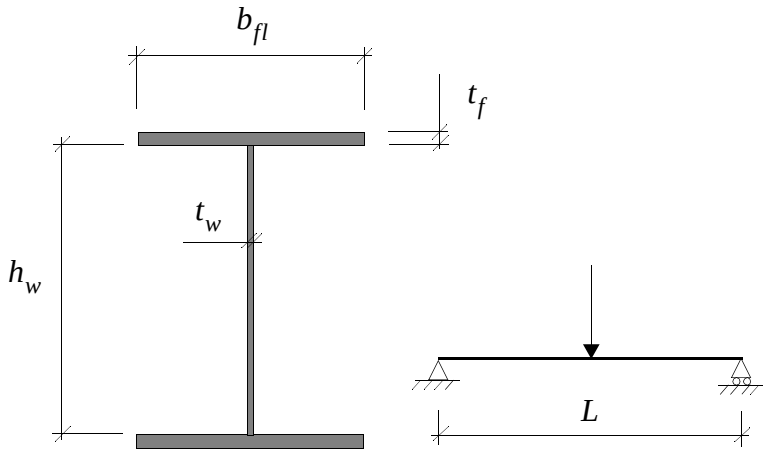

Figure 3.1 Explanation to notations used in table 3.1.1

Table 3.1.1 Geometry of tested girders

Girder	h_w [mm]	t_w [mm]	b_{fl} [mm]	t_f [mm]	L [mm]
A1	239.8	3.8	118.5	12.0	5014
A2	278.1	3.8	119.9	12.0	5011

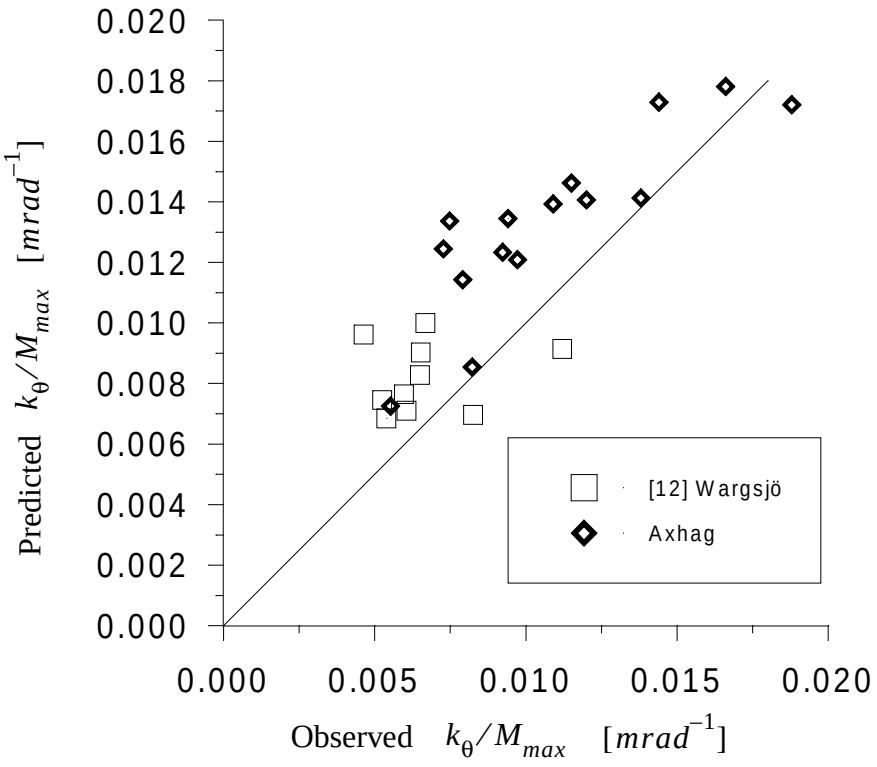

Figure 4.2.6 Observed versus predicted values (equation 4.2.8) for k_θ/M_{max}

Since the Q^2 values are improved for equation (4.2.7) and (4.2.8) compared to (4.2.5) and (4.2.6) it is clear that the former two equations represent an improvement. Further studies are necessary in order to predict the moment-rotation relation accurately.

Table 4.2.4 Values from analyses of variance describing the quality of the model

	$\log\theta_{fk}$	$\log\,(k_\theta/M_{max})$
Q^2	64 %	63 %
s_e	0.131 $[mrad]$	0.101 $[mrad^{-1}]$

hence yields the following formulae for θ_{fk} and k_θ/M_{max}:

$$\hat{\theta}_{fk} = 10^{-(1,260)} \cdot \left(\frac{b_f}{t_f}\right)^{-(1,483)} \cdot \left(\sqrt{\frac{E}{f_y}}\right)^{2,858} \cdot \left(\frac{M_{max}}{M_p}\right)^{10,33} \tag{4.2.7}$$

$$\hat{k}_\theta/M_{max} = 10^{0,213} \cdot \left(\frac{V}{V_{cd}}\right)^{0,413} \cdot \left(\sqrt{\frac{E}{f_y}}\right)^{-(1,664)} \cdot \left(\frac{M_{max}}{M_p}\right)^{-(3,526)} \tag{4.2.8}$$

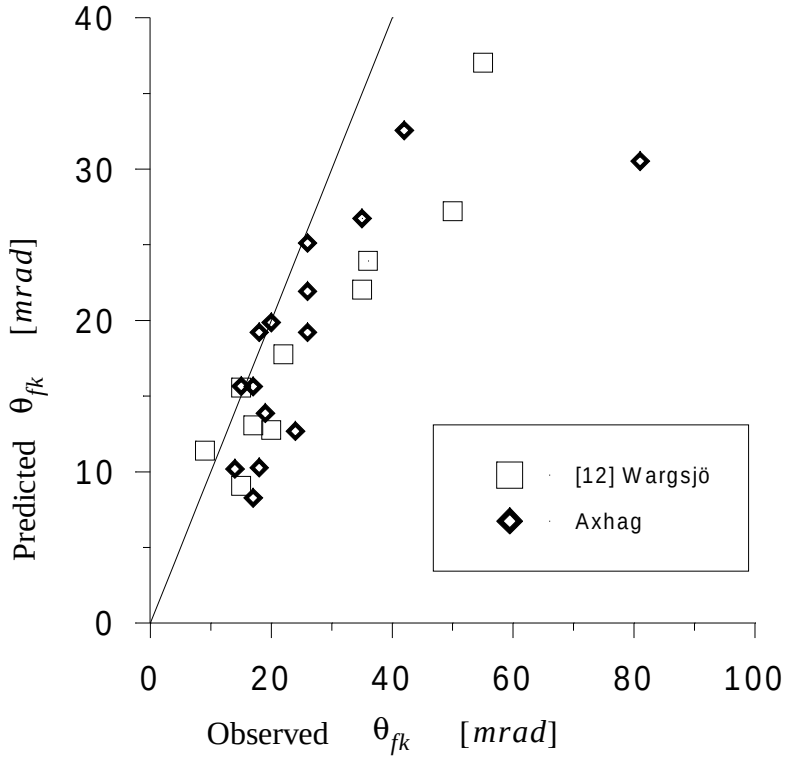

Figure 4.2.5 Observed versus predicted values (equation 4.2.7) for θ_{fk}.

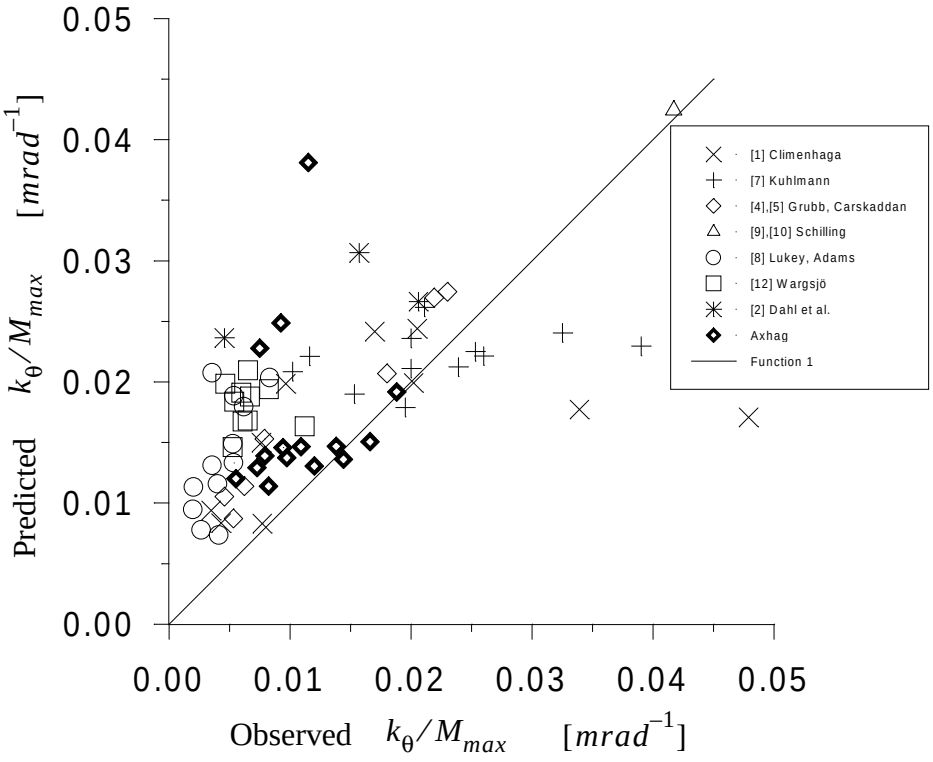

Figure 4.2.4 Observed versus predicted values (equation 4.2.5) for k_θ/M_{max}, magnified scale.

As stated previously, the Q^2 value in table 4.2.2 indicates that the models for $\log\ \theta_{fk}$ and $\log\ (k_\theta/M_{max})$ (and hence equations 4.2.5 and 4.2.6) is not very good. therefore we will try to improve this by only using the results from Wargsjö [12] and from the results in this report (table 4.1.2). These tests were performed in the same laboratory using similar test setups. This yields:

Table 4.2.3 Constants derived from regression analyses

β	$\log\theta_{fk}$	$\log\ (k_\theta/M_{max})$
β_0	-1.129	0.112
β_1	0	0
β_2	-1.483	0
β_3	2.858	-1.664
β_4	0	0
β_5	0	0.413
β_6	10.33	-3.526

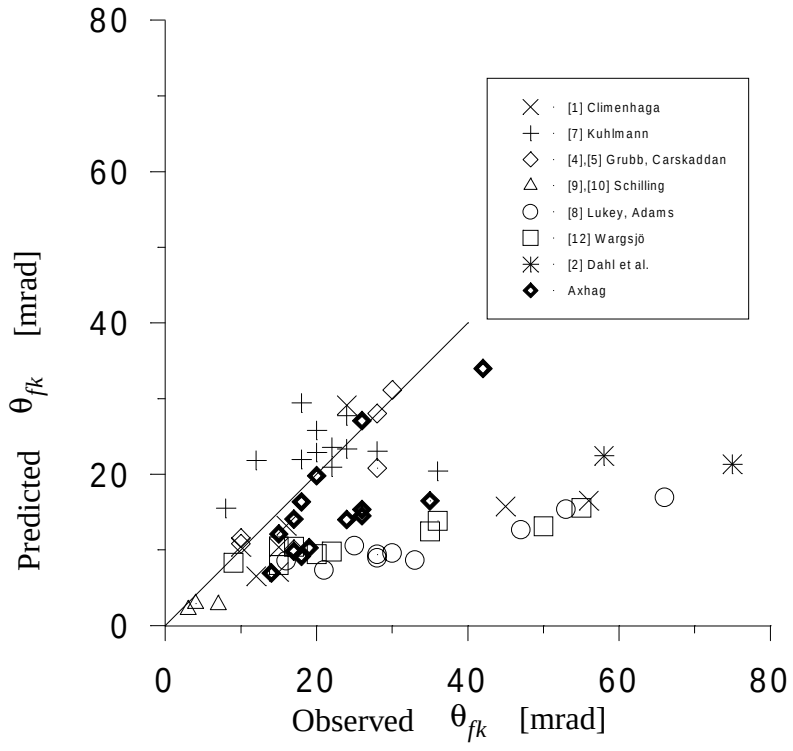

Figure 4.2.2 Observed versus predicted values (equation 4.2.4) for θ_{fk}, magnified scale.

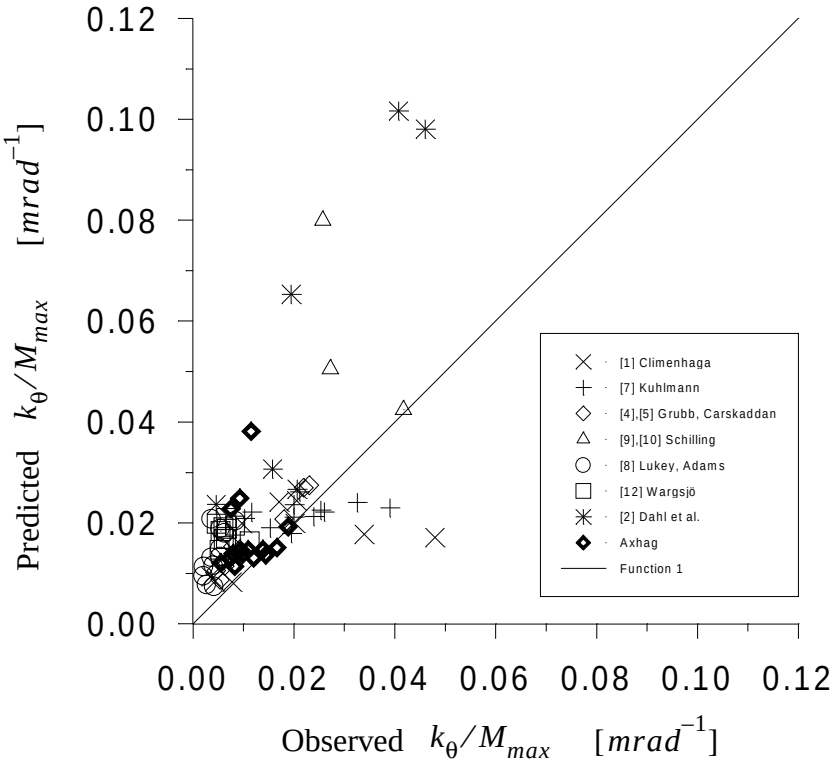

Figure 4.2.3 Observed versus predicted values (equation 4.2.5) for k_θ/M_{max}

$$k_\theta / M_{max} = 10^{-(0,278)} \cdot \left(\frac{V}{V_{cd}}\right)^{0,529} \cdot \left(\frac{2h_{wc}}{t_w}\right)^{-(0,867)} \cdot \left(\frac{b_f}{t_f}\right)^{2,060} \cdot \left(\sqrt{\frac{E}{f_y}}\right)^{-(1,167)} \cdot \left(\frac{M_{max}}{M_p}\right)^{-(3,365)}$$

(4.2.4)

We cannot use equations (4.2.3) and (4.2.4) directly. These equations are corrected with the residual standard error S.E. in table 4.2.2, so that θ_{fk} is corrected with the factor $10^{-(0,249)}$ and k_θ / M_{max} with $10^{0,251}$.

Hence the corrected values of the predicted values of θ_{fk} and k_θ are:

$$\hat{\theta}_{fk} = 10^{2,401} \cdot \left(\frac{2h_{wc}}{t_w}\right)^{-(1,040)} \cdot \left(\frac{b_f}{t_f}\right)^{-(1,707)} \cdot \left(\sqrt{\frac{E}{f_y}}\right)^{1,546} \cdot \left(\frac{M_{max}}{M_p}\right)^{1,684} \qquad (4.2.5)$$

$$\hat{k}_\theta / M_{max} = 10^{-(0,027)} \cdot \left(\frac{V}{V_{cd}}\right)^{0,529} \cdot \left(\frac{2h_{wc}}{t_w}\right)^{-(0,867)} \cdot \left(\frac{b_f}{t_f}\right)^{2,060} \cdot \left(\sqrt{\frac{E}{f_y}}\right)^{-(1,167)} \cdot \left(\frac{M_{max}}{M_p}\right)^{-(3,365)}$$

(4.2.6)

Equation (4.2.5) is compared with observed values in figures 4.2.1 and 4.2.2. Equation (4.2.6) is compared with observed values in figures 4.2.3 and 4.2.4.

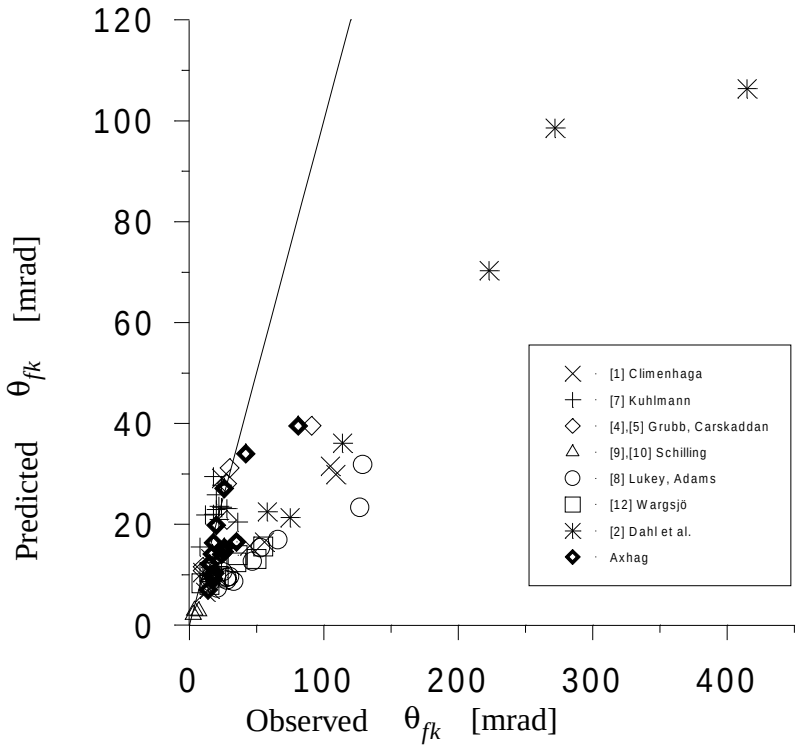

Figure 4.2.1 Observed versus predicted values (equation 4.2.4) for θ_{fk}.

Table 4.2.2 Values from analyses of variance describing the quality of the model

	$\log\theta_{fk}$	$\log\,(k_\theta / M_{max})$
Q^2	58 %	44 %
s_e	0.249 $[mrad]$	0.251 $[mrad^{-1}]$

the definitions of Q^2 and s_e are:

$$Q^2 = 1 - \left(\frac{n-1}{n-p}\right) \cdot \left(1 - \frac{\sum_{i=1}^{n} \left(\hat{y}_i - \bar{y}\right)^2}{\sum_{i=1}^{n} \left(y_i - \bar{y}\right)^2} \right)$$

and

$$s_e = \sqrt{\frac{1}{n-p} \cdot \sum_{i=1}^{n} \left(y_i - \hat{y}_i\right)^2}$$

where:

n = Number of observations

p = Number of coefficients estimated (β)

y_i = Observation number i

$\hat{y}_i$ = Predicted value by regression analysis

$\bar{y}$ = Mean value of the observations

The Q^2 value implies that the models for $\log\theta_{fk}$ and $\log k_\theta$ is not very good. However, the β values from table 4.2.1 are input into equations (4.2.1) and (4.2.2) and these are raised with base 10, which yields:

$$\theta_{fk} = 10^{2,\,650} \cdot \left(\frac{2h_{wc}}{t_w}\right)^{-(1,\,040)} \cdot \left(\frac{b_f}{t_f}\right)^{-(1,\,707)} \cdot \left(\sqrt{\frac{E}{f_y}}\right)^{1,\,546} \cdot \left(\frac{M_{max}}{M_p}\right)^{1,\,684} \qquad (4.2.3)$$

4.2 Statistical evaluation

The purpose of performing the laboratory tests, is to find empirical relationships for θ_{fk} and k_θ. The relationships will be derived with the help of the statistical computer program, Statgraphics [17]. We start by assuming a model for the relationships (the denotation log is the logarithm of the argument with base 10):

$$\log\theta_{fk} = \beta_{0,\theta} + \beta_{1,\theta}\log\left(\frac{2h_{wc}}{t_w}\right) + \beta_{2,\theta}\log\left(\frac{b_f}{t_f}\right) + \beta_{3,\theta}\log\left(\sqrt{\frac{E}{f_y}}\right) + \beta_{4,\theta}\log\left(\frac{L}{2h_w}\right) + \beta_{5,\theta}\log\left(\frac{V}{V_{cd}}\right) + \beta_{6,\theta}\log\left(\frac{M_{max}}{M_p}\right) + \varepsilon \quad (4.2.1)$$

$$\log\left(k_\theta / M_{max}\right) = \beta_{0,k} + \beta_{1,k}\log\left(\frac{2h_{wc}}{t_w}\right) + \beta_{2,k}\log\left(\frac{b_f}{t_f}\right) + \beta_{3,k}\log\left(\sqrt{\frac{E}{f_y}}\right) + \beta_{4,k}\log\left(\frac{L}{2h_w}\right) + \beta_{5,k}\log\left(\frac{V}{V_{cd}}\right) + \beta_{6,k}\log\left(\frac{M_{max}}{M_p}\right) + \varepsilon \quad (4.2.2)$$

where ε is the error in the observations and assumed independently and identically distributed random variables with mean value = 0 and variance σ^2, or equivalently IID N(0, σ^2).

Performing multiple regression analyses with the hypothesis that $\beta = 0$, we can reject the hypothesis for some of the β's, with a 5 % risk or less. The following values according to table 4.2.1 were found from the analyses using the results from the literature survey (table2.2) and the experimental results (table 4.1.2):

Table 4.2.1 Constants derived from regression analyses

β	$\log\theta_{fk}$	$\log\left(k_\theta / M_{max}\right)$
β_0	2.650	-0.278
β_1	-1.040	-0.867
β_2	-1.707	2.060
β_3	1.546	-1.167
β_4	0	0
β_5	0	0.529
β_6	1.684	-3.365

The Q^2 value expresses the percentage of variation explained by the model and s_e is the standard error of the estimate. These values are presented in table 4.2.2.

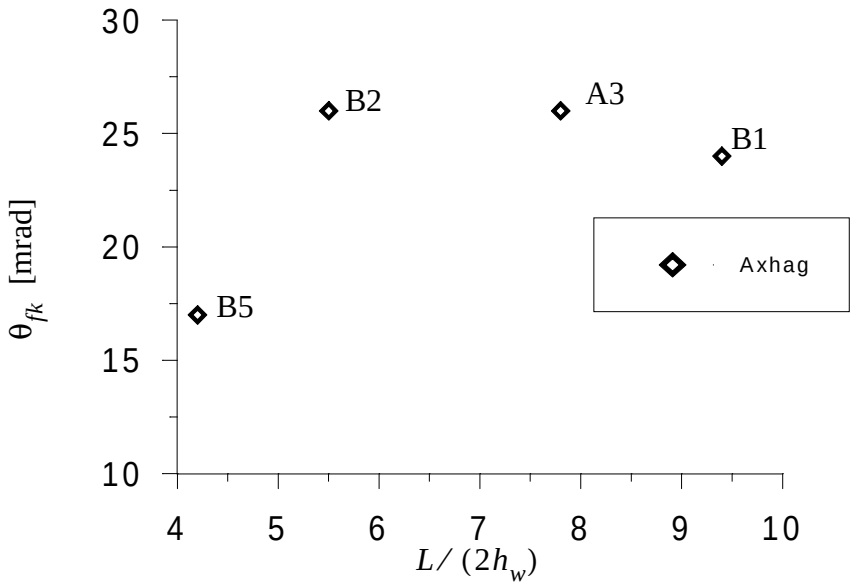

Figure 4.1.17 $\theta_{fk} - L/(2h_w)$ *diagram*

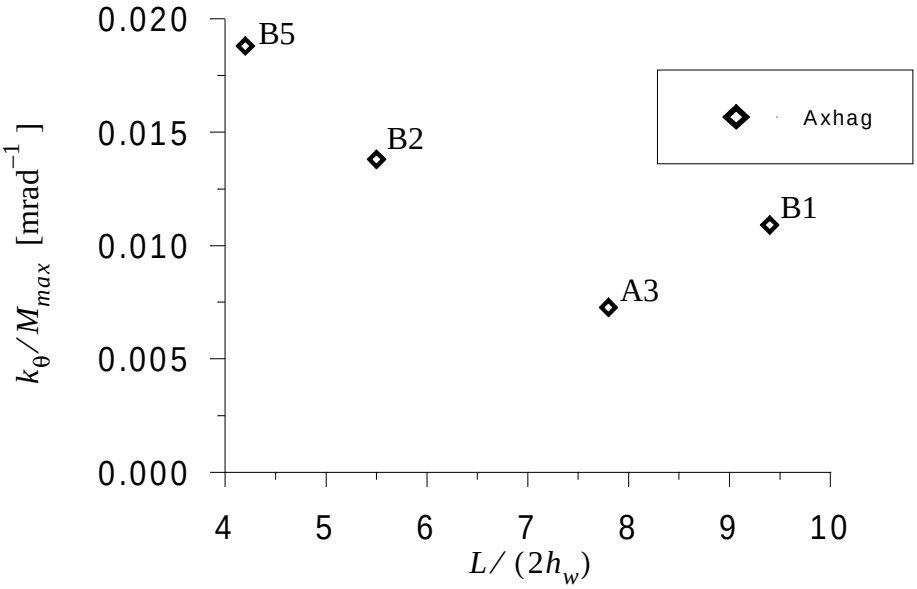

Figure 4.1.18 $k_\theta - L/(2h_w)$ *diagram*

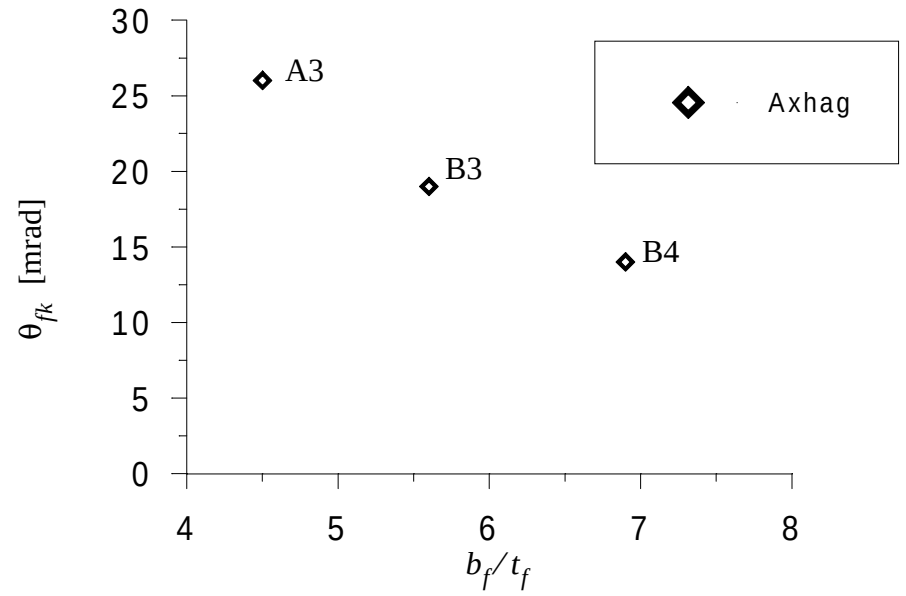

Figure 4.1.15 $\theta_{fk} - b_f/t_f$ *diagram*

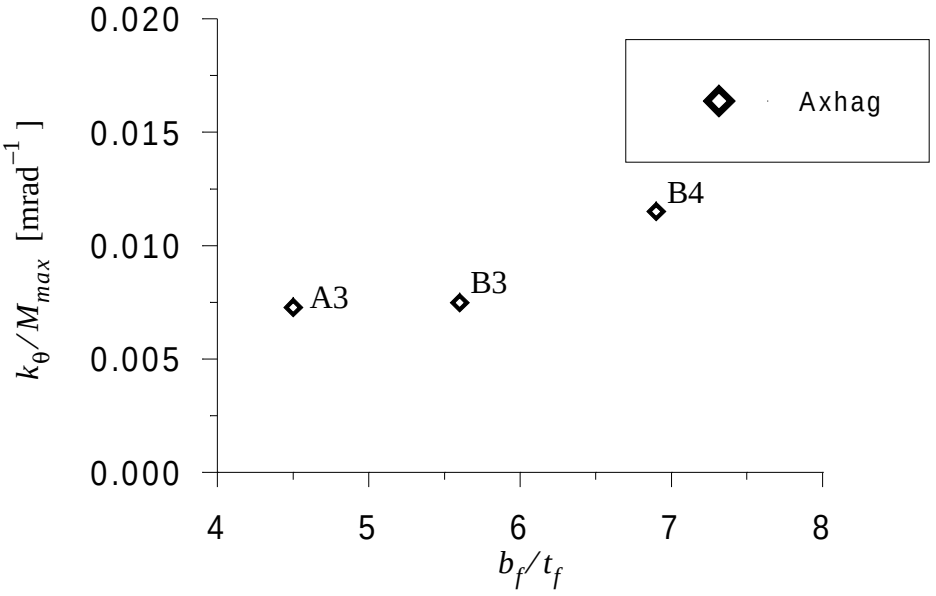

Figure 4.1.16 $k_\theta - b_f/t_f$ *diagram*

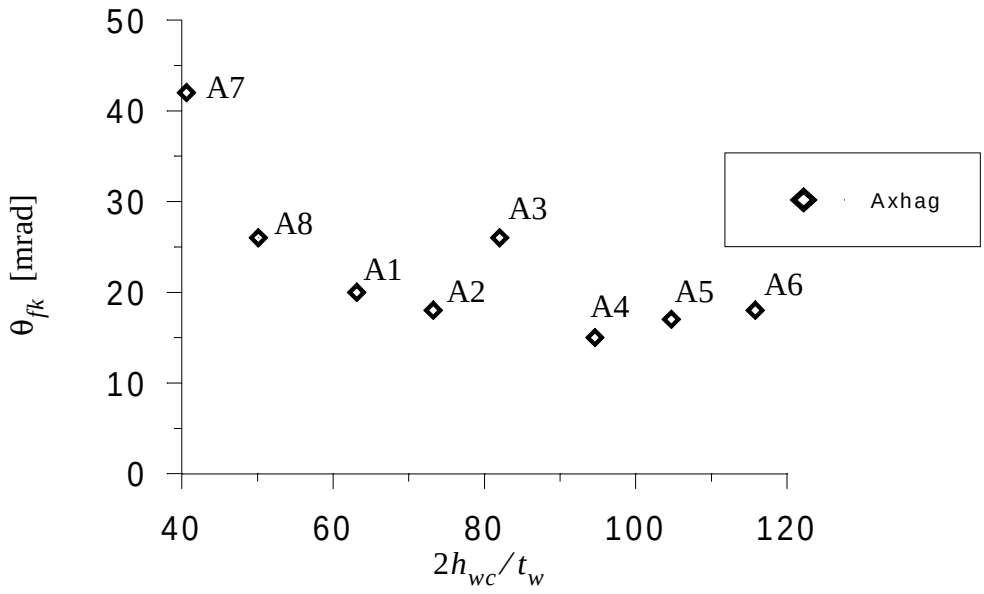

Figure 4.1.13 $\theta_{fk} - (2h_{wc})/t_w$ *diagram*

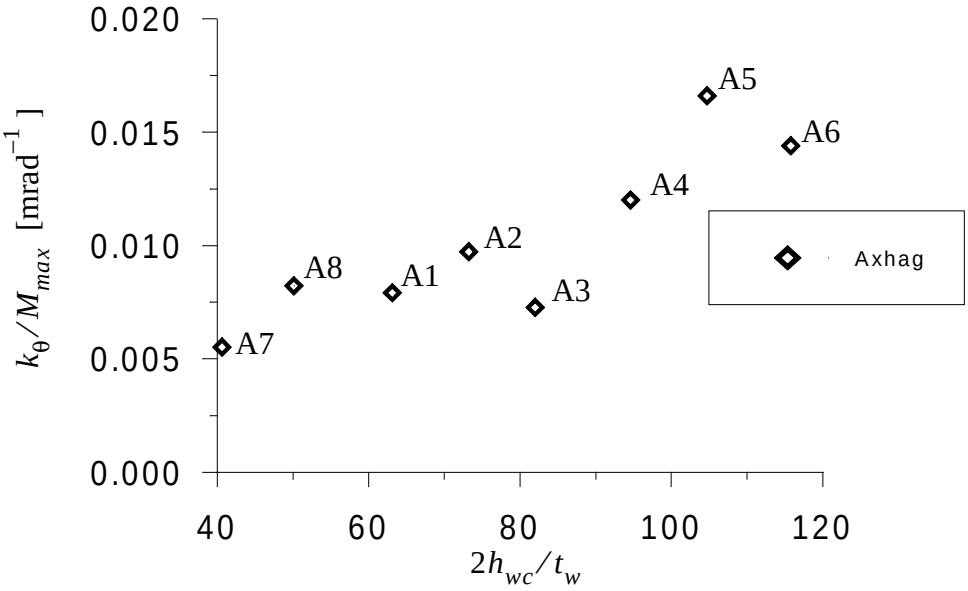

Figure 4.1.14 $k_\theta - (2h_{wc})/t_w$ *diagram*

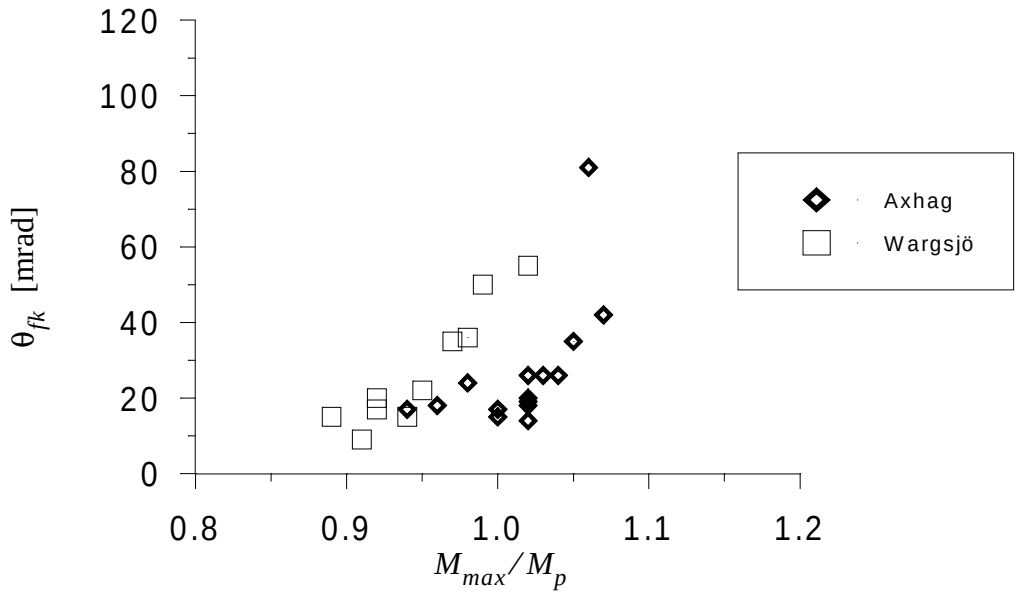

Figure 4.1.11 $\theta_{fk} - M_{max}/M_p$ *diagram*

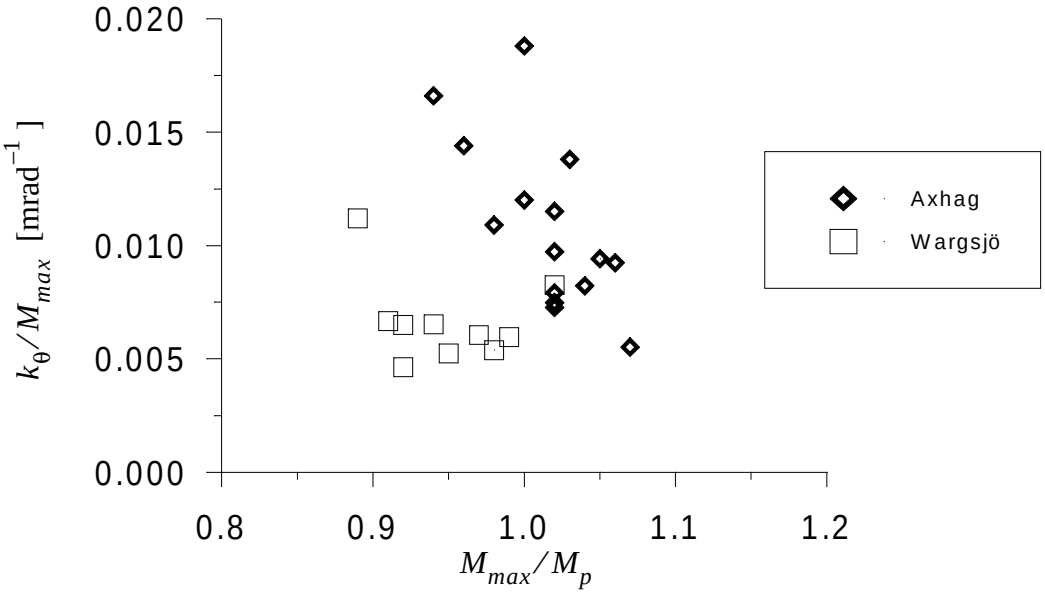

Figure 4.1.12 $k_\theta - M_{max}/M_p$ *diagram*

Plots in figures 4.1.1 to 4.1.12 are difficult to analyse like the plots in chapter two. Therefore additional plots from the laboratory tests only, are added (figures 4.1.13 to 4.1.18). Here θ_{fk} and k_θ/M_{max} are plotted as a function of the variables which were varied in the tests i.e. $(2h_{wc})/t_w$, b_f/t_f and $L/(2h_w)$ (hybrid girders excluded).

Hence in figures 4.1.13 through 4.1.18 only one variable is varied while all the others are kept constant. So for instance in figures 4.1.13 and 4.1.14 only $(2h_{wc})/t_w$ is varied while all the other variables are kept constant.

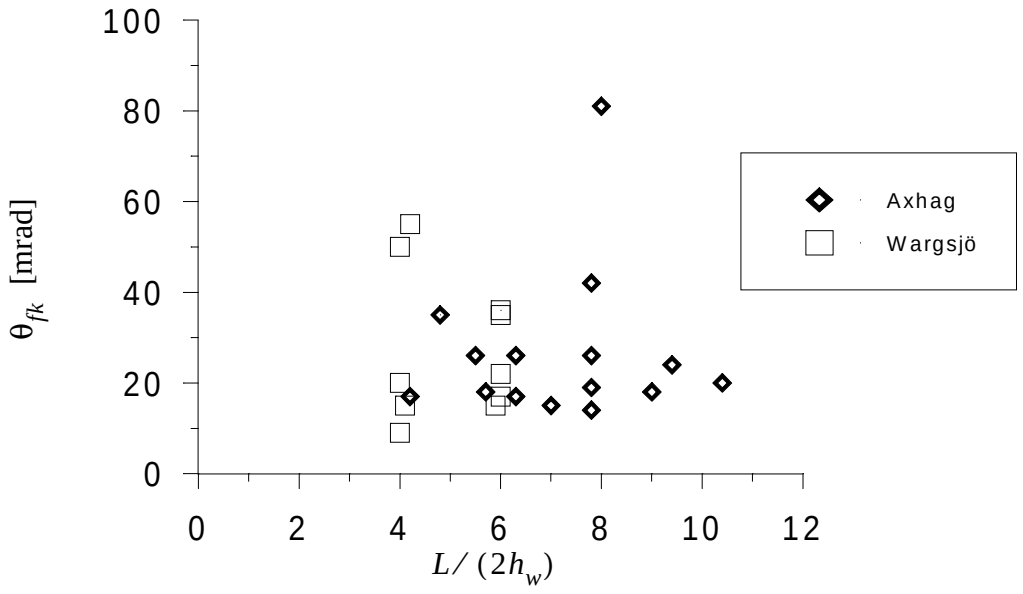

Figure 4.1.9 $\theta_{fk} - L/(2h_w)$ *diagram*

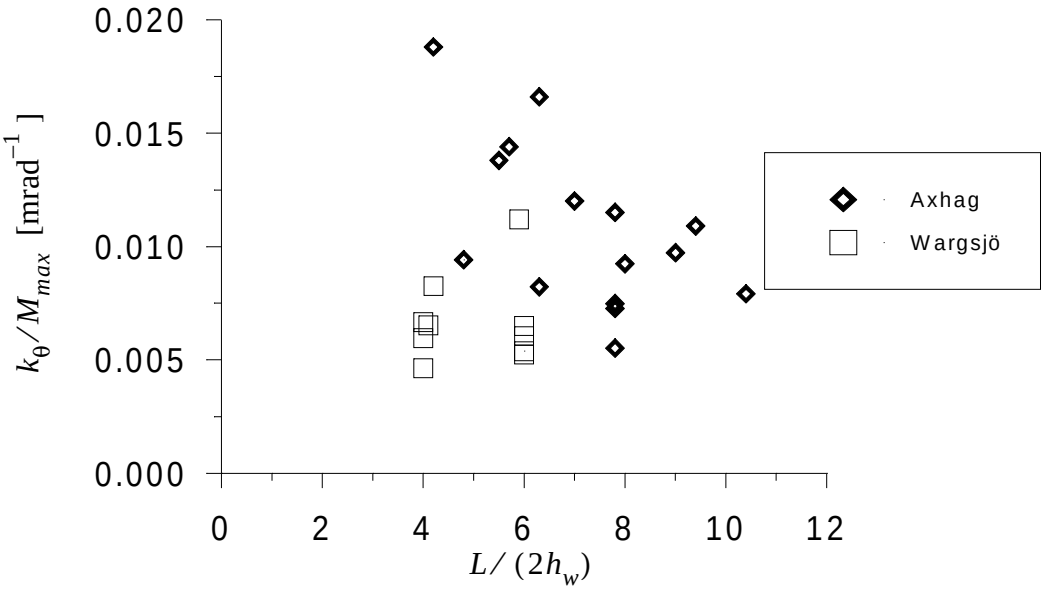

Figure 4.1.10 $k_\theta - L/(2h_w)$ *diagram*

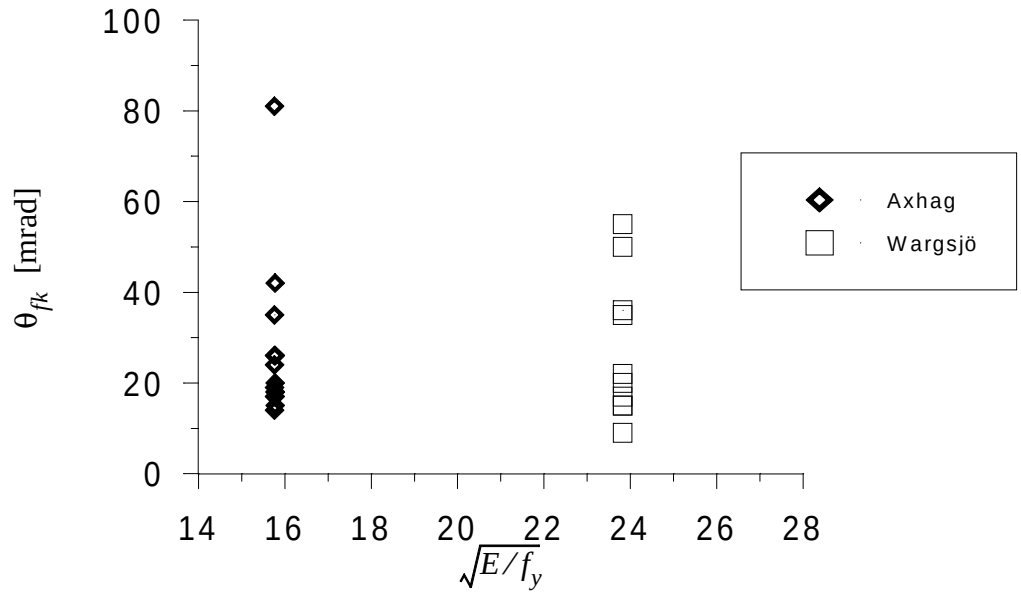

Figure 4.1.7 $\theta_{fk} - \sqrt{E/f_y}$ *diagram*

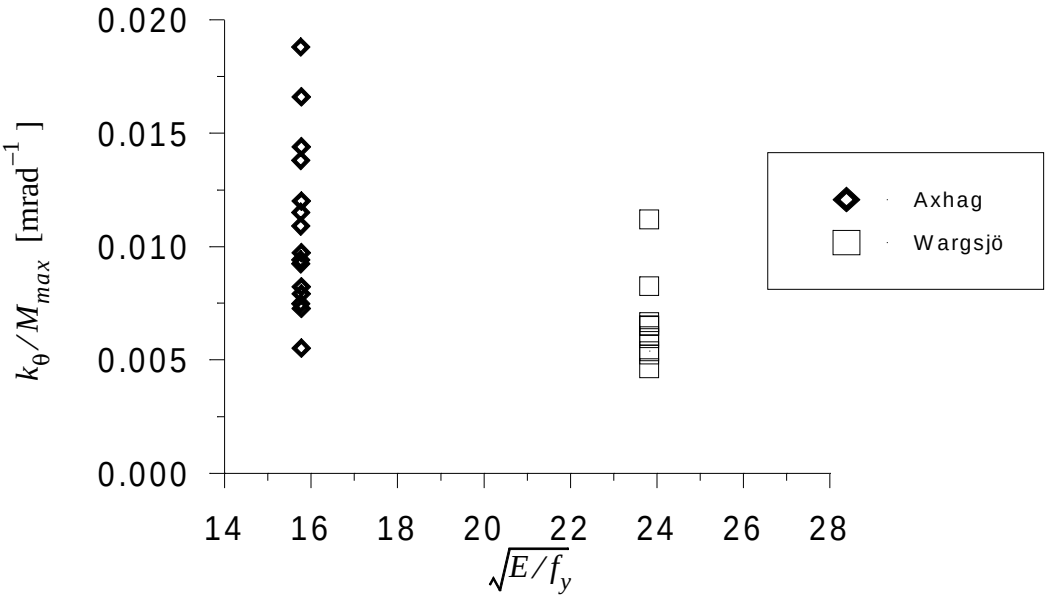

Figure 4.1.8 $k_\theta - \sqrt{E/f_y}$ *diagram*

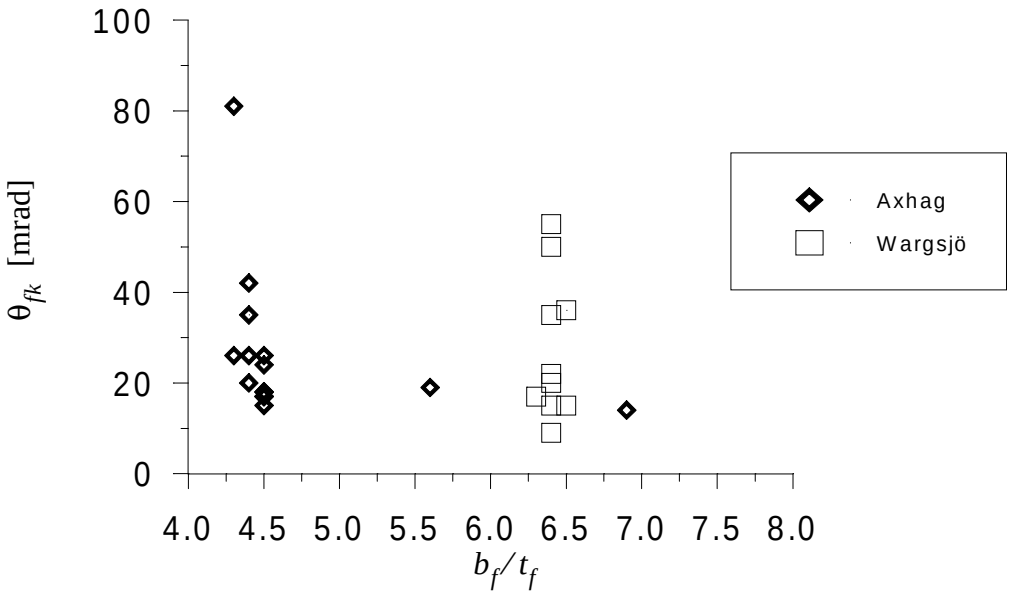

Figure 4.1.5 $\theta_{fk} - b_f/t_f$ *diagram*

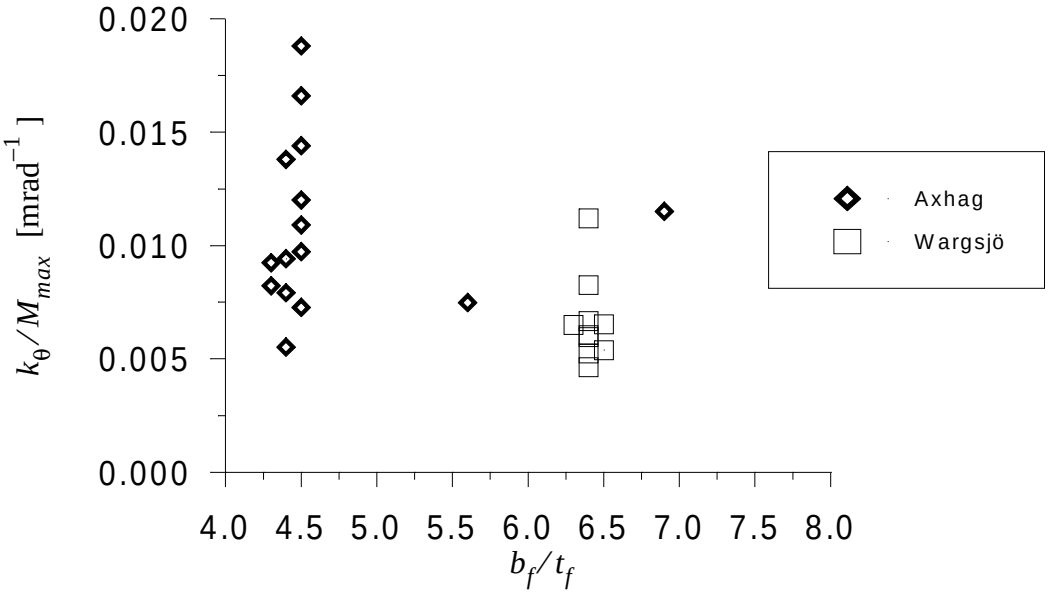

Figure 4.1.6 $k_\theta - b_f/t_f$ *diagram*

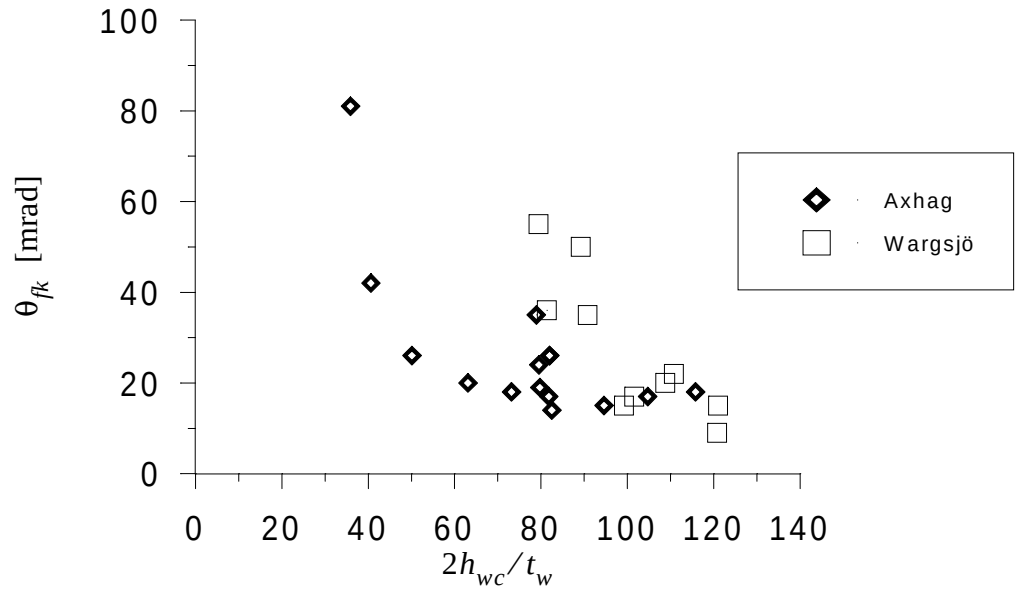

Figure 4.1.3 $\theta_{fk} - (2h_{wc})/t_w$ *diagram*

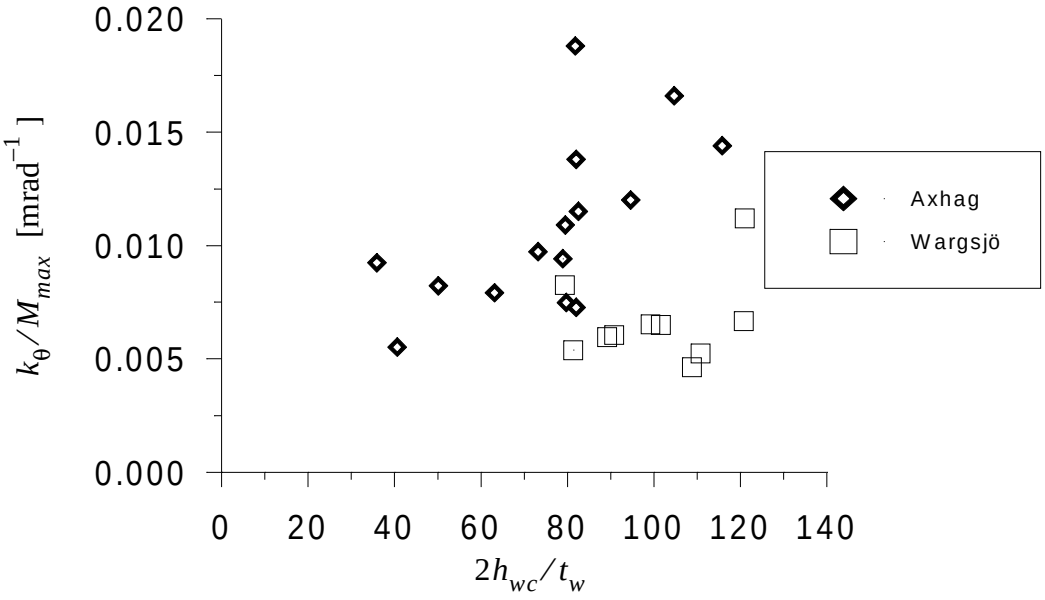

Figure 4.1.4 $k_\theta - (2h_{wc})/t_w$ *diagram*

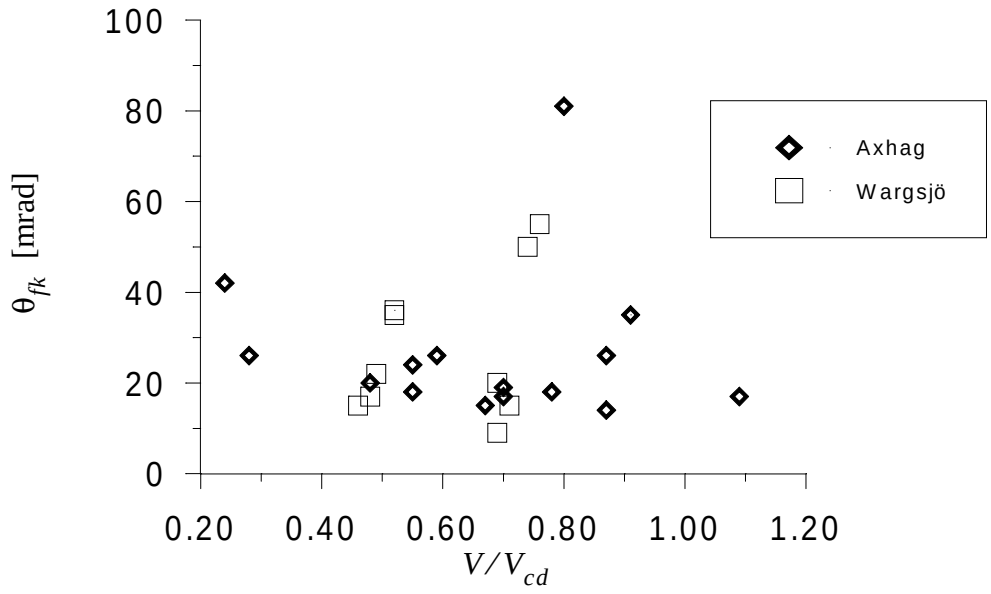

Figure 4.1.1 $\theta_{fk} - V/V_{cd}$ *diagram*

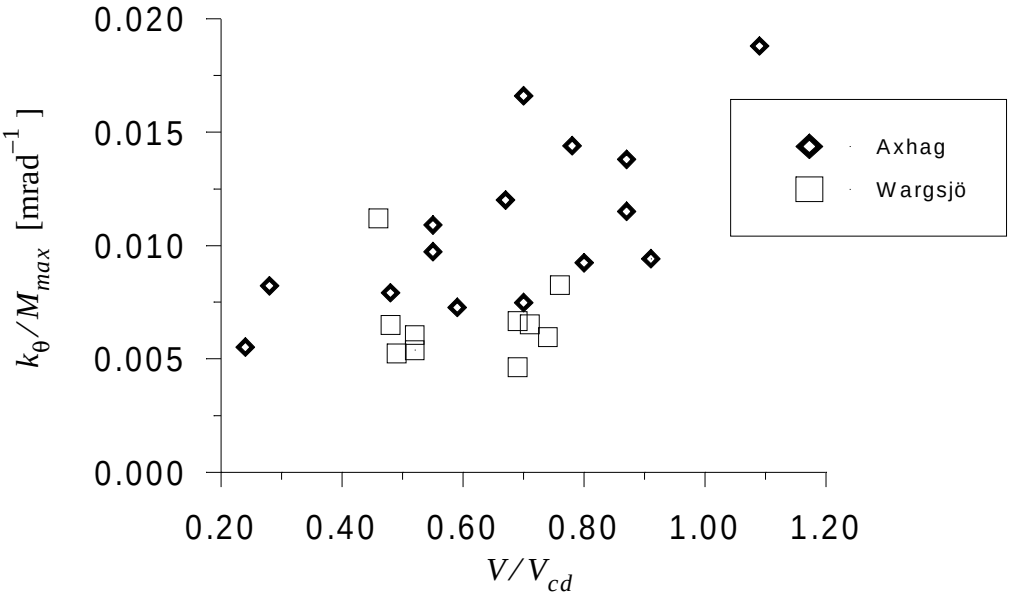

Figure 4.1.2 $k_\theta - V/V_{cd}$ *diagram*

Table 4.1.1 Maximum shear force and moment obtained from tests

B3	241	602
B4	288	719
B5	363	484
HB1	185	325
HB2	318	733

Table 4.1.2 Test results from laboratory tests

Balk	$\frac{2h_{wc}}{t_w}$	$\frac{b_f}{t_f}$	$\sqrt{\frac{E}{f_y}}$	$\frac{L}{2h_w}$	$\frac{V_{max}}{V_{cd}}$	$\frac{M_{max}}{M_p}$	θ_{fk} $[mrad]$	k_θ / M_{max} $[mrad^{-1}]$
A1	63.1	4.4	15.77	10.45	0.48	1.02	20	$7,91 \cdot 10^{-3}$
A2	73.2	4.5	15.77	9.01	0.55	1.02	18	$9,72 \cdot 10^{-3}$
A3	82.0	4.5	15.77	7.83	0.59	1.02	26	$7,27 \cdot 10^{-3}$
A4	94.6	4.5	15.77	6.96	0.67	1.00	15	$12,0 \cdot 10^{-3}$
A5	104.7	4.5	15.77	6.29	0.70	0.94	17	$16,6 \cdot 10^{-3}$
A6	115.8	4.5	15.77	5.69	0.78	0.96	18	$14,4 \cdot 10^{-3}$
A7	40.6	4.4	15.77	7.81	0.24	1.07	42	$5,52 \cdot 10^{-3}$
A8	50.1	4.3	15.77	6.26	0.28	1.04	26	$8,22 \cdot 10^{-3}$
B1	79.5	4.5	15.76	9.43	0.55	0.98	24	$10,9 \cdot 10^{-3}$
B2	82.0	4.4	15.76	5.47	0.87	1.03	26	$13,8 \cdot 10^{-3}$
B3	79.7	5.6	15.76	7.84	0.70	1.02	19	$7,48 \cdot 10^{-3}$
B4	82.5	6.9	15.76	7.76	0.87	1.02	14	$11,5 \cdot 10^{-3}$
B5	81.8	4.5	15.76	4.18	1.09	1.00	17	$18,8 \cdot 10^{-3}$
HB1	35.9	4.3	15.76	8.02	0.80	1.06	81	$9,23 \cdot 10^{-3}$
HB2	78.9	4.4	15.76	4.79	0.91	1.05	35	$9,41 \cdot 10^{-3}$

Table 4.1.2 Test results from laboratory tests

4 Evaluation of laboratory tests

In this chapter an attempt is made to derive the moment-rotation relationship based on the results from the laboratory tests. The test results are presented in table 4.1.1 and 4.1.2 together with those parameters that is believed to influence the moment-rotation relationship.

Plots like the ones in chapter two of the results from the literature survey, have also been made for the results of the fifteen girders from the laboratory tests. In addition the test results from Wargsjö [12] are also included in these plots. Wargsjö's results have been included since these tests are well documented and have been performed in the same laboratory, using the same equipment and test setup. Wargsjö has also used another steel grade which was not varied in the current laboratory tests.

4.1 Presentation of results

The test results in table 4.1.2 and from Wargsjö [12] are plotted in diagram 4.1.1 to 4.1.12. The two variables θ_{fk} and k_θ / M_{max} are plotted against each of the six variables in table 4.1.2. The diagrams are presented to visualize any dependence between the variables versus θ_{fk} and k_θ / M_{max}. It seems however difficult to make any conclusions from the diagrams alone.

Table 4.1.1 Maximum shear force and moment obtained from tests

Balk	V_{max} [kN]	M_{max} [kNm]
A1	141	354
A2	168	422
A3	198	495
A4	220	551
A5	235	589
A6	269	673
A7	239	598
A8	311	779
B1	159	476
B2	291	508

responding increase 100 MPa. In the next part the yield stress is decreased 100 MPa and at the web decreased 200 MPa.

A3-020:

Same as A3-018 but imperfections are introduced in the web and the compressed flange. The maximum imperfection in the flange is 1 mm at the edges and directed towards the lower flange (in tension). The maximum imperfection in the web was also 1 mm and situated 37 mm below the compressed flange.

A3-011:

Same as A3-010 but the $\sigma - \varepsilon$ diagram modified such that E = 0 after f_{uk} is reached.

A3-012:

Same as A3-011 but the number of integration points over the thickness of the elements is increased from five to eleven.

A3-013:

Same as A3-011 but the yield strength of the material in the compressed flange has been increased 100 MPa at the edges and decreased 100 MPa in the vicinity of the web. This is a way of implementing residual stresses in the model.

A3-014:

Same as A3-011 but the $\sigma - \varepsilon$ diagram has been modified such that E < 0 after f_{uk} is reached.

A3-015:

Same as A3-011 but only a quarter of the girder is modelled (the symmetryplanes used are one through the vertical stiffener at midspan and one in the plane of the web). However the model did not converge.

A3-016:

Same as A3-013 but the imperfection in the compressed flange is decreased to 0.5 mm. The yield strength of the material in the compressed flange has been increased an additional 100 MPa at the edges and decreased an additional 100 MPa in the vicinity of the web, compared to A3-013.

A3-017:

Same as A3-009 but the elements in the midpart are 9-node shell elements, S9R5 in ABAQUS. The 4-node shell elements are changed to S4R5 from S4R.

A3-018:

The mesh is refined in the midpart of the girder.

A3-019:

Same as A3-018 but the effect of residual stresses have been accounted for. The compressed flange have been divided in eight parts, four on each side of the web, over the width. At the edges the yield stress of the material has been increased by 200 MPa. In the adjacent part is the cor-

A3-002:

Imperfection in compressed flange included in the model. Imperfection 1 mm situated approximately 100 mm from midspan.

A3-003:

The element mesh is made coarser at midspan of the girder.

A3-004:

Imperfection in compressed flange included with + 1 mm imperfection at one edge and - 1 mm at the other edge of the flange. The imperfection decreases to zero on a length of 107 mm on both sides of the maximum imperfection. The maximum imperfection is situated approximately 100 mm from midspan.

A3-005:

Same model as A3-004 but the imperfection is increased from 1 mm to 5 mm.

A3-006:

It is the same model as A3-003 but the whole girder is modelled (not just half the girder).

A3-007:

The same model as A3-001 but the $\sigma - \varepsilon$ diagram is modified such that the yield plateau has been taken away.

A3-008:

The yield plateau $\sigma - \varepsilon$ diagram is modified such that the yield plateau has been taken away (as in A3-007). In addition the element mesh has been refined in midspan of the girder.

A3-009:

The element mesh has been refined (as in A3-008). In addition an imperfection of + 2 mm at one edge of the compressed flange and - 2 mm at the other edge. An imperfection of 1 mm is also included in the web. The $\sigma - \varepsilon$ diagram has been refined in the hardening range such that the slope has been modelled more exact

A3-010:

8-node shell elements are used in the midpart of the girder. Also the $\sigma - \varepsilon$ diagram is modified such that no yield plateau is included. In the compressed flange a imperfection of + 1 mm at one edge and - 1 mm at the other edge is included near midspan.

Table 5.1 Matrix representation of variation of FEM-models from A3-001

Model	1[a]	2[b]	3[c]	4[d]	5[e]	6[f]	7[g]	8[h]	9[i]	10[j]	11[k]	12[l]	13[m]
A3-002	*												
A3-003			*										
A3-004	*												
A3-005	*												
A3-006			*			*							
A3-007							*						
A3-008				*			*						
A3-009	*	*		*									
A3-010	*						*			*			
A3-011	*						*	*		*			
A3-012	*						*	*		*		*	
A3-013	*						*	*		*			*
A3-014	*						*		*	*			
A3-015	*				*		*	*		*			
A3-016	*						*	*		*			*
A3-017	*	*		*							*		
A3-018				*									
A3-019				*									*
A3-020	*	*		*									

a. Imperfection in flange
b. Imperfection in web
c. Coarser element mesh
d. Finer element mesh
e. One quarter of the girder modelled
f. The whole girder modelled
g. No yield plateau in sigma-epsilon diagram
h. E = 0 after f_{uk} is reached
i. E < 0 after f_{uk} is reached
j. 8-node elements in midpart of model
k. 9-node elements in midpart of model
l. Increase of integration points over the thickness of the elements
m. Residual stresses in flange

A3-001:

Referencemodel with 776 elements and 801 nodes, using S4R and STRI35 elements in ABAQUS.

5. FEM analyses

Based on the results from the experiments, the intention was to develop a FEM computer model which could simulate the behaviour of the tested girders. The girder A3 was chosen to be modelled first in the computer. For this the FEM program ABAQUS [23] was employed. Various parameters in the model were varied trying to match the experimental moment-rotation relationship with the one derived from the computer model. A total of 20 runs were performed, numbered A3-001 to A3-020, each varying one parameter. A short description of each run is presented in this chapter and a table is provided for clearness.

The simulations were however stopped after the 20th simulation, due to lack of time in the project. Some of the best simulations conform fairly well to the experimental results. It is believed that the conformity can be further improved and then be checked for all the other girders. This work has however been postponed for a later stage. In appendix E, comparisons of experimental and FEM moment-rotation relationships are presented.

The main problem is that the FEM-model appears stiffer in the descending part of the moment-rotation relationship compared to the test results. Table 5.1 shows the differences of the nineteen analyses from the reference model A3-001. Following the table is a short description of each model.

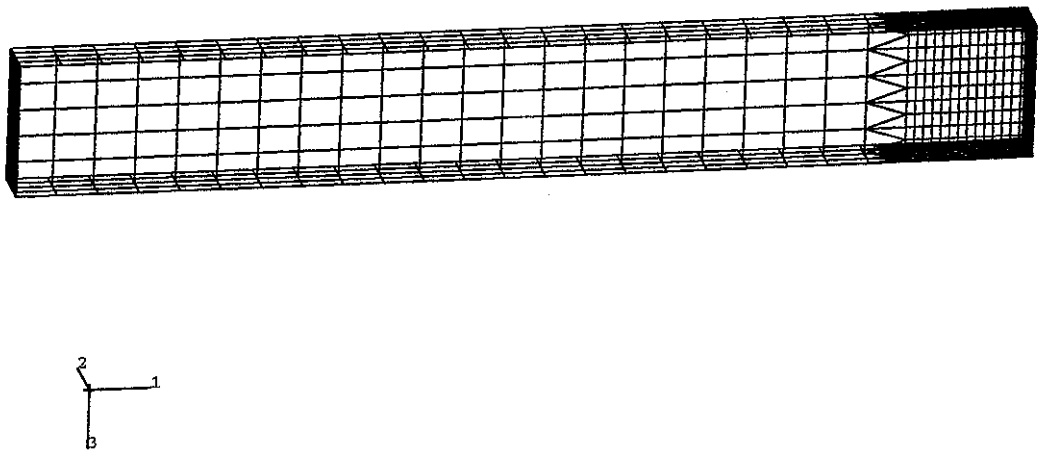

Figure 5.1 FEM-mesh of reference model A3-001 using shell elements

$$\theta_B = 0,7578 \cdot \frac{M_P L}{EI}$$

If we had assumed the last plastic hinge to occur at B then we would have put $\theta_B = 0$ and the result would have been:

$$\theta_C = 0,3258 \cdot \frac{M_P L}{EI}$$

Thus θ_C is positive while $M_C = -M_P$ is negative. Thus this is not the correct mechanism as the work in a plastic hinge always is positive.

The purpose of the simple example given, is to demonstrate the use of the principle of virtual work when determining the plastic rotations in the plastic hinges. In the example the last hinge to form was at the internal support and hence the hinge in B had to undergo plastic rotation. For a composite bridge this is usually not a problem since the cross-section in midspan often have sufficient plastic rotation capacity. The problem arises when the first hinge to form is the one at the internal support. This section has less rotation capacity compared to the one at midspan.

A composite bridge is subjected to both concentrated and distributed loads. It also has a varying flexural stiffness EI along the length of the bridge. This will make the use of (6.2) more laborious but the equation is still valid. If the rotation capacity θ_{fk} for a cross section is not sufficient and the descending part of the moment-rotation curve has to be employed, then an iterative procedure could be used. A reduced moment capacity is then tried thus enabling to take into account a larger rotation capacity θ_{fk}. This reduced moment from the moment-rotation relationship shall be equal (or greater) than the assumed moment capacity at the support. The method is examplified in chapter 8.

After a plastic hinge has formed in B the plastic rotation in this point is according to (6.9). The elastic rotation in C is then, using (6.4), (6.5) and (6.8):

$$\varphi_C = 0 + \frac{L}{3 \cdot EI} \cdot \frac{1}{1,754} (PL - 4,080 M_P) = \frac{L}{6 \cdot EI} (1,1402 PL - 4,6522 M_P)$$

At the start of rotation in the plastic hinge in B φ_C is:

$$\varphi_C = 0,1409 \cdot \frac{M_P L}{EI}$$

A mechanism is developed when φ_C is:

$$\varphi_C = \frac{1}{3} \cdot \frac{M_P L}{EI}$$

and at the same time the plastic rotation in B, using (6.9), is:

$$\theta_B = \frac{L}{6 \cdot EI} (-7,8723 (-M_P) - 3,3256 M_P) = 0,7578 \cdot \frac{M_P L}{EI}$$

Hence, $\theta_B = 0,7578 \cdot \frac{M_P L}{EI}$ is the required plastic rotation at midspan just before a plastic hinge is developed in C.

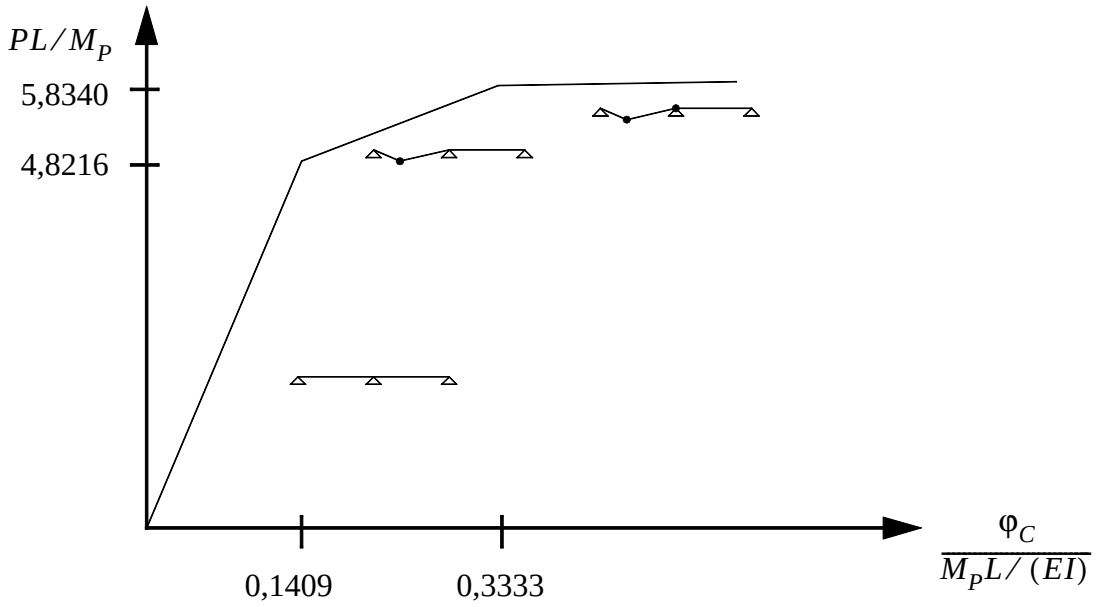

It is not necessary to go through the loading sequence as we did previously to find the plastic rotation at collapse. This can be calculated directly by putting $M_B = M_P$, $M_C = -M_P$ and $\theta_C = 0$ in equation (6.7):

$$P < \frac{M_P}{0,2074L} \approx 4,8216 \cdot \frac{M_P}{L}$$

When P exceeds this value, a plastic hinge will form at B and $M_B = M_P$. With a plastic hinge at B, (6.6) becomes:

$$M_C = \frac{1}{1,754}(4,080M_P - PL) \tag{6.8}$$

and (6.7) with $\theta_C = 0$:

$$\theta_B = \frac{L}{6 \cdot EI}(7,8723M_C - 3,3256M_P) \tag{6.9}$$

A plastic hinge will form at C when $M_C = -M_P$. Equation (6.8) then give:

$$P = 5,834 \cdot \frac{M_P}{L}$$

At this point a mechanism is formed. To calculate the rotation at point C, a virtual moment $\delta M = 1$ is applied in point C. The only requirement is that the moment distribution is in equilibrium with the virtual moment δM. There are an infinite number of such distributions. Let us choose one with part ABC being a cantilever which yields a virtual moment distribution given by figure 6.4

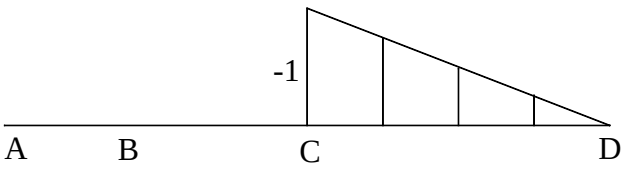

Figure 6.4 Virtual moment distribution.

Equations (6.4) and (6.5) give:

$$\varphi_C = (-1)\,\theta_C + \frac{L}{6 \cdot EI} \cdot 2\,(-1)\,M_C = 0 + \frac{L}{3 \cdot EI} \cdot 0,087PL = 29,2 \cdot 10^{-3} \cdot \frac{PL^2}{EI}$$

Where φ_C denotes elastic rotation in C. The same procedure for calculation of elastic rotation in B can be performed by applying a virtual moment in B.

The rotations θ in figure 6.2 gives

$$\theta_A = \frac{d}{0,43L} \qquad \theta_B = d\left(\frac{1}{0,43L} + \frac{1}{0,57L}\right) \qquad \theta_C = -\frac{d}{0,57L}$$

The principle of virtual work gives:

$$M_B \cdot d\left(\frac{1}{0,43L} + \frac{1}{0,57L}\right) - M_C \cdot \frac{d}{0,57L} = P \cdot d$$

$$4,080 \cdot M_B - 1,754 \cdot M_C = P \cdot L \qquad (6.6)$$

This equilibrium equation must always hold. The minus sign in (6.6) is because M_C is negative therefore θ_c must be negative since work in hinges always is positive.

The number of redundancy of the girder is one, therefore one residual bending moment set, δm exists.

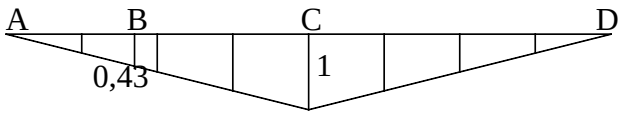

Figure 6.3 Residual bending moment δm.

Equations (6.3) and (6.5) yields:

$$0,43 \cdot \theta_B + \theta_C + \frac{0,43L}{6 \cdot EI}\left[2\,(0 + 0,43M_B) + 0\right] +$$

$$+ \frac{0,57L}{6 \cdot EI}\left[2\,(0,43M_B + M_C) + (M_B + 0,43M_C)\right] + \frac{L}{6 \cdot EI}\left(\left[2\,(M_C + 0) + 0\right]\right) = 0$$

$$0,43\theta_B + \theta_C + \frac{L}{6 \cdot EI}\left[1,4300M_B + 3,3851M_C\right] = 0 \qquad (6.7)$$

For an elastic solution, $\theta_B = \theta_C = 0$ and equations (6.6), (6.7) give:

$$M_B = 0,2074PL \qquad M_C = -0,0876PL$$

This elastic solution is valid as long as M_B and M_C are less than M_p or equivalent when:

If for simplicity only concentrated loads acts upon the girder then M varies linearly along the girder. The residual moment δm always vary linearly. If also EI = constant then

$$\int_0^L \delta m \cdot \frac{M}{EI} dx = \frac{L}{6 \cdot EI} [2 (M_A \delta m_A + M_B \delta m_B) + (M_A \delta m_B + M_B \delta m_A)] \qquad (6.5)$$

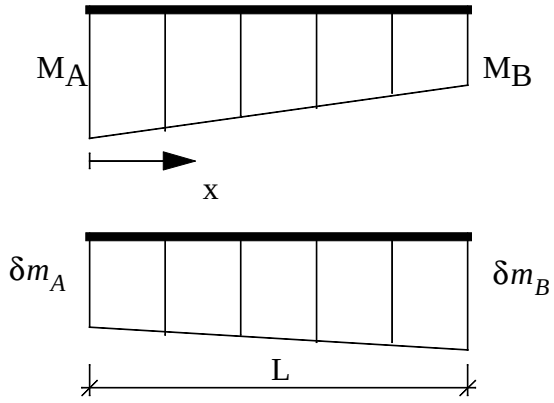

Figure 6.1 Linearly varying M and δm.

An example of the use of the principle of virtual work is presented below.

Example:

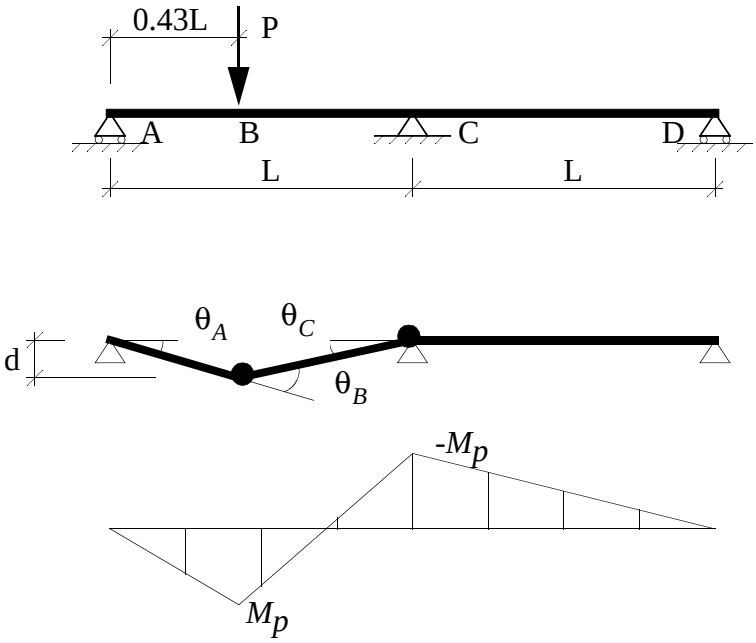

Figure 6.2 Two span girder with concentrated load P and plastic hinge mechanism.

6. Required Rotation Capacity

In the previous chapters, effort has been put in to determine the available rotation capacity θ_{fk} of steel girders. θ_{fk} must however be related to the required rotation capacity θ_{rk} for a mechanism to form. Calculation of θ_{rk} can be performed by different methods. One method is the moment-area method described in for example [3] where use is made of the equation:

$$\kappa = -\frac{d^2 y}{dx^2} \text{ (small to moderate deflections)} \qquad (6.1)$$

If the moment-curvature relationship is known then the end slope θ can be computed from the area under the curvature diagram.

Another method, which is employed in this chapter, is the principle of virtual work described in for example [13], [14] and [15]. The principle of virtual work states according to [13] that if a body in equilibrium is given a set of small displacements, then the work done by the external loads on the external displacements is equal to the work done by the internal forces on the internal displacements. The following is valid:

- The system of displacements must be compatible i.e. internal deformations must correspond to external displacements. The body may however be arbitrarily distorted without reference to any loading system, hence the word virtual.

- Internal forces must be in equilibrium with external loads, but the internal forces need not to be the actual forces due those loads. Any equilibrium set of forces may be used in the equation of virtual work.

In this chapter we are seeking the real deformations of the girder, therefore the real deformations of the girder will be combined with equilibrium states which might have nothing to do with the actual loading on the girder.

Studying elastic-plastic deformations we have elastic curvature M/EI and plastic hinge discontinuities θ, leading to deflections Δ. Virtual bending moments δM are in equilibrium with external virtual loads δF. According to [14], the principle of virtual work then gives:

$$\sum \delta F \cdot \Delta = \sum \delta M \cdot \theta + \int \delta M \cdot \frac{M}{EI} ds \qquad (6.2)$$

Since we are working with statically indeterminate structures we can always find residual moments, $\delta m = \delta m(s)$ to exist in the girder which are in self equilibrium. Then we have from (6.2):

$$\sum \delta m \theta + \int \delta m \cdot \frac{M}{EI} ds = 0 \qquad (6.3)$$

When the state of the girder is known from (6.3) the deflections Δ can be determined by again using (6.2) and $\delta F = 1$, which yields:

$$\Delta = \sum \delta M \cdot \theta + \int \delta M \cdot \frac{M}{EI} ds \qquad (6.4)$$

To give a sense of the magnitude of equation (7.4.4) we put in the values used in the example of chapter 8 we get:

$$\theta_{cs,\,\Delta T} = \frac{1500 \cdot 10^{6} \cdot 80 \cdot 10^{3}}{2 \cdot 2,1 \cdot 10^{5} \cdot 43,3 \cdot 10^{9}} \approx 7 \cdot 10^{-3} \text{ rad}$$

This rotation is larger than from linearly varying temperature and differential settlement. It is not obvious which is most favourable, to decrease the the rotation capacity by $\theta_{cs,\,\Delta T}$ or using the constraint forces from shrinkage and different temperature in design.

To sum up our findings from the two span bridge example, the table below suggests the required plastic rotation at the internal support to cancel out the forces from constraints. In the cases where it might be better to include the constraint forces in the design instead of cancelling them out an “F” (meaning include **F**orces instead of plastic rotation in calculations) is marked in the table.

Table 7.4.1

		Linearly varying temperature		Differential settlement		Different temperature in concrete and steel		Shrinkage
Required plastic rotation at internal support	Check of cross-section at internal support	1.5 mrad	0	2 mrad	0	“F” or $\theta_{\Delta T}$	“F” or $\theta_{\Delta T}$	“F” or θ_{cs}
	Check of cross-section at mid-span	1.5 mrad	0 or “F”	2 mrad	0 or “F”	“F” or $\theta_{\Delta T}$	“F” or $\theta_{\Delta T}$	“F” or θ_{cs}

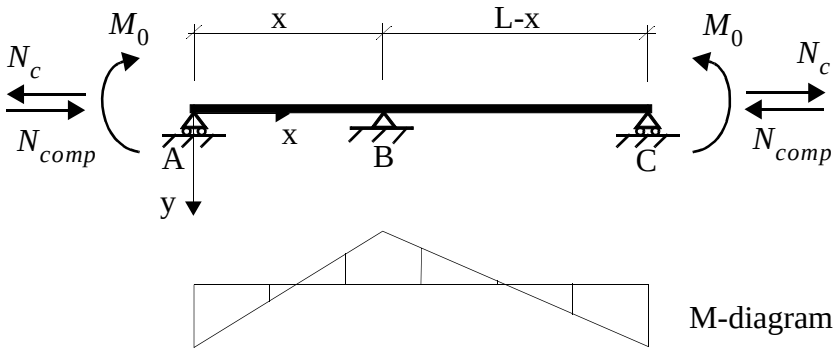

Figure 7.4.6 Moment diagram from different temperature in concrete and steel or from shrinkage in concrete.

If we cut the girder at the internal support B we would get two simply supported girders with a discontinuity at the support corresponding to the amount of plastic rotation to cancel out shrinkage or different temperature in steel and concrete, see figure 7.4.7.

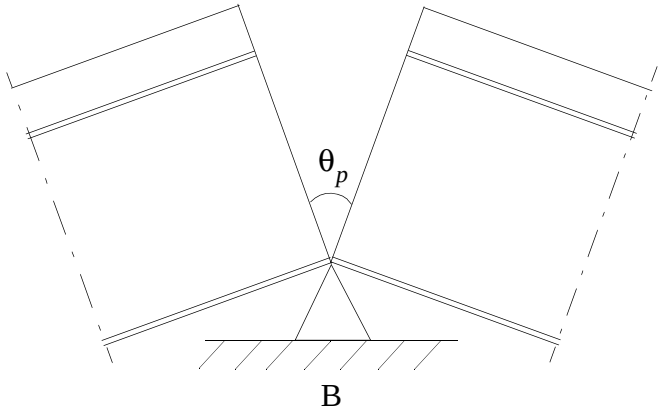

Figure 7.4.7 Bridge subjected to shrinkage and different temperature "cut" at the interior support.

There are still stresses present in the two "simply supported" parts from shrinkage and different temperature. These stresses are refered to primary effects in EC4, part 2 and need not be considered in design. The "cutting" of the bridge at the internal support relieves the stresses from the continuity of the bridge. These stresses are refered to secondary effects and shall be considered in design according to EC4, part 2.

By applying the same procedure as for linearly varying temperature and differential settlement (see figure 7.4.4.), we can write (deflection y from concentrated, equal moments at the ends of the bridge):

$$\theta_{cs,\Delta T} = \theta_1 + \theta_2 = y_{cs,\Delta T}\left(\frac{1}{x} + \frac{1}{L-x}\right) = \frac{M_0 L \cdot x}{2EI} \cdot \left(\frac{1}{x} + \frac{1}{L-x}\right) = \frac{M_0 L}{2EI} \qquad (7.4.4)$$

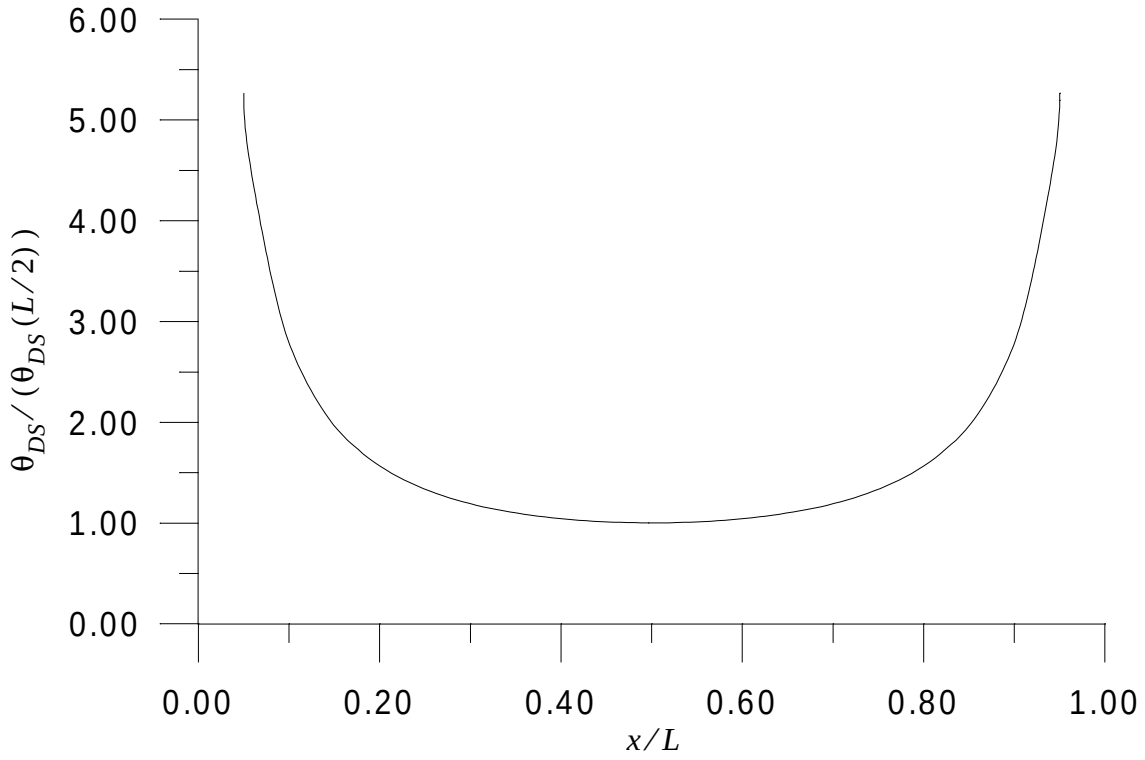

Figure 7.4.5 $\theta_{DS}/\theta_{DS}(L/2)$ *as a function of* $x = L/2$.

The linearly varying temperature can of course be of opposite sign and the differential settlement may appear at the internal support giving a moment diagram of opposite sign to that presented in figure 7.4.2. Such a moment diagram giving tensile stresses in the bottom flange at the internal support (and at all other cross-sections) can be disregarded as this is a conservative approach for the cross-section at the internal support.

For a cross-section at midspan with tension in the bottom flange from temperature and settlement, the influence of these imposed deformations can be neglected if the first plastic hinge forms at midspan and the plastic rotation is such of an amount that it cancels out the imposed deformations. In other cases the forces from constraints have to be included in the design.

If we finally assess the case where we have different temperature in steel and concrete, see figure 7.4.1 or shrinkage in concrete and use the example of a two span bridge as previous , we get a moment diagram according to figure 7.4.6. The model to take into account shrinkage and different temperature consists of applying moments and normal forces at the ends of the bridge. The normalforce N_c acts only on the concrete and corresponds to free shrinkage or temperature difference. The direction of forces in figure 7.4.6 is for shrinkage or with regards to temperature when the concrete slab is colder than the girders.

N_{comp} acts on the whole composite section and the moment M_0 is an eccentricity moment that is applied when N_{comp} is moved from the center of the concrete slab to the gravity center of the composite section.

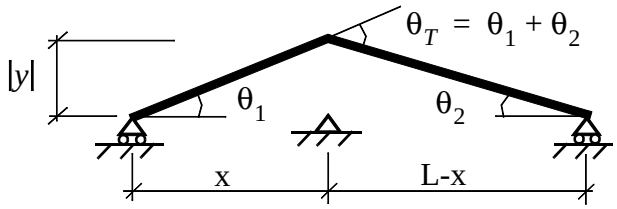

Figure 7.4.4 Permanent deflection $|y|$ from plastic rotation at support assuming girder set free.

Using the geometry from figure 7.4.4 and equation (7.4.2):

$$\theta_T = \theta_1 + \theta_2 = y_T\left(\frac{1}{x} + \frac{1}{L-x}\right) = \frac{\varepsilon_T \cdot L}{2H}\left(x - \frac{x^2}{L}\right) \cdot \frac{L}{x\,(L-x)} = \frac{\varepsilon_T \cdot L}{2H} \qquad (7.4.3)$$

If we set all load coefficients $\psi\gamma$ (Bro 94) equal to unity, the design value of ε_T is:

$$\varepsilon_T = \psi\gamma \cdot \alpha \cdot \Delta T = 1,0 \cdot 1 \cdot 10^{-5} \cdot 10 = 1,0 \cdot 10^{-4}$$

Assume $L/H = 20$ then

$$\theta_T = \frac{1,0 \cdot 10^{-4}}{2} \cdot 20 = 1,0 \cdot 10^{-3}$$

Thus the required plastic rotation at internal support to cancel out linearly varying temperature would be 1.0 mrad.

Performing a similar assessment for differential settlement with settlements of the end supports we find from Bro 94 that the design settlement is:

$$y_{DS} = \psi\gamma_{max} \cdot y_{k,\,DS} = 1,0 \cdot 10 = 10 \;\; mm$$

Using equation (7.4.3) we get:

$$\theta_{DS} = y_{DS}\left(\frac{1}{x} + \frac{1}{L-x}\right) = y_{DS} \cdot \frac{L}{x\,(L-x)}$$

$\theta_{DS} = \theta_{DS}(x)$ has a minimum for $x = L/2$. Plotting $\theta_{DS}/\theta_{DS}(L/2)$ as a function of x/L according to figure 7.4.5, we see that the required plastic rotation increases rapidly if the length of the spans differ substantially. One conclusion from this is that a plastic design method will be less suitable the more the lengths of the spans differ. However, for all realistic span ratios the value $\theta_{DS}/\theta_{DS}(L/2) \approx 1$. For $x = L/2$ and L = 20 m $\theta_{DS} = 2 \cdot 10^{-3} = 2 \;\; mrad$.

Let us estimate the amount of plastic rotation at midspan that is required to cancel out linearly varying temperature and differential settlement at end supports according to figure 7.4.2. If we first assess the linearly varying temperature and remove the internal support, the linear stress distribution according to figure 7.4.3 will exist for all cross-sections in the girder. There will be no normal stresses but the girder will deflect y_T.

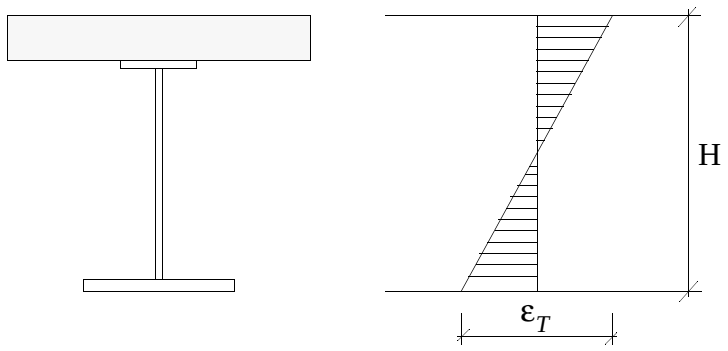

Figure 7.4.3 Strain distribution over the depth of the girder from linearly varying temperature.

With a coordinate system according to figure 7.4.2 the curvature from linearly varying temperature is:

$$\kappa = \frac{d^2 y_T}{dx^2} = -\frac{\varepsilon_T}{H} \tag{7.4.1}$$

Integrating two times gives:

$$y_T = -\frac{\varepsilon_T \cdot x^2}{2H} + C_1 x + C_2$$

Boundary conditions $y_T(0) = y_T(L) = 0$ yields:

$$y_T = \frac{\varepsilon_T \cdot L}{2H}\left(x - \frac{x^2}{L}\right) \tag{7.4.2}$$

If the girder was set free from the internal support, the plastic rotation at the internal support that would leave a permanent deflection of y_T in the negative direction, would be the sought rotation that would cancel out the moment from linearly varying temperature, see figure 7.4.4.

7.4 Effects of imposed deformations

According to the Swedish bridge code, Bro 94, effects of temperature, shrinkage and differential settlement shall be accounted for in the ultimate limit states. However, these loads originate from constraints which implies that if the bridge undergoes sufficient plastic deformations, these effects will disappear. It would be preferable if these effects could be disregarded in ultimate limit states as this would simplify the design work. An attempt is therefore made in this chapter to assess if these loads can be neglected.

Temperature can either be linearly varying over the depth of the girder or different temperatures may exist in the concrete slab and the steel girder according to Bro94, see figure 7.4.1.

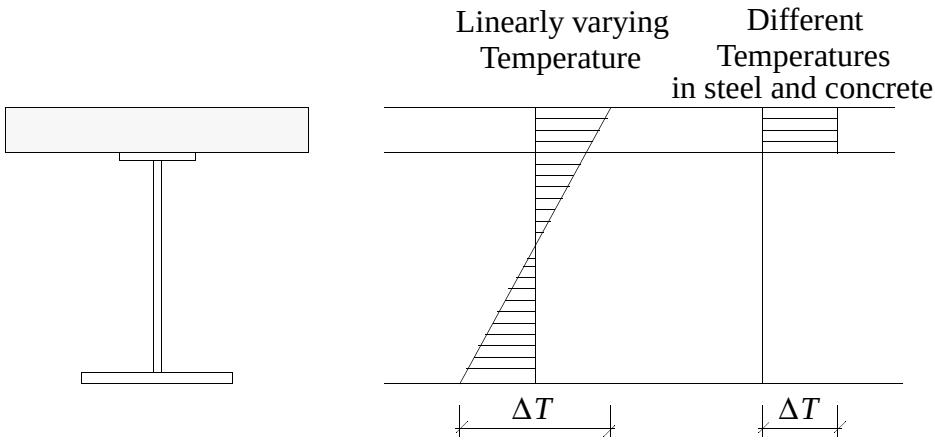

Figure 7.4.1 Temperature gradient over depth of cross section

The linearly varying temperature, with the higher temperature at the lower flange and differential settlement in positive y-direction at the end supports, give rise to a moment diagram for a two span bridge according to figure 7.4.2.

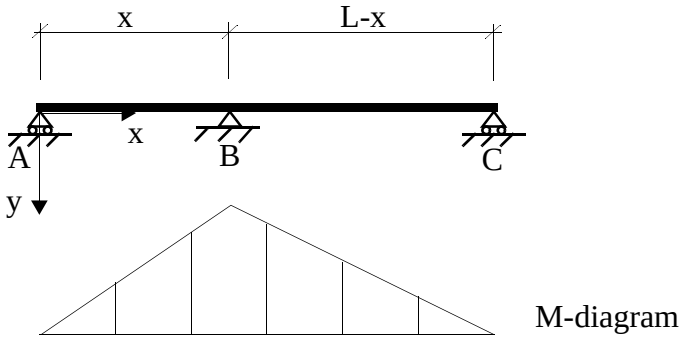

Figure 7.4.2 Moment diagram from linearly varying temperature or differential settlement at end supports.

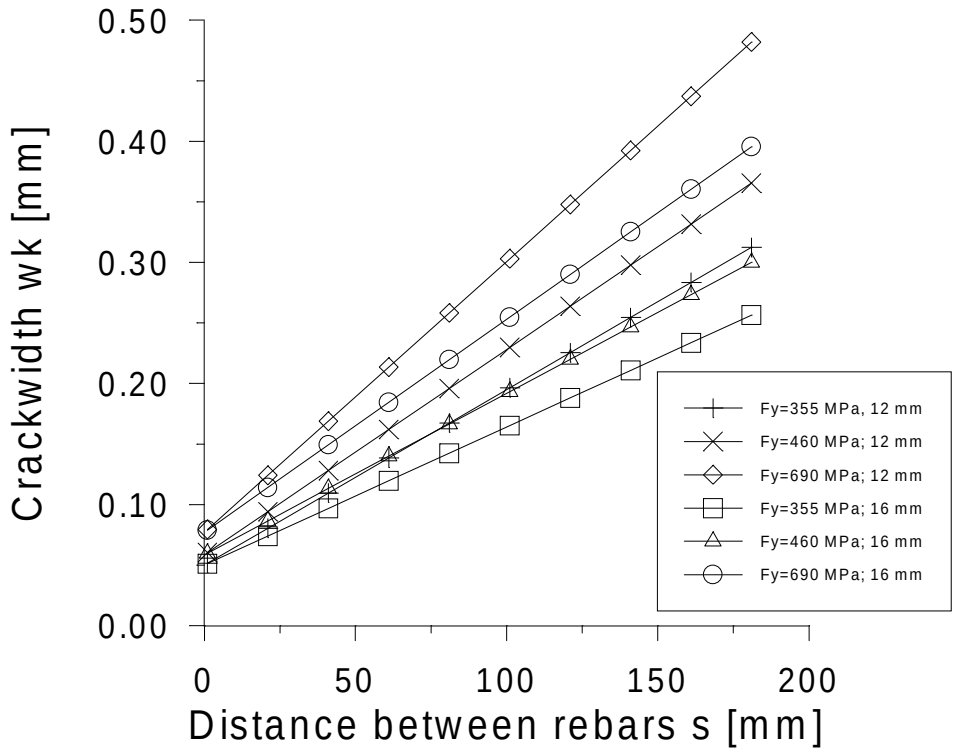

Figure 7.3.2 Crackwidth as a function of distance between rebars.

The value of ρ_r when the curves of figure 7.3.2 intersect $w_k = 0,20$ mm presented in table 7.3.3.

Table 7.3.3 Required amount of reinforcement for different steel grades and diameters of rebars

ρ_r [%]			
ϕ [*mm*]]	$f_{yf} = 355\ MPa$	$f_{yf} = 460\ MPa$	$f_{yf} = 690\ MPa$
12	1.3	1.7	2.5
16	1.8	2.2	3.3

We can conclude that it is possible to use a plastic design method in ultimate limit states with respect to limiting crackwidth values in serviceability limit states. However, as can be seen from figure 7.3.3 it may be necessary to use considerable amount of reinforcement, especially for higher steel grades, if the minimum spacing of shear studs is not used.

Table 7.3.2 Comparison of maximum mean distance between cracks for different steel grades.

Steel grade [MPa]	s_{rm} [mm]
355	200
460	171
690	130

According to Bro 94 the values of s_{rm} may be set equal to the spacing of the shear studs. The minimum spacing according to Bro 94 is 6d, where d is the diameter of the stud. Hence, using studs with diameter 22 mm, s_{rm} can be set to $6 \cdot 22 = 132\ mm$. According to table 7.3.2 this means that using steel grade S690 is possible with respect to crackwidth (130 mm $\approx 132\ mm$).

If the stud spacing is large the mean distance between cracks is taken from BBK94. The equation for s_{rm} in BBK94 (equation (7.3.9)) is:

$$s_{rm} = 50 + \kappa_1 \kappa_2 \cdot \frac{\phi}{\rho_r} \qquad (7.3.9)$$

Another way of assessing the cracking in concrete is to describe the relation between crackwidth w_k and distance between center of rebars s. If we use rebars with $\phi = 12\ mm$ and $\phi = 16$ mm in our comparison and assume that $\kappa_1 \kappa_2 \approx 1/6$, then equation (7.3.9) is simplified to:

$$s_{rm} = 50 + \frac{2s \cdot (2c + \phi)}{3\pi\phi} \qquad (7.3.10)$$

The concrete cover of reinforcement, c is set to 35 mm. Equations (7.3.7) and (7.3.10) yields

$$w_k = 1,7\left(0,20 \cdot \frac{f_{yf}}{E} + 0,25 \cdot 10^{-3}\right) \cdot \left(50 + \frac{2s \cdot (70 + \phi)}{3\pi\phi}\right) \qquad (7.3.11)$$

Putting $f_{yf} = 355, 460, 690\ MPa$ into equation (7.3.11) we get the results in figure 7.3.2.

$$y'' = -\frac{2\varepsilon_f}{h} = -\frac{M}{EI} \tag{7.3.3}$$

In the serviceability state, $M = 0,2 \cdot M_p$ and thus equation (7.3.3) yields:

$$\varepsilon_f = \frac{h}{2} \cdot \frac{0,2 M_p}{1,2 \cdot EI} \tag{7.3.4}$$

Putting (7.3.1) and (7.3.2) in (7.3.4) yields:

$$\varepsilon_f = \frac{1}{6} \cdot \frac{f_{yf}}{E} \tag{7.3.5}$$

If we assume that the distance from the upper flange to the rebars is 0.1h, then the strain in the rebars are:

$$\varepsilon_s = 0,20 \cdot \frac{f_{yf}}{E} \tag{7.3.6}$$

According to BBK94, the crackwidth is calculated according to:

$$w_k = 1,7 \cdot \frac{\sigma_s}{E_s} \cdot \nu \cdot s_{rm} \tag{7.3.7}$$

If we replace σ_s / E_s in equation (7.3.7) with $(\varepsilon_s + \varepsilon_{cs})$ where $\varepsilon_{cs} = 0,25 \cdot 10^{-3}$ is the shrinkage of the concrete, set $\nu = 1$ and $w_k = 0,20\ mm$, we get an expression for the maximum allowable mean distance between cracks, s_{rm}.

$$s_{rm} \leq \frac{0,20}{1,7 \cdot \left(0,20 \cdot \frac{f_{yf}}{E} + 0,25 \cdot 10^{-3} \right)} \quad \text{[mm]} \tag{7.3.8}$$

Assessing equation (7.3.8) for three different steel grades we get results according to table 7.3.2.

Table 7.3.1 Comparison of support moment in ultimate and serviceability states.

Load	Loadcoefficient in ultimate limit state	Loadcoefficient in serviceability state	Moment in ultimate limit state	Moment in serviceability state
Dead	1.05	1.0	0.4	$\frac{1,0}{1,05} \cdot 0,4 \cdot 0,2 = 0,08$
Traffic	1.5	0.3	0.6	$\frac{0,3}{1,5} \cdot 0,6 = 0,12$
Sum			1.0	0,2

According to table 7.3.1 the support moment in serviceability states is 20 % of the moment in ultimate limit states. Let us assume that the girder at the internal support can be assessed as a double symmetric girder including the rebars, figure 7.3.1. Also assume that only the flanges (rebars included in upper flange) resist the applied moment.

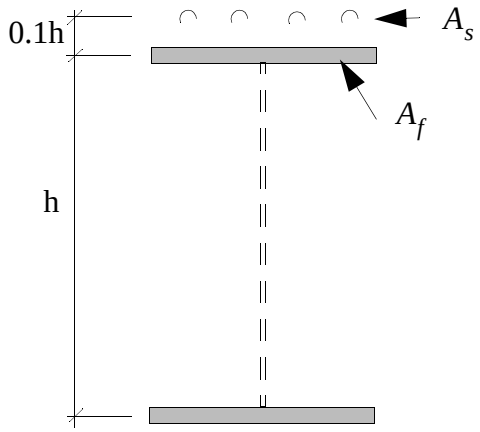

Figure 7.3.1 Assumed cross-section of girder at internal support.

The plastic moment is:

$$M_p \approx f_{yf} \cdot A_f \cdot h \tag{7.3.1}$$

and the moment of inertia:

$$I \approx A_f \cdot \frac{h^2}{2} \tag{7.3.2}$$

The curvature can be expressed as:

$$-\frac{1,86M_y}{5,5258\cdot M_p} = \frac{x_p}{L}\left(1-\frac{1,86}{5,5258}\right)-\left(\frac{x_p}{L}\right)^2 \qquad (7.2.30)$$

For an I-section $M_p/M_y \approx 1,1$ which with equation (7.2.30) gives:

$$\frac{x_p}{L} \approx 0,985$$

Hence the length at which the lower flange has yielded in one span is:

$$(1-x_p/L)\,L = 0,6\ m$$

This value corresponds fairly well with equation (7.2.28A) in which the critical length with respect to lateral torsion buckling is $L_{cr} = 716$ mm.

The derivation of the distance of bracings performed in this report is believed to be somewhat conservative. The recommendation is to use the requirement according to [20].

7.3 Crackwidth in concrete

Requirements in serviceability limit states may govern the dimensions of the cross-section. One factor is the crackwidth in the concrete at internal supports. The crackwidth is limited in the swedish bridge code, Bro94, to $w_k = 0,20\ mm$ for the type of bridge studied in this report. The question is how does this affect the possibility of using a plastic design method in ultimate limit state?

For a common two span bridge with a length of each span of about 40 m and a width of the bridge of 9 m approximately, 40 % of the moment at the pier in ultimate limit states originates from dead load and 60 % from the traffic load. Let us assume that casting of the concrete slab at the internal supports is made last, then the deadload of girders and concrete slab will not influence the calculations of crackwidths. Thus from deadloads, only surfacing will influence the crackwitdh. Let us further assume that surfacing is about 20 % of the total deadweight. Using the load coefficients $\psi\gamma$ of Bro 94 we can set up the values in table 7.3.1.

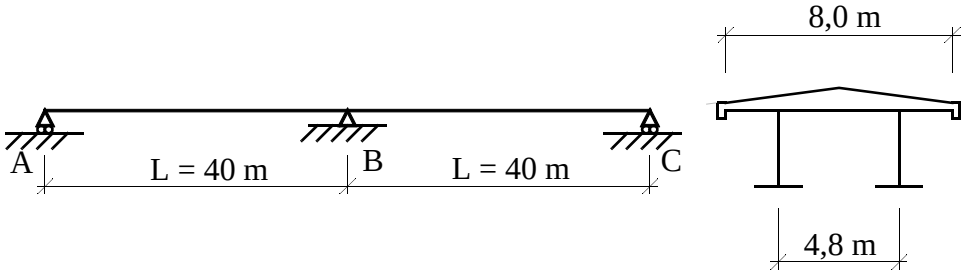

Figure 7.2.7 Example of bridge for determining the length of the yielded zone of the lower flange.

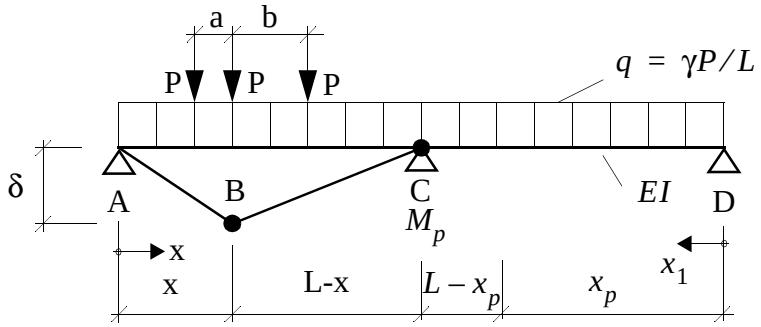

Figure 7.2.8 Loads and plastic mechanism of example bridge.

The plastic moment M_p at the internal support B can be calculated with equations (8.2.3), which gives the location of the hinge in midspan, and (8.2.2) which gives M_p. The following assumptions is made for this example:

a = 1.5 m; b = 6 m; L = 40 m; $\gamma = 5,5258$

The length $L - x_p$ designates the zone where the lower flange has yielded. With the assumptions given $M_c = M_p = -0,93PL$ (the minus sign because moment is defined positive when giving tensile stress in the lower flange). The momentdistribution for part C-D is:

$$M(x_1) = x_1\left(\frac{qL}{2} + \frac{M_c}{L}\right) - \frac{qx_1^2}{2} \qquad (7.2.29)$$

We are interested in finding the value of x_p i.e the point where yielding starts. Hence $M(x_1) = M_y, x_1 = x_p, qL = 5,5258P$ and $M_p = -0,93PL$ are input into equation (7.2.29), which gives:

$E_T = 1250$ MPa

$G = 0,81 \cdot 10^5$ MPa

Equation (7.2.28) gives:

$L_{cr} = 716$ mm (7.2.28A)

From BSK94 6:2441:

$$L \leq 0,3 \cdot b_{fl2} \cdot \sqrt{\frac{E_k}{f_{yk}}} = 0,3 \cdot 550 \cdot \sqrt{\frac{2,1 \cdot 10^5}{845}} = 2601 \text{ mm}$$

and from [20] describing the autostress method:

$$L_b = \frac{(3,6 - 2,2 \cdot M_1 / M_u) \cdot 10^6 \cdot r_y}{F_y}$$

in which:

L_b = Distance between points of bracing [in].

r_y = Radius of gyration with respect to the y-axis [in].

F_y = Yield strength of the steel [psi].

and M_1 and M_u are the moments at the two adjacent braced points. So:

$$L_b = \frac{(3,6 - 2,2 \cdot 1) \cdot 10^6 \cdot 4,02}{122557} \approx 46 \text{ in } \approx 1166 \ mm$$

Thus equation (7.2.28) is the most stringent of the three equations compared.

It is of interest to estimate the length of which the lower flange has yielded. Let us therefore use an example similar to that in chapter 8, i.e. a bridge in two spans according to figure 7.2.7 and 7.2.8.

The area A is divided by the plastic neutral axis into A_1 and A_2, in which A_1 is the part subjected to tensile stress and A_2 subjected to compressive stress. The plastic critical buckling length L_{cr} is:

$$L_{cr} = \sqrt{\frac{\alpha_p}{2}\left(\sqrt{1-\frac{4\beta}{\alpha_p{}^2}}-1\right)} \qquad (7.2.28)$$

Assuming the cross-section has reached M_p then E equals the strain hardening modulus E_T. The shear modulus is assumed not to be reduced i.e. $G_T = G$ At the instance of lateral-torsional buckling, some parts of the cross-section will be subjected to unloading (double modulus concept) but we will consider that the path of unloading follows the same path as loading (tangent modulus concept) thus $E = E_T$ for the whole cross-section. The tangent modulus concept gives a lower bound of the critical moment.

Example:

To compare equation (7.2.28) with BSK94 and the American code [20], an example is calculated.

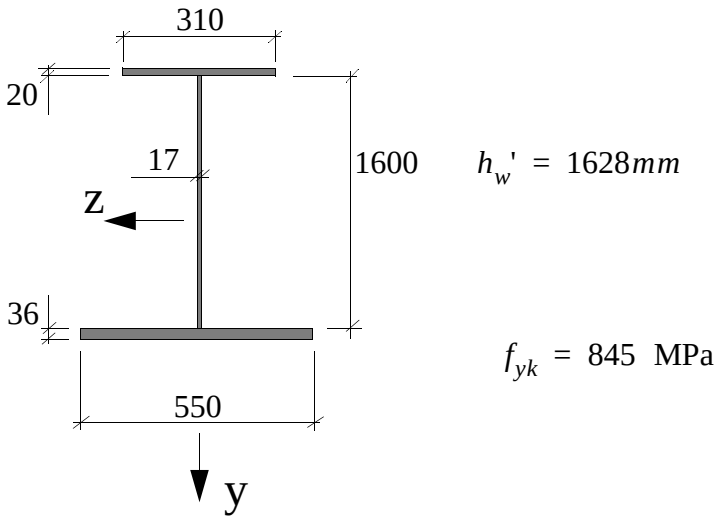

Figure 7.2.6 Dimensions of example girder.

$I_y = 548,78 \cdot 10^6$ mm^4

$K_v = 12,0 \cdot 10^6$ mm^4

$K_w = 127,68 \cdot 10^{12}$ mm^6

$\bar{K} = 25,808 \cdot 10^{12}$ Nmm^2

$M_p = 24826 \cdot 10^6$ Nmm

$$\frac{\partial \Pi}{\partial B} = 0 \tag{7.2.22}$$

Which gives:

$$\frac{\partial \Pi}{\partial A} = (L^4 + \alpha L^2 + \beta) A + \gamma L^2 B = 0 \tag{7.2.23}$$

$$\frac{\partial \Pi}{\partial B} = \gamma L^2 A + (L^4 + 4\alpha L^2 + 16\beta) B = 0 \tag{7.2.24}$$

where

$$\alpha = \frac{\pi^2}{k_r}\left(GK_v + M_{z1}(\mu + 1) \cdot \frac{1}{2I_z}\int_A \left(y_S^2 + z_S^2 \right) y dA - M_{z1}(\mu + 1) e \right)$$

$$\beta = \frac{\pi^4 E}{k_r}\left(K_w + I_y e^2 \right)$$

$$\gamma = \frac{32 M_{z1}(1 - \mu)}{9 k_r}\left(\frac{1}{2I_z}\int_A \left(y_S^2 + z_S^2 \right) y dA - 5e \right)$$

Note that α, β and γ are not non-dimensional. Equations (7.2.23) and (7.2.24) form a system of equations. The vanishing of the determinant of the coefficients of A and B gives the elastic critical buckling length $L_{cr,\,el}$. This leads to rather laborious expressions why we should try to simplify the assumption of ϕ according to equation (7.2.19), to:

$$\phi = A \sin \frac{\pi x}{L} \tag{7.2.25}$$

Equation (7.2.23) yields the elastic critical buckling length (with $B = 0$ and $A \neq 0$):

$$L_{cr,\,el} = \sqrt{\frac{\alpha}{2}\left(\sqrt{1 - \frac{4\beta}{\alpha^2}} - 1 \right)} \tag{7.2.26}$$

We are however interested in the plastic critical buckling length. It is therefore necessary to adjust equation (7.2.26) accordingly. When we performed the integration of equation (7.2.20) we assumed that GK_v, EK_w and EI_y were constants. For the plastic case with a varying moment this is not the case. If we are studying the part of the girder in which the lower flange has yielded, we should put $\mu = 1$. Then the assumption of constant GK_v, EK_w and EI_y in the plastic range can be considered correct.

For a plastic case $\alpha = \alpha_p$, where:

$$\alpha_p = \frac{\pi^2}{k_r}\left(GK_v + |f_y| \int_{A_1} \left(y_S^2 + z_S^2 \right) dA_1 - |f_y| \int_{A_2} \left(y_S^2 + z_S^2 \right) dA_2 - 2M_{z1} e \right) \tag{7.2.27}$$

these are independent of each other it must hold that $\Pi_v = min$ and $\Pi_\phi = min$. Thus:

$$\Pi_\phi = \frac{1}{2}\cdot\int_0^L\left(\left[GK_v + \frac{M_z(x)}{I_z}\cdot\int_A\left(y_s^2+z_s^2\right)ydA\right]\cdot\left(\frac{d\phi}{dx}\right)^2 - EK_w\cdot\frac{d^3\phi}{dx^3}\cdot\frac{d\phi}{dx}\right)dx +$$

$$+\frac{1}{2}\int_0^L\left(E\,I_y e^2\left(\frac{d^2\phi}{dx^2}\right)^2 + k_r\phi^2\right)dx + \int_0^L M_z(x)\,e\cdot\frac{d^2\phi}{dx^2}\cdot\phi\;dx = min \qquad (7.2.17)$$

Let us put $M_{z2} = \mu M_{z1}$, this gives:

$$M_z(x) = M_{z1}\left(1 + (\mu-1)\frac{x}{L}\right) \qquad (7.2.18)$$

Assuming

$$\phi = A\sin\frac{\pi x}{L} + B\sin\frac{2\pi x}{L} \qquad (7.2.19)$$

and using equation (7.2.18), we perform the integrations of equation (7.2.17) and get:

$$\Pi_\phi = \frac{\pi^2 GK_v}{4L}\cdot(A^2+4B^2) +$$

$$+\frac{M_{z1}\pi^2}{8LI_z}\cdot\int_A\left(y_S^2+z_S^2\right)ydA\cdot\left((\mu+1)(A^2+4B^2) + \frac{64}{9\pi^2}(1-\mu)AB\right) +$$

$$+\frac{EK_w\pi^4}{4L^3}(A^2+16B^2) + \frac{EI_y e^2\pi^4}{4L^3}(A^2+16B^2) + \frac{k_r L}{4}(A^2+B^2) +$$

$$-\frac{M_{z1}\pi^2 e}{4L}\left((A^2+4B^2)(\mu+1) + \frac{320}{9\pi^2}(1-\mu)AB\right) \qquad (7.2.20)$$

Equation (7.2.20) can be seen as representing a surface in the Π, A, B Cartesian coordinate system. The condition for minimum potential is then:

$$\frac{\partial\Pi}{\partial A} = 0 \qquad (7.2.21)$$

and

$$U = \int_0^L M_z(x)\ (v'' + u''\phi)\, dx \tag{7.2.14}$$

Now according to Rayleigh-Ritz method the following is valid for the potential Π:

$$\Pi = W + U = min \tag{7.2.15}$$

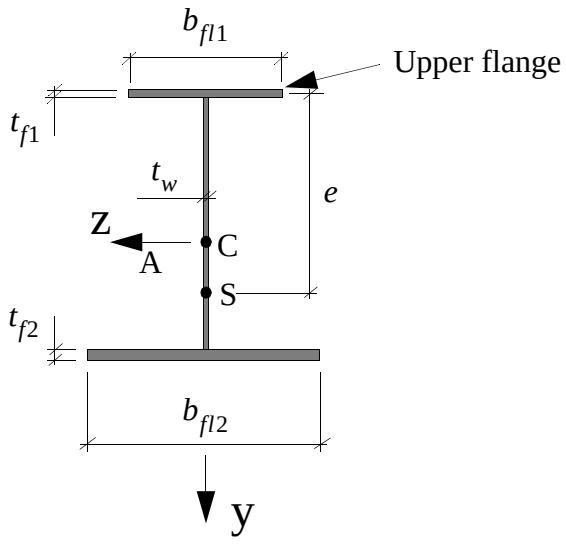

Figure 7.2.4 Distance e from upper flange to shear centre.

In our case the girder is restrained by the concrete slab i.e. the axis of rotation is situated at the upper flange and therefore we set $u = e \cdot \phi$ in equations (7.2.15), where e is the distance from the upper flange to the shear centre.The potential Π for our system according to figure (7.2.1) is then:

$$\Pi = \frac{1}{2} \cdot \int_0^L \left(\left[GK_v + \frac{M_z(x)}{I_z} \cdot \int_A \left(y_s^2 + z_s^2 \right) y dA \right] \cdot \left(\frac{d\phi}{dx} \right)^2 - EK_w \cdot \frac{d^3\phi}{dx^3} \cdot \frac{d\phi}{dx} \right) dx +$$

$$+ \frac{1}{2} \int_0^L \left(E I_z \left(\frac{d^2 v}{dx^2} \right)^2 + EI_y e^2 \left(\frac{d^2\phi}{dx^2} \right)^2 + k_r \phi^2 \right) dx + \int_0^L M_z(x) \left(\frac{d^2 v}{dx^2} + e \cdot \frac{d^2\phi}{dx^2} \cdot \phi \right) dx \tag{7.2.16}$$

Equation (7.2.16) can be divided into two parts $\Pi_v = \Pi(v'')$ and $\Pi_\phi = \Pi(\phi, \phi', \phi'', \phi''')$, since

$$0 = \left(\frac{dv}{dx}\right)_{x=o} \cdot L + \int_0^L (L-s)\, v''\left(1 - \frac{1}{2}\phi^2\right) ds + \int_0^L (L-s)\, u''\phi\, ds \quad \text{or:}$$

$$\left(\frac{dv}{dx}\right)_{x=0} = -\frac{1}{L} \cdot \int_0^L (L-s)\, v''\left(1 - \frac{1}{2}\phi^2\right) ds - \frac{1}{L} \cdot \int_0^L (L-s)\, u''\phi\, ds \qquad (7.2.11)$$

In (7.2.11) use of the relation $\cos\phi \approx 1 - \frac{1}{2}\phi^2$ has been made. The potential due to end moments M_{z1} and M_{z2} is:

$$U = -M_{z1}\left(\frac{dv}{dx}\right)_{x=0} + M_{z2}\left(\frac{dv}{dx}\right)_{x=L} \qquad (7.2.12)$$

To find the potential of the end moments we need the rotations at the supports. Therefore, we differentiate equation (7.2.10).

$$\frac{dv}{dx} = \left(\frac{dv}{dx}\right)_{x=o} + \int_0^x v''\left(1 - \frac{1}{2}\phi^2\right) ds + \int_0^x u''\phi\, ds \qquad (7.2.12)$$

Equations (7.2.11) and (7.2.12) gives with $\phi^2 \ll 1$ and exchanging ds with dx:

$$U = -M_{z1} \cdot \left(\frac{dv}{dx}\right)_{x=0} + M_{z2} \cdot \left(\left(\frac{dv}{dx}\right)_{x=0} + \int_0^L v''\, dx + \int_0^L u''\phi\, dx\right) \qquad (7.2.13)$$

Putting equation (7.2.11) into (7.2.13) yields with $\phi^2 \ll 1$ and exchanging s with x yields:

$$U = \int_0^L \left(M_{z1} + (M_{z2} - M_{z1}) \cdot \frac{x}{L}\right) v''\, dx + \int_0^L \left(M_{z1} + (M_{z2} - M_{z1}) \cdot \frac{x}{L}\right) u''\phi\, dx \quad \text{or:}$$

In deriving the potential of the external load, it is based in the deformation of the shear centre axis, according to [19], see figure 7.2.3.

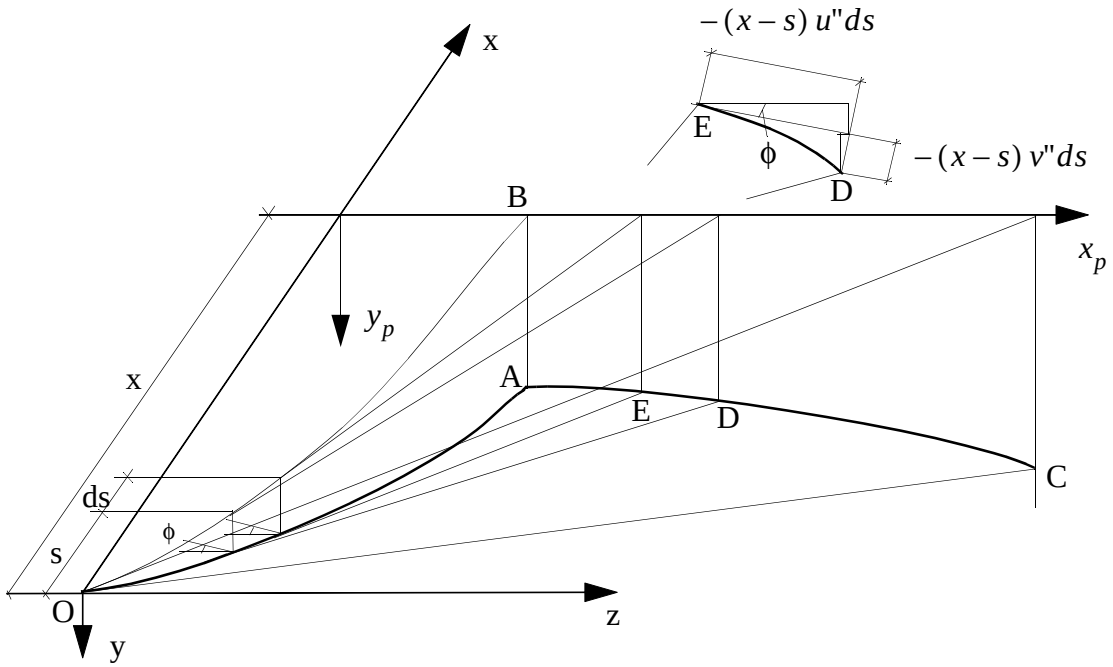

Figure 7.2.3 Deformation of the shear centre axis.

Let $x_p - y_p$ define a movable plane and the curve OA be the deformed shear centre axis. If a tangent to OA is moving along OA, then the point of intersection of this tangent with the $x_p - y_p$ plane will describe a curve CA.

The vertical deflection v is:

$$v = \left(\frac{dv}{dx}\right)_{x=o} \cdot x + \int_0^x (x-s)\,v''\left(1-\frac{1}{2}\phi^2\right)ds + \int_0^x (x-s)\,u''\phi\,ds \qquad (7.2.10)$$

$\left(\frac{dv}{dx}\right)_{x=0}$ can be found by the boundary condition that $v((L) = 0)$ which gives:

The component in z-direction gives a moment:

$$\sigma dA \cdot y_S \cdot \frac{d\phi}{dx} \cdot y_S \tag{7.2.2}$$

The component in y-direction gives a moment:

$$\sigma dA \cdot z_S \cdot \frac{d\phi}{dx} \cdot z_S \tag{7.2.3}$$

where y_S and z_S denotes a coordinate system with origo in the shear centre. The normal stress can in this case be expressed as:

$$\sigma = \frac{M_z(x)}{I_z} y \tag{7.2.4}$$

Thus from equation (7.2.1), (7.2.2), (7.2.3) and (7.2.4) we can express the torsion T as:

$$T = GK_v \cdot \frac{d\phi}{dx} - EK_w \cdot \frac{d^3\phi}{dx^3} + \frac{M_z(x)}{I_z} \cdot \frac{d\phi}{dx} \cdot \int_A \left(y_s^2 + z_s^2 \right) y dA \tag{7.2.5}$$

The internal energy stored from torsion is then:

$$W_{i,T} = \frac{1}{2} \cdot \int_0^L \left(\left[GK_v + \frac{M_z(x)}{I_z} \cdot \int_A \left(y_s^2 + z_s^2 \right) y dA \right] \cdot \left(\frac{d\phi}{dx} \right)^2 - EK_w \cdot \frac{d^3\phi}{dx^3} \cdot \frac{d\phi}{dx} \right) dx \tag{7.2.6}$$

The internal energy stored due to the upper flange being clamped to the concrete slab is:

$$W_{i,c} = \frac{1}{2} \cdot \int_0^L k_r \cdot \phi^2 dx \tag{7.2.7}$$

Where k_r is the rotation stiffness in the connection between the upper flange and the web.

Finally, the energy stored from bending is:

$$W_{i,b} = \frac{1}{2} \int_0^L EI_z (v'')^2 dx + \frac{1}{2} \int_0^L EI_y (u'')^2 dx \tag{7.2.8}$$

Thus the total internal energy stored is

$$W_i = W_{i,T} + W_{i,c} + W_{i,b} \tag{7.2.9}$$

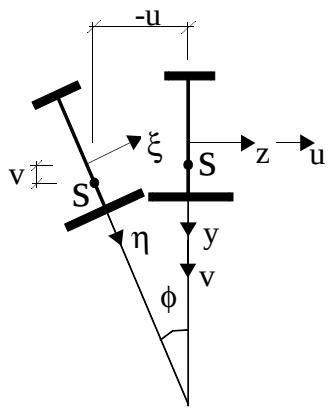

Figure 7.2.2 Lateral-torsional buckling of girder.

A coordinate system $\xi - \eta - \zeta$ should be introduced on the buckled mode. However for simplicity the potential will be derived from the fixed x-y-z system. This approach is acceptable if v' and v'' are small when the load acts in the plane of maximum flexural rigidity according to [19].

From structural mechanics we know that:

$$T_{SV} + T_W = GK_v \cdot \frac{d\phi}{dx} - EK_w \cdot \frac{d^3\phi}{dx^3} \qquad (7.2.1)$$

The increase in ϕ on an infinitesimal length dx is $d\phi$. The normal stresses in the girder thus have components in the y-z plane giving rise to torsion about the shear centre S.

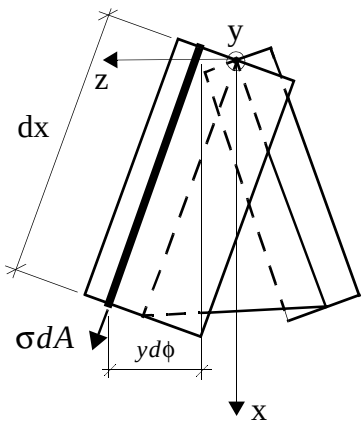

Figure 7.2.3 σdA giving components in y-z plane.

A restriction of h_w / t_w is defined in EC3 which is:

$$\frac{d}{t_w} \leq 0,55 \cdot \frac{E}{f_{yf}} \sqrt{\frac{A_w}{A_{fc}}}$$

for flange in class 3 or 4 in order to avoid buckling in the elastic range. The most stringent requirement of the two should be applied.

Table 7.1.4

Girder	θ_p [rad]	$\frac{h_w}{t_w}$	Eq. (7.1.2)
A4	$45 \cdot 10^{-3}$	94	73
A5	$35 \cdot 10^{-3}$	105	86
A6	$30 \cdot 10^{-3}$	116	98

From table 7.1.4 it can be seen that the requirement according to equation (7.1.6) is a bit conservative.

7.2 Lateral bracings

This chapter will assess the lateral-torsional buckling of the lower flange at internal supports. The attempt will be according to the Rayleigh-Ritz method which is based on the principle that the total potential (or the change in potential) must be a minimum, if the system is to be in static equilibrium. First we will define the potential for the system in figure 7.2.1. The course of action follows in principle the way it is presented in [19].

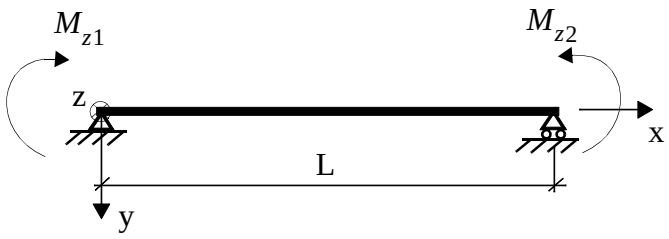

Figure 7.2.1 Girder between lateral bracings subjected to end moments. Definition of positive direction of end moments.

During buckling the cross-section rotates an angle ϕ and the displacements of the shear centre S, are u and v.

Table 7.1.3 Vianello's method for calculation of N_{cr}

Point	z_{ass}	$1/EI$	z_R	z_N	$z_R + z_N$	$\frac{z_{ass}}{z_R + z_N}$
9	4.5	1.1	1.95(- 44.5) = - 86.8	174.6	87.8	51.3
10	0	1.0	0	0	0	-
Factor		$\frac{1}{EI_0}$	$\frac{Nh_w^2}{10^2 EI_0}$	$\frac{Nh_w^2}{10^2 EI_0}$	$\frac{Nh_w^2}{10^2 EI_0}$	$10^{-3} \cdot \frac{Nh_w^2}{10^2 EI_0}$
$\sum$	175.2				3421.4	

The critical load can now be determined:

$$\frac{N_{cr}}{N} = \frac{175,2}{3421,4 \cdot \frac{Nh_w^2}{10^2 EI_0}}$$

Thus

$$N_{cr} \approx 0,52 \cdot \frac{\pi^2 \cdot EI_0}{h_w^2} = 0,52 \cdot \frac{\pi^2 \cdot E \cdot 2h_w t_w^3}{12\,(1-\nu^2) \cdot h_w^2} \qquad (7.1.5)$$

The criterion must be that $N_{cr} \geq f_{yf} \cdot A_{fc} \cdot \theta_p$ in which θ_p is the total hinge rotation, which with (7.1.5) gives

$$\frac{h_w}{t_w} \leq 1,0 \cdot \sqrt{\frac{A_w}{A_{fc}}} \cdot \frac{1}{\sqrt{\theta_p}} \cdot \sqrt{\frac{E}{f_{yf}}} \qquad (\theta_p \text{ in [rad]}) \qquad (7.1.6)$$

Equation (7.1.6) is the restriction on the web slenderness to avoid buckling of the compressed flange into the web. To compare equation (7.1.6) with the experiments, the data from girders A4, A5 and A6 has been put into (7.1.6) together with θ_p (in the descending part of the moment-rotation curve) at which the first sign of the flange buckling into the web occurs. The result is presented in table 7.1.4.

$$\varphi_R = 49,54 \cdot \frac{Rh_w^2}{10^3 EI_0}$$

It is also valid that $\varphi_R - \varphi_N = \varphi$, where $\varphi = -Rh_w / C_M$. This gives:

$$R = \frac{174,59 \cdot 10^2 N}{\left(\frac{EI_0}{C_M h_w} \cdot 10^3 + 49,54\right) h_w}$$

so that:

$$\frac{Rh_w^3}{10^4 EI_0} = \frac{174,59}{\left(\frac{10^3}{25} + 49,54\right)} \cdot \frac{Nh_w^2}{10^2 EI_0} \approx 1,950 \cdot \frac{Nh_w^2}{10^2 EI_0}$$

Table 7.1.3 Vianello's method for calculation of N_{cr}

Point	z_{ass}	$1/EI$	z_R	z_N	$z_R + z_N$	$\frac{z_{ass}}{z_R + z_N}$
0	0	$1 \cdot 10^6$	0	0	0	-
1	16.5	10	1.95(- 44.9) = - 87.6	409.0	321.4	51.3
2	25.5	5	1.95(- 79.7) = - 155.4	653.0	497.6	51.2
3	29.0	3.3	1.95(- 104.6) = - 204.0	769.5	565.5	51.3
4	28.5	2.5	1.95(- 119.5) = - 233.0	790.3	557.3	51.1
5	25.4	2	1.95(- 124.5) = - 242.8	740.0	497.2	51.1
6	20.8	1.7	1.95(- 119.5) = - 233.0	638.8	405.8	51.3
7	15.3	1.4	1.95(- 104.2) = - 203.2	502.2	299.0	51.2
8	9.7	1.2	1.95(- 79.2) = - 154.4	344.2	189.8	51.1

Table 7.1.2 Vianello's method for calculation of N_{cr}

Point	z_{ass}	$1/EI$	M_R	z''_R	z'_R	z_R
0	0	$1 \cdot 10^6$	0	0		0
					$-94.4 + \varphi_R$	
1	16.5	10	1	10		$-94.4 + \varphi_R$
					$-84.4 + \varphi_R$	
2	25.5	5	2	10		$-178.8 + 2\varphi_R$
					$-74.4 + \varphi_R$	
3	29.0	3.3	3	9.9		$-253.2 + 3\varphi_R$
					$-64.5 + \varphi_R$	
4	28.5	2.5	4	10		$-317.7 + 4\varphi_R$
					$-54.5 + \varphi_R$	
5	25.4	2	5	10		$-372.2 + 5\varphi_R$
					$-44.5 + \varphi_R$	
6	20.8	1.7	6	10.2		$-416.7 + 6\varphi_R$
					$-34.3 + \varphi_R$	
7	15.3	1.4	7	9.8		$-451.0 + 7\varphi_R$
					$-24.5 + \varphi_R$	
8	9.7	1.2	8	9.6		$-475.8 + 8\varphi_R$
					$-14.9 + \varphi_R$	
9	4.5	1.1	9	9.9		$-490.4 + 9\varphi_R$
					$-5 + \varphi_R$	
10	0	1.0	10	10	φ_R	$-495.4 + 10\varphi_R$
Factor		$\frac{1}{EI_0}$	$-\frac{Rh_w}{10^2}$	$-\frac{Rh_w}{10^2 EI_0}$	$\frac{Rh_w^2}{10^3 EI_0}$	$\frac{Rh_w^3}{10^4 EI_0}$
$\sum$	175.2					

The conditions that $z_N(L) = z_R(L) = 0$ (at point 10) gives:

$$\varphi_N = 174,59 \cdot \frac{Nh_w}{10EI_0}$$

Table 7.1.1 Vianello's method for calculation of N_{cr}

Point	z_{ass}	$1/EI$	M_N	z''_N	z'_N	z_N
0	0	$1 \cdot 10^6$	0	0		0
					583.6 - φ_N	
1	16.5	10	16.5	165		583.6 - φ_N
					418.6 - φ_N	
2	25.5	5	25.5	127.5		1002.2 - $2\varphi_N$
					291.1 - φ_N	
3	29.0	3.3	29.0	95.7		1293.3 - $3\varphi_N$
					195.4 - φ_N	
4	28.5	2.5	28.5	71.2		1488.7 - $4\varphi_N$
					124.2 - φ_N	
5	25.4	2	25.4	50.8		1612.9 - $5\varphi_N$
					73.4 - φ_N	
6	20.8	1.7	20.8	35.4		1686.3 - $6\varphi_N$
					38.0 - φ_N	
7	15.3	1.4	15.3	21.4		1724.3 - $7\varphi_N$
					16.6 - φ_N	
8	9.7	1.2	9.7	11.6		1740.9 - $8\varphi_N$
					5.0 - φ_N	
9	4.5	1.1	4.5	5.0		1745.9 - $9\varphi_N$
					- φ_N	
10	0	1.0	0	0	- φ_N	1745.9 - $10\varphi_N$
Factor		$\frac{1}{EI_0}$	N	$-\frac{N}{EI_0}$	$\frac{Nh_w}{10EI_0}$	$\frac{Nh_w^2}{10^2 EI_0}$
$\sum$	175.2					

Now let us assess $C_M \cdot L / (EI)$. If the flange induced buckling occurs at a distance of $h_w/2$ from the internal support, and the lower flange is assumed to be clamped with respect to torsion at the transverse stiffener at the support we get by using $\varphi' = T/(GK_v)$:

$$C_M = \frac{T}{\varphi} = \frac{2GK_v}{h_w} \tag{7.1.3}$$

With $L = h_w$ and conservatively choosing:

$$I = I_0 = \frac{t_w \cdot h_w^3}{12(1-\nu^2)}$$

and noting that $G = E/(2(1+\nu))$, we get:

$$\frac{C_M \cdot L}{EI} = \frac{24(1-\nu^2)GK_v}{Eh_w t_w^3} = 12(1-\nu) \cdot \frac{b_{fl} \cdot t_f^3}{3h_w \cdot t_w^3}$$

If we assume that $b_{fl} = h_w/3$ and $t_f = 3t_w$ (where b_{fl} and t_f denotes the dimensions of the lower flange) then:

$$\frac{C_M \cdot L}{EI} \approx 25 \tag{7.1.4}$$

The buckling of the flange into the web, appears near the internal support where the web is stiffened with vertical stiffeners. The stiffeners have an favourable effect of the resistance with respect to flange induced buckling. This has conservatively not been taken into account by the model in figure 7.1.2, except for the restraint at the lower flange.

The critical load N_{cr} of the column is solved by the method of Vianello's. This is an iterative procedure where a deflection is assumed and from this a new deflection is calculated. The iterative procedure is continued until the assumed deflection has the same shape as the calculated. The critical load N_{cr} is then

$$\frac{N_{cr}}{N} = \frac{\sum z_{assumed}}{\sum z_{calculated}}$$

Only the last iteration in the Vianello method is presented here in the tables below. Table 7.1.1 includes the influence of load N, table 7.1.2 the influence of reaction force R and table 7.1.3 the sum of load N and reaction force R.

The derivatives of z in table 7.1.2 is with respect to coordinate y.

Using:

$$\frac{d^2 z}{dy^2} = -\frac{M}{EI} = -\frac{1}{EI}\left(N \cdot z - \frac{C_M \cdot \varphi}{L} \cdot y \right)$$

gives:

$$z'' + \frac{N}{EI} \cdot z = \frac{C_M \cdot \varphi}{EIL} \cdot y$$

the solution is:

$$z = C_1 \cdot \cos\left(\sqrt{\frac{N}{EI}} \cdot y \right) + C_2 \cdot \sin\left(\sqrt{\frac{N}{EI}} \cdot y \right) + \frac{C_M \cdot \varphi}{\frac{N}{EI} \cdot EIL} \cdot y \qquad (7.1.1)$$

Using following boundary conditions:

$$z(0) = 0$$

$$z(L) = 0$$

$$z'(L) = -\varphi$$

we get:

$$\frac{C_M \cdot L}{EI} = \frac{\left(\sqrt{\frac{N}{EI}} \cdot L \right)^2}{\sqrt{\frac{N}{EI}} \cdot L \cdot \cot\left(\sqrt{\frac{N}{EI}} \cdot L \right) - 1} \qquad (7.1.2)$$

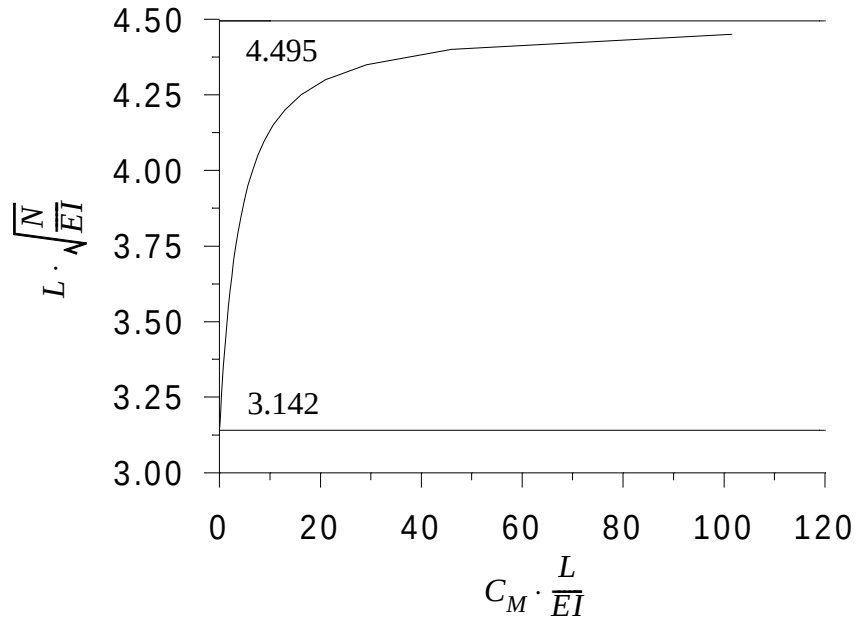

Figure 7.1.4 Plot of equation (7.1.2).

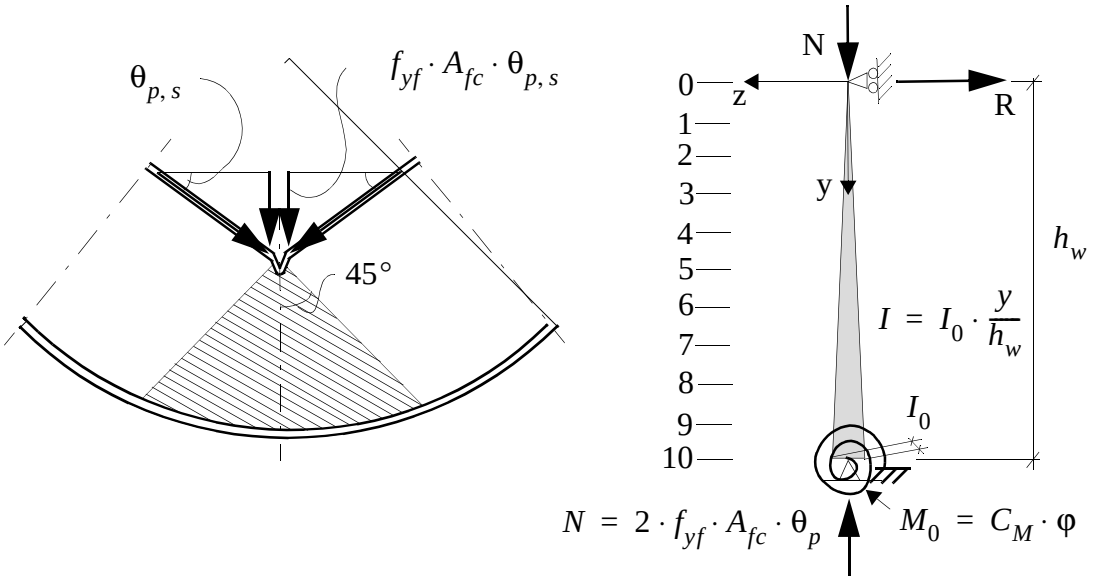

Figure 7.1.2 Model of web subjected to forces from the compressed flange.

The model according to figure 7.1.2 assumes elastic conditions and also the elastic curvature has been neglected.

The web is subjected to a concentrated force $N = 2 \cdot f_{yf} \cdot A_{fc} \cdot \theta_{p,s}$. The force is assumed to be distributed over an angle of $45°$ to a vertical axis. The web is modelled as an equivalent column, pinned at the top and elastically restrained ($C_M \cdot \varphi$) at the bottom and with a linearly varying moment of inertia $I = I_0 \cdot y / h_w$.

The motive of assuming elastically restrained conditions at the bottom flange is based on the following discussion. Figure 7.1.3 shows a column subjected to a normal force N and elastically restrained at the bottom, represented in figure 7.1.3 with a rotational spring stiffness C_M.

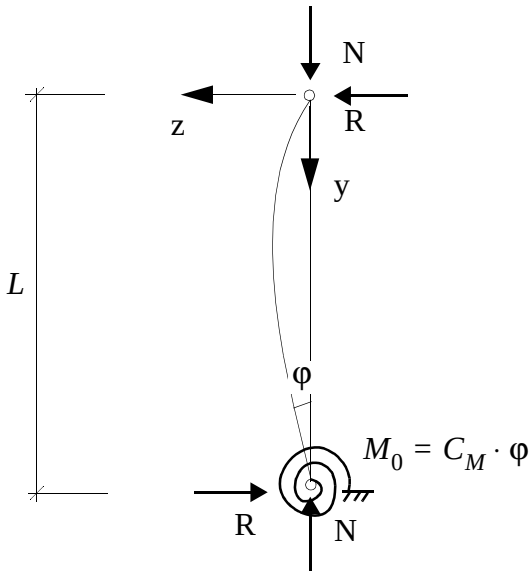

Figure 7.1.3 Buckling of column elastically restrained at the bottom.

7. Subjects connected to Design of Composite Bridges

7.1 Buckling of flange into the web

During the laboratory tests, a failure mode was observed which consisted of the compressed flange buckling into the web. This failure mode is denoted “flange induced buckling” in EC3 and “vertical buckling of the flange” in American literature. In this chapter we will use the denotation by EC3. In [21] is flange induced buckling assessed.

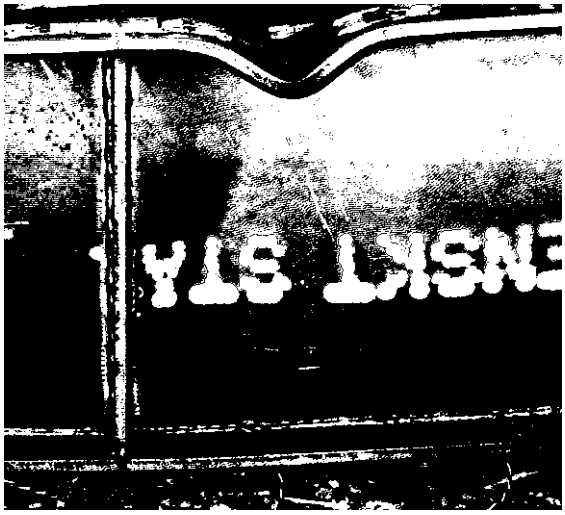

Figure 7.1.1 Failure mode where the compressed flange has buckled into the web.

This phenomenon was observed for girders A4, A5 and A6. This flange induced buckling leads to a severe drop in the descending part of the moment-rotation relationship and is therefore to be avoided. The failure mode seems to arise when the web is slender. Hence, the attempt is to restrict the web slenderness h_w / t_w . The following model according to figure 7.1.2 is assumed.

The required plastic rotation at the internal support (point C) is:

$$\theta_C = -0,3895\frac{PL^2}{EI} = -0,3832 \cdot \frac{485 \cdot 10^3 \cdot (40 \cdot 10^3)^2}{2,1 \cdot 10^5 \cdot 43,3 \cdot 10^9} \approx -32,7 \cdot 10^{-3} \text{ rad}$$

To θ_C we shall add 1,5 + 2 = 3,5 mrad according to table 7.4.1 to take into account linearly varying temperature and differential settlement.

If we instead of using the formulae of moment rotation relationships according to chapter 4, use the results from test of girder A5, we get $M_R/M_{Rp} = 0,72$ for $\left|\theta_{C,TOT}\right| = 32,7 + 3,5 \approx 37\ mrad$.

The plastic moment capacity of the cross-section in figure 8.2.7 is $M_{Rp} = 24887\ kNm$. With $M_R/M_{Rp} = 0,72$ this gives $M_R = 0,72 \cdot 24887 = 17918$ kNm which is the capacity of the cross-section in figure 8.2.7 at an plastic rotation of $\left|\theta_{C,TOT}\right| = 37$ mrad.

The capacity we assumed at the beginning for the cross section at the internal support was:

$$\alpha M_p = 0,84 \cdot 19591 = 16456\ \ kNm$$

which is approximately equal to M_R. If $M_R < \alpha M_p$ or there would have been a large discrepany in these values, then we would have to assume a new cross-section at the support and perform the calculations all over again.

Finally, comparing the required amount of steel in the girders from plastic and elastic design, one finds that the plastic design requires approximately 90 % of the amount of steel required in the elastic analysis.

The required cross-section for M_p is according to figure 8.2.6, which is the same cross-section as in the elastic analysis but the lower flange has been reduced.

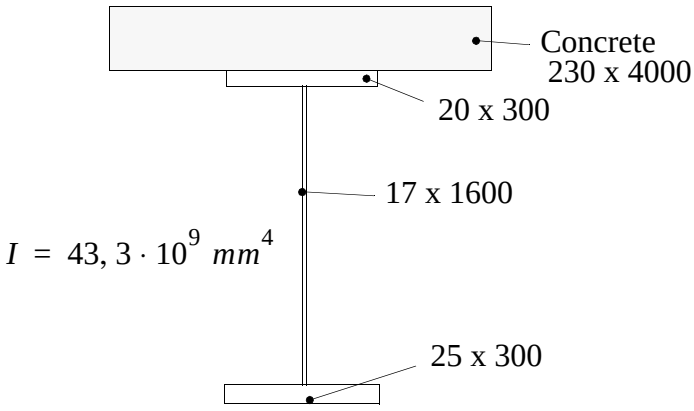

Span cross-section

$$0 \le x < (1 - \xi)\, L$$

$$(1 + \xi)\, L < x \le 2L$$

Figure 8.2.6 Required cross-section in the spans, using plastic design method

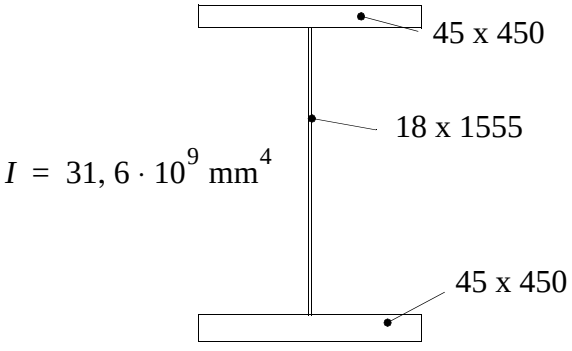

Internal support
cross-section

$$(1 - \xi)\, L < x < (1 + \xi)\, L$$

Figure 8.2.7 Required cross-section at the internal support, using plastic design method

$$\sum m\theta + \int m \cdot \frac{M}{EI} ds = \frac{x}{L} \cdot \theta_B + \theta_C - \frac{PL^2}{6EI} \cdot \frac{(x-a)^3 + x^3 + (x+b)^3}{L^3} +$$

$$+ \frac{L^2}{\eta EI}\left[\left[\frac{M_B - M_0}{L} \cdot \frac{L}{x} + \frac{qL}{2} \cdot \frac{x}{L} + P\left(1 - \frac{a}{x}\right)\right] \cdot \frac{1}{3} - \frac{qL}{8} - P - \frac{P}{2} \cdot \frac{a-b-3x}{L} + \frac{M_0}{2L}\right] +$$

$$+ \left(1 - \frac{1}{\eta}\right) \cdot \frac{(1-\xi)^3 L^2}{3EI}\left[\frac{M_B - M_0}{L} \cdot \frac{L}{x} + \frac{qL}{2} \cdot \frac{x}{L} + P\left(1 - \frac{a}{x}\right)\right] +$$

$$+ \left(1 - \frac{1}{\eta}\right) \cdot \frac{(1-\xi)^2 L^2}{EI}\left[-\frac{(1-\xi)^2 qL}{8} - (1-\xi) P - \frac{P}{2} \cdot \frac{a-b-3x}{L} + \frac{M_0}{2L}\right] +$$

$$+ \frac{L^2}{\eta EI}\left[\frac{1}{3L}\left(M_C + \frac{qL^2}{2} - M_0\right) + \frac{M_0}{2L} - \frac{qL}{8}\right] +$$

$$- \left(1 - \frac{1}{\eta}\right) \cdot \frac{(1-\xi)^2 L^2}{EI}\left[\frac{(1-\xi)}{3L}\left(M_C + \frac{qL^2}{2} - M_0\right) + \frac{M_0}{2L} - (1-\xi)^2 \cdot \frac{qL}{8}\right] = 0 \quad (8.2.4)$$

Equation (8.2.4) with the given values yields:

$$0,4097\theta_B + \theta_C + 0,9297 \cdot \frac{M_B L}{EI} + 0,5323 \cdot \frac{M_C L}{EI} - 104,1 \cdot 10^{-3} \cdot \frac{PL^2}{EI} = 0$$

Putting $M_B = M_p \approx 1,009834PL$, $M_C = -\alpha M_p$ and $\theta_B = 0$ we finally get:

$$\theta_C = -0,3832\frac{PL^2}{EI}$$

This is the required plastic rotation at the internal support for the assumed values in our example.

The plastic moment M_p as found previously, is:

$$M_p = 1,009834 \cdot 485 \cdot 40 = 19591\ kNm$$

$$\gamma = \frac{qL}{P} = \frac{67 \cdot 40}{485} \approx 5,5258$$

$$\beta = \frac{M_0}{PL} = \frac{1500}{485 \cdot 40} = 0,08$$

$$\alpha = 0,84$$

$$\eta = 0,73$$

$$\xi = 0,15$$

then x from equation (8.2.2) can be calculated using a = 1.5 m and b = 6 m according to Bro 94 which gives

$$x_{max} \approx 16,4 \ \ m$$

With the value of x known M_p is calculated using equation (8.2.3), giving:

$$M_p \approx 1,009834PL$$

Using equation (6.3) and choosing our residual moment m = m(x) according to figure 8.2.5:

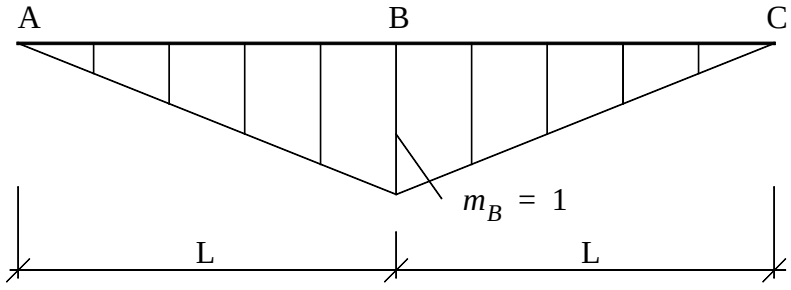

Figure 8.2.5 Distribution of residual moment m.

Equation (6.3):

$$\sum m\theta + \int m \cdot \frac{M}{EI} ds = 0$$

Which in our case is:

8.2 Plastic design method taking into account local buckling

We will start by assuming a plastic hinge mechanism according to figure 8.2.1

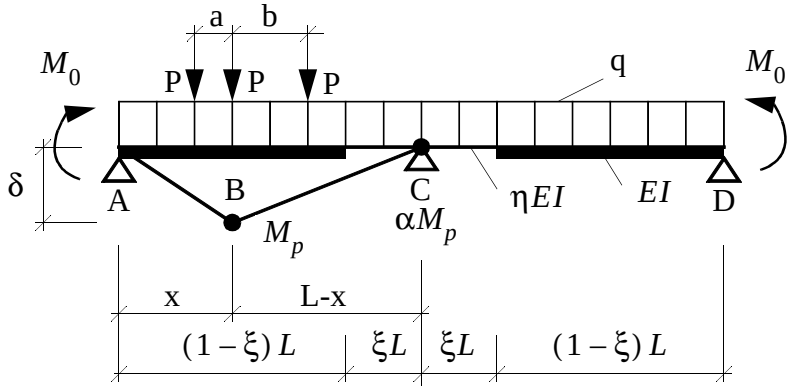

Figure 8.2.1 Assumed plastic hinge mechanism.

The plastic hinge is assumed to be situated under the concentrated force in the middle. Under these assumptions the following is valid:

$$M_0 \cdot \frac{\delta}{x} + P\delta\left(\frac{x-a}{x} + 1 + \frac{L-x-b}{L-x}\right) + qL \cdot \frac{\delta}{2} = M_p\delta\left(\frac{1}{x} + \frac{1}{L-x} + \frac{\alpha}{L-x}\right) \qquad (8.2.1)$$

Put

$qL = \gamma P$ and $M_0 = \beta PL$.

Rearranging equation (8.2.1.) to $M_p = M_p(x)$ and then putting $\frac{dM_p}{dx} = 0$ yields:

$$x = \frac{L}{\alpha}\left(\sqrt{1 + \frac{\alpha}{(6+\gamma)\,L}\left(2a\,(1+\alpha) - 2b + (6+\gamma)\,L - 2\beta L\,(1+\alpha)\right)} - 1\right) \qquad (8.2.2)$$

With x from equation (8.2.2) the extreme value of M_p can be calculated by input of x into equation (8.2.3).

$$M_p = \frac{\left[(2a - 2b + (6+\gamma)\,L)\,\frac{x}{L} - (6+\gamma)\,\frac{x^2}{L} - 2a + 2\beta\,(L-x)\right]}{2\,(\alpha x + L)} \cdot PL \qquad (8.2.3)$$

Let us assume the following:

For simplicity, $q_d = q$, $P_d = P$ and $M_{0,d} = M_0$ in the further discussion of this chapter.

8.1 Elastic design of bridge

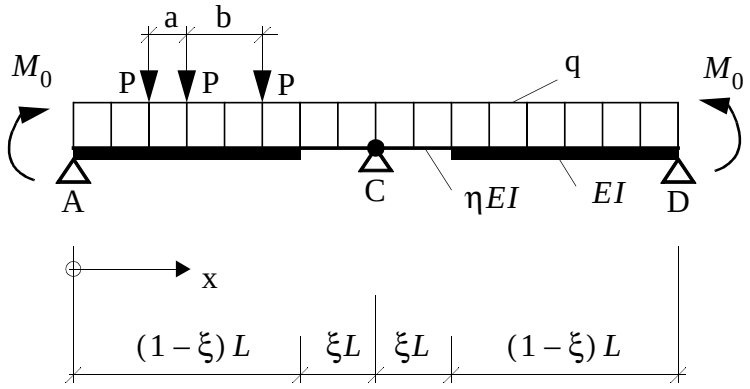

Figure 8.1.1 Outline of bridge model for elastic analysis

An elastic analysis of the bridge has been performed using the computer programs sk88 [16] and Strip-Step 2 [18]. The cross sections of the steel girders are changed at the distance $(1-\xi)L$ from the end supports. The zone of cracked concrete around the internal support is also assumed to start there with $\xi = 0,15$. The results of the analysis are presented in figure 8.1.2. which are required cross-sections in span and at the pier.

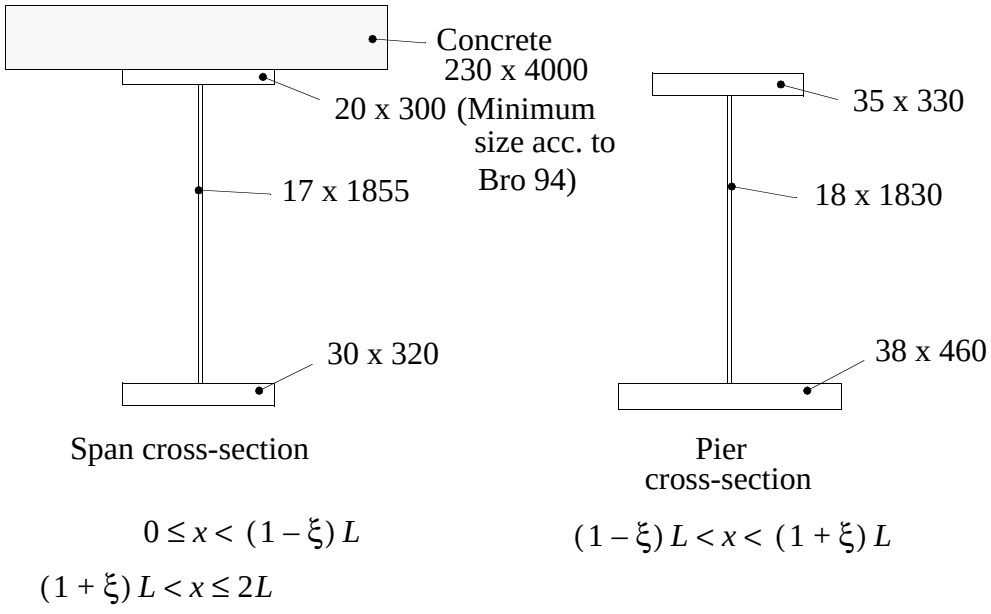

$0 \le x < (1-\xi)L$

$(1+\xi)L < x \le 2L$

$(1-\xi)L < x < (1+\xi)L$

Figure 8.1.2 Cross sections derived from elastic analysis

8. Comparison of Design Methods

In this chapter, the principle way of designing a continuous composite bridge according to a plastic design method, will be outlined. Use of findings and conclusions from previous chapters are included in the outlined design. In addition, an elastic design will be performed and the results from plastic and elastic design will be compared.

The bridge under consideration is a two span bridge, each span is 40 m. The width of the carriage way is 8,0 m and is resting on two steel girders in composite action with the carriage way.The steel is assumed to be S690 with $f_{yd} = 575\ MPa$ and the concrete K40 with $f_{cc} = 15,8\ MPa$.

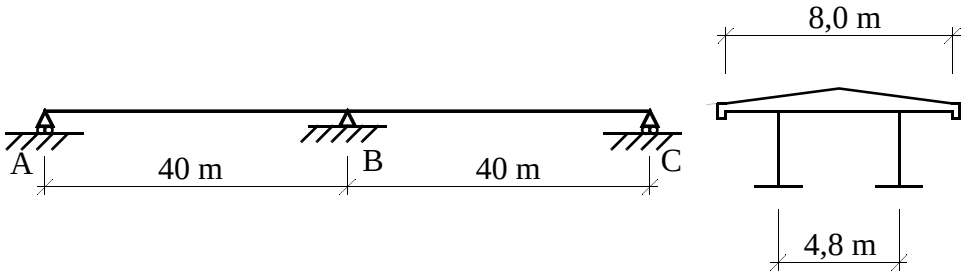

Figure 8.1 Dimensions of bridge in the design comparison.

The following loads, according to table 8.1 (Bro94) are assumed to act on the bridge. The effect of eccentricity of the traffic load has been included in the values for the traffic load. The values of the loads in table 8.1 refer to load on one girder.

.

Table 8.1

Load	q [kN/m]	P [kN]	$M_{0,k}$ [kNm]	ψγ	q_d [kN/m]	P_d [kN]	$M_{0,d}$ [kNm]
Structure	30	-	-	1.05	31.5	-	-
Pave-ment	8.4	-	-	1.2	10.1	-	-
Traffic	17.0	322	-	1.5	25.5	483	-
Temp.	-	-	642	0.6	-	-	385
Shrink.	-	-	1104	1.0	-	-	1104
∑					≈ 67	≈ 485	≈ 1500

Table 8.1 Assumed loads on one girder of the bridge.

9. Proposal of Plastic Design Method taking into account Local Buckling

In the preceding chapters, some of the problems about plastic design including local buckling have been discussed. Some of these may require a more in depth investigation, for example lateral torsion buckling and crackwidth limitation at piers. Other related problems have not been discussed at all, for instance fatigue and shakedown. However, one may hopefully come to the conclusion after having read this report, that a plastic design of a composite bridge is not only feasible but also favourable.

The proposal in this chapter follows in principle the comparison made in chapter 8, with the difference that here the principles for design will be stated in words.

- After the global outline of the bridge has been been decided, the flexural stiffness and the plastic moment capacity at supports of the bridge is assumed.

- Find the governing positions of the load using plastic hinge method. This could readily be done by a computer program to assure that the governing loadpositions are assessed.

- Calculate the required rotation capacity at support using for example the principle of virtual work (be aware of that spans, differing much in length and concentrated forces near supports often require a high rotation capacity). This is easiest performed using an numerical integration method. To the required rotation, add an additional amount of rotation to account for linearly varying temperature and differential settlement, according to chapter 7.4.

- With the required rotation, use formulae derived in chapter 4 or the moment-rotation relationships from the laboratory tests and find the moment capacity of the supports. If this differ from the assumed moment capacity at support, do the calculations all over until assumed and predicted moment capacity is equal.

One major advantage of using a plastic design method in ultimate limit state, is that creep in the concrete is set to zero for all loads, whereas for elastic design several different cross-section properties must be calculated, using different creep factors depending on the type of load.

About 10 % of material savings in the girders is possible is plastic instead of elastic design is used. However to this must be added that a plastic design might need more rigorous arrangements in other aspects for example with respect to lateral torsional buckling of the lower flange at piers. On a whole, cost savings are most certainly in favour of the plastic design.

[15] Mrazik, A., Skaloud, M., Tochacek, M., *Plastic Design of Steel Structures.* ISBN 0-85312-381-0, Ellis Horwood Limited, 1987.

[16] sk88, version 1.0 (93-04-08), computer program for elastic design of composite bridges according to the swedish bridge code, owned by the Swedish Institute of Steel Construction (Stålbyggnadsinstitutet), Stockholm, Sweden.

[17] Statgraphics, version 6.0, computer program for statistical evaluation of observations, owned by STSC, Inc., Rockville, Maryland, U.S.A.

[18] Strip-Step 2, version 2.1, computer program for calculation of forces in two dimensional frames, owned by the swedish consultant company ELU Konsult AB, Stockholm, Sweden.

[19] Nylander, H., *Torsion, Bending and Lateral Buckling of I-Beams*, Bulletin no. 22 from the Division of Building Statics and Structural Engineering, The Royal Institute of Technology, Stockholm, Sweden, 1956.

[20] AASHTO (The American Association of State Highway and Transportation Officials) *Standard Specification for Highway Bridges,*1989, Part "*Guide Specification for Alternate Load Factor Design Procedures for Steel Beam Bridges Using Braced Compact Sections, 1986"*.

[21] Basler, K., Thürlimann, B., *Strength of Plate Girders in Bending,* ASCE Journal, St 6, August 1961.

[22] Johnson, R.P., Dongjie Huang, *Composite Bridge Beams with Mixed-Class Cross-Sections,* Research Report CE46, Univ. of Warwick U.K., Dept. of Engineering, June 1994.

[23] ABAQUS, version 5.3, general finite element program, owned by Hibbitt, Karlsson & Sorensen Inc., 1080 Main Street, Pawtucket, RI 02860-4847, U.S.A.

[24] Ahlenius, E., *Hybridbalkar i stål, dimensioneringsmodell*, publikation 147, Stålbyggnadsinstitutet, 1994.

References

[1] Climenhaga, J.J., *Local Buckling in Composite Beams.* Dissertation submitted to the University of Cambridge for the degree of Doctor of Philosophy, Cambridge 1970.

[2] Dahl, W., Langenberg, P., Sedlacek G., et al., *Elastisch-Plastisches Verhalten von Stahlkonstruktionen Anforderungen und Werkstoffkennwerte.* Doc.-Nr. 7210-Sa/118(91-F6.05), Rheinisch-Westfälischen Technischen Hochschule Aachen, Germany, March 1992.

[3] Galambos, T.V., *Structural Members and Frames.* Prentice-Hall, Library of Congress Catalog Card Number: 68-17530, 1968.

[4] Grubb, M.A. and Carskaddan, P.S., *Autostress Design of Highway Bridges Phase 3: Initial Moment-Rotation Tests.* AISI Project 188, 97-H-045(019-4), April 1979.

[5] Grubb, M.A. and Carskaddan, P.S., *Autostress Design of Highway Bridges Phase 3: Moment-Rotation Requirements.* AISI Project 188, 97-H-045(018-1), July 1981.

[6] Johnson, R.P. and Chen S., *Local Buckling and Moment Redistribution in Class 2 Composite Beams*. Structural Engineering International 4/91, p. 27-34, IABSE.

[7] Kuhlmann, U., *Definition of Flange Slenderness Limits on the Basis of Rotation Capacity Values.* Journal of Construct. Steel Research 14 (1989) pp. 21-40.

[8] Lukey, A.F. and Adams P.F., *Rotation Capacity of Beams under Moment Gradient.* Journal of the Structural Division, Proc. ASCE, Vol 95, No. ST6, June 1969 pp. 1173-1188

[9] Schilling, C.G., *Moment-Rotation Tests of Steel Bridge Girders*. Journal of Structural Engineering, ASCE, Vol. 114, No. 1, Jan. 1988, pp. 134-149.

[10] Schilling, C.G., *Moment-Rotation Tests of Steel Girders with Ultracompact Flanges.* Proc. 1990 Annual Technical Session, Stability of Bridges, Structural Stability Research Council, St. Louis, Missouri, April 10-11, 1990.

[11] Spangemacher, R., *Zum Rotationsnachweis von Stahlkonstruktionen, die nach dem Traglastverfahren berechnet werden*. Thesis, Institut für Stahlbau, RWTH Aachen, ISSN 0722-1037.

[12] Wargsjö, A., *Plastisk Rotationskapacitet hos Svetsade Stålbalkar,* Licentiate Thesis, 1991:15L, Division of Steel Structures, Luleå University of Technology, Sweden, ISSN 0280-8242 (in Swedish).

[13] Baker, J., Heyman, J., *Plastic Design of Frames*, Vol.1, Cambridge University Press, 1969.

[14] Heyman, J., *Plastic Design of Frames*, Vol. 2, Cambridge University Press, 1971.